Åbo Akademi University

Yongchao Zhang

Formic Acid Fractionation of Bamboo and Valorization of Isolated Lignin

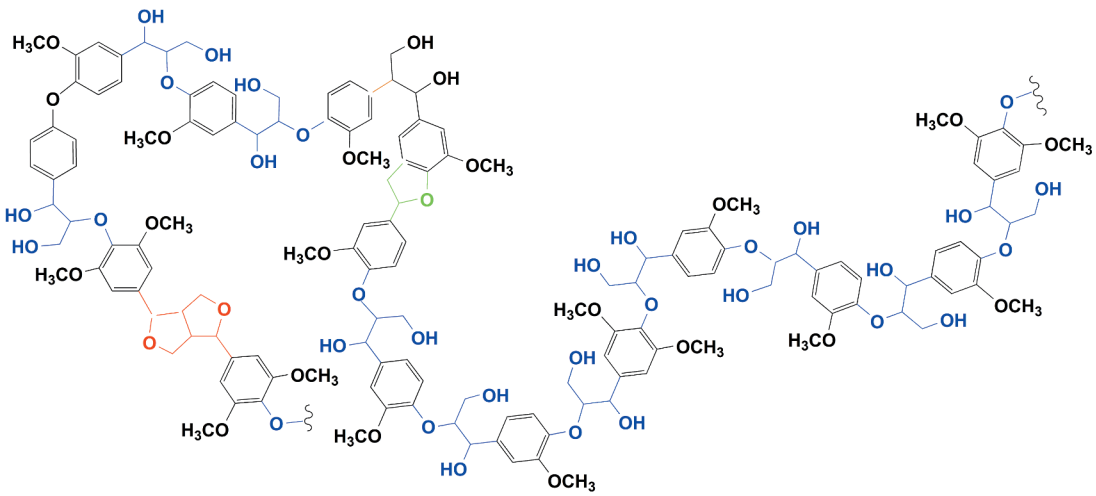

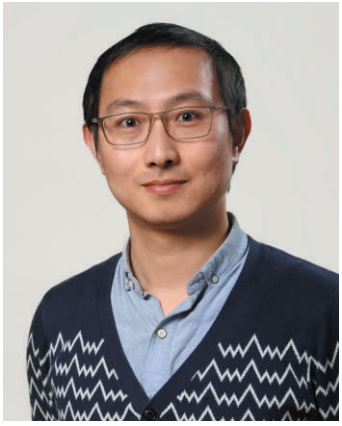

Yongchao Zhang

Born in 1988, Binzhou, Shandong, P.R. China

B.Sc. Chemical Engineering, 2012

Qilu University of Technology, Jinan, Shandong, China

M.Sc. Pulp and Papermaking, 2015

Qilu University of Technology, Jinan, Shandong, China

Ph.D. studies at the Laboratory of Natural Materials Technology from September of 2016

Åbo Akademi University, Turku/Åbo, Finland

Formic acid fractionation of bamboo and valorization of isolated lignin

Yongchao Zhang

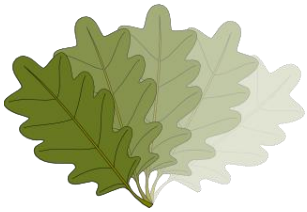

Wood and Paper Chemistry
Laboratory of Natural Materials Technology
Johan Gadolin Process Chemistry Centre
Faculty of Science and Engineering
Åbo Akademi University
Turku/Åbo, Finland, 2020

Supervisors:

Docent Chunlin Xu
Laboratory of Natural Materials Technology
Johan Gadolin Process Chemistry Centre
Åbo Akademi University
Åbo, Finland

Professor Stefan Willför
Laboratory of Natural Materials Technology
Johan Gadolin Process Chemistry Centre
Åbo Akademi University
Åbo, Finland

Reviewers:

Professor Antje Potthast
Department of Chemistry
University of Natural Resources and Life Sciences Vienna (BOKU University)
Tulln, Austria

Associate Professor Martin Lawoko
Fiber and Polymer Technology
Wallenberg Wood Science Center
KTH Royal Institute of Technology
Stockholm, Sweden

Opponent:

Professor Thomas Rosenau
Department of Chemistry
University of Natural Resources and Life Sciences Vienna (BOKU University)
Tulln, Austria

ISBN 978-952-12-3919-9 (printed)
ISBN 978-952-12-3920-5 (electronic)
Painosalama Oy, Turku, Finland 2020

Stay Hungry

Stay Foolish

To Xiaodi and my families

Contents

Perface

List of publications

I **Yongchao Zhang**, Qingxi Hou, Yingjuan Fu, Chunlin Xu, Annika I. Smeds, Stefan Willför, Zhaojiang Wang, Zongquan Li, Menghua Qin. One-step fractionation of the main components of bamboo by formic acid-based organosolv process under pressure. *Journal of Wood Chemistry and Technology*, 2018, 38(3), 170-182.

II **Yongchao Zhang**, Qingxi Hou, Wenyang Xu, Menghua Qin, Yingjuan Fu, Zhaojiang Wang, Stefan Willför, Chunlin Xu. Revealing the structure of bamboo lignin obtained by formic acid delignification at different pressure levels. *Industrial Crops and Products*, 2017, 108, 864-871.

III **Yongchao Zhang**, Menghua Qin, Wenyang Xu, Yingjuan Fu, Zhaojiang Wang, Zongquan Li, Stefan Willför, Chunlin Xu, Qingxi Hou. Structural changes of bamboo-derived lignin in an integrated process of autohydrolysis and formic acid inducing rapid delignification. *Industrial Crops and Products,* 2018, 115, 194-201.

IV **Yongchao Zhang**, Wenyang Xu, Xiaoju Wang, Shuzhen Ni, Emil Rosqvist, Jan-Henrik Smått, Jouko Peltone, Qingxi Hou, Menghua Qin, Stefan Willför, Chunlin Xu. From biomass feedstock to nanomaterials: A green procedure for preparation of holistic bamboo multifunctional nanocomposites based on rapid-formic acid fractionation. *ACS Sustainable Chemistry & Engineering*, 2019, 7 (7), 6592-6600.

V **Yongchao Zhang**, Shuzhen Ni, Xiaoju Wang, Weihua Zhang, Lucas Lagerquist, Menghua Qin, Stefan Willför, Chunlin Xu. Ultrafast adsorption of heavy metal ions onto functionalized lignin-based hybrid magnetic nanoparticles. *Chemical Engineering Journal*, 2019, 372, 82-91.

This work was carried out at the Laboratory of Natural Materials Technology during the years of 2016-2019 under the supervision of Professor Stefan Willför and Docent Chunlin Xu at Åbo Akademi University. Part of the work was carried out at Tianjin Key Laboratory of Pulp & Paper, Tianjin University of Science & Technology, China, and Department of Chemical Engineering, Lakehead University, Canada.

Contribution of the author

The author was responsible for planning, experimental work, and writing the articles of **I**, **II**, **III**, and **V**. The author was responsible for planning, experimental work, and writing the articles of paper **IV** except antibacterial activity analysis.

Supporting publications, proceedings, and presentations

1. **Yongchao Zhang**, Singhi Wang, Andrey Pranovich, Wenyang Xu, Annika Smeds, Stefan Willför, Chunlin Xu. Valorization of lignin-carbohydrate complexes from hydrolysates of Norway spruce: Efficient separation, structural characterization and antioxidant activity. *ACS Sustainable Chemistry & Engineering*. 2018, 7(1), 1447-1456.
2. **Yongchao Zhang**, Xiaoju Wang, Stefan Willför, Chunlin Xu, Pedram Fatehi, Menghua Qin. Magnetic hybrid lignin nanoparticles for ultrafast removal of heavy metal ions, 20th International Symposium on Wood, Fiber, and Pulping Chemistry, Tokyo, Japan, September 9th-11th, 2019. (Oral Presentation by Yongchao Zhang)
3. **Yongchao Zhang**, Qingxi Hou, Xiaoju Wang, Stefan Willför, Chunlin Xu, Menghua Qin. Preparation and characterization of functional nanocomposites based on lignin nanoparticles and cellulose nanocrystals from holistic rapid-formic acid fractionation of bamboo. Proceedings of 5th International Conference on Pulping, Papermaking and Biotechnology, Nanjing, China, November 12th-14th, 2018. (Oral presentation by Yongchao Zhang)
4. **Yongchao Zhang**, Xiaoju Wang, Chunlin Xu, Stefan Willför. Preparation and characterization of functional nanocomposite based on lignin nanoparticles and cellulose nanofibers from holistic rapid-formic acid fractionation of bamboo. Younger Researcher Seminar of the Marcus Wallenberg Prize, Stockholm, Sweden, September 23th-26th, 2018. (Oral presentation and Poster presentation by Yongchao Zhang)
5. **Yongchao Zhang**, Menghua Qin, Zhaojiang Wang. Fractionation of lignocellulosic biomass into cellulose fiber, functional sugars and lignin-based organic fertilizer by recyclable green solvent. 3rd International Symposium on Green Chemistry, La Rochelle, France, May 16th-19th, 2017. (Poster presentation by Yongchao Zhang)
6. **Yongchao Zhang**, Menghua Qin, Zhaojiang Wang. Functional Nanocrystalline cellulose produced directly from lignocellulosic biomass using recyclable formic acid. 3rd International Symposium on Green Chemistry, La Rochelle, France, May 16th-19th, 2017. (Poster presentation by Yongchao Zhang)
7. **Yongchao Zhang**, Menghua Qin, Qingxi Hou, Yingjuan Fu, Zhaojiang Wang. Structural changes of bamboo lignin during formic acid and performic acid treatments. 5th International Symposium on Emerging Technologies of Pulping and Papermaking & 3rd International Papermaking and Environment Conference, Guangzhou, China, November 7th-9th, 2016. (Poster presentation by Yongchao Zhang)

Abstract

Lignocellulosic biomass is the most abundant and renewable natural resource on earth. It has been regarded as an environmentally sustainable raw material to be converted into chemicals and biomaterials. To profitably use the entire lignocellulosic biomass, its dominant components, *i.e.*, cellulose, hemicelluloses and lignin, must be fractionated effectively based on a green pathway. Moreover, a fractionation process suitable for a flexible and economically feasible integrated biorefinery should be beneficial for the subsequent valorization of each obtained stream. In this thesis, formic acid fractionation of bamboo was developed to separate its major components. The obtained fractions were thoroughly analyzed by using advanced instruments analysis methods. Furthermore, valorization processes for the production of lignin nanoparticles, lignin-based composite and hybrid nanoparticles were developed to achieve integration of the concept of current biorefinery into nanomaterials production.

Firstly, one-step formic acid fractionation approach was developed for converting bamboo (*Neosinocalamus affinis*) to its main components focusing on the selective separation of lignin and hemicelluloses. Under the optimized conditions (*i.e.*, 85% formic acid, a liquor-to-solid ratio of 7:1, and a temperature of 145 °C for 45 min), this process provided a high efficient way to produce 42.2% cellulose pulp, 31.5% lignin, 8.5% hemicellulose fractions. An integrated process combining autohydrolysis and formic acid rapid-delignification for bamboo chips was also explored. Autohydrolysis pretreatment facilitated oligosaccharide production, while the subsequent rapid-delignification using formic acid at a low liquid/solid ratio with a relatively short reaction time allowed to obtain cellulose fibers and lignin with a high purity.

Then, the structural characterization of lignin obtained from formic acid fractionation of bamboo was conducted. The results indicated that the formic acid fractionation under pressure presented a quick and efficient delignification method by enhancing the cleavage of interunitary bonds in lignin, however, condensation reaction of dissolved lignin also occurred. Compared to atmospheric formic acid lignin, high-pressure formic acid lignins obtained from both original and autohydrolyzed bamboo showed a higher purity and yield, and had relatively higher contents of phenolic and carboxylic groups.

The dissolved lignin was processed into nanoparticles (lignin-NPs), which exhibited spherical morphology and a uniform particle size distribution. Moreover, the obtained cellulose was easily converted into cellulose nanocrystals (CNCs) by using TEMPO oxidation in a relatively short time. Mixtures of lignin-NPs and CNCs were prepared and further filtrated to form nanocomposite films. The lignin-NPs were homogeneously dispersed in the CNCs matrix and the obtained nanocomposite films exhibited a very smooth surface. Most impressively, at CNCs/lignin-NPs ratio of 5:1, the tensile strength

and Young's modulus were improved by 44% and 47%, respectively, compared to the pure CNC film. Owning to the presence of lignin-NPs, the nanocomposites also exhibited an effective antibacterial activity against *E. coli* (ATCC 11229).

Additionally, novel hybrid nanoparticles were prepared by a facile method involving epichlorohydrin as a cross-linker between carboxymethylated lignin and amino-functionalized magnetic nanoparticles. Both the special nanostructures and the abundant active sites produced from the carboxymethylated lignin are beneficial for achieving excellent performance for the adsorption of heavy metal ions. The as-synthesized magnetic hybrid nanoparticles exhibited adsorption capacities of 152.4 and 71.4 mg/L for Pb^{2+} and Cu^{2+}, respectively. More importantly, the adsorption equilibrium of Pb^{2+} and Cu^{2+} onto hybrid nanoparticles can be achieved within 30 s, which was among the fastest of those previously reported for Pb^{2+} and Cu^{2+} adsorbents. The binding mechanism of Pb^{2+} and Cu^{2+} by hybrid nanoparticles could be attributed to ion exchange and hydrogen bonding.

Keywords

autohydrolysis, biorefinery, formic acid fractionation, functional nanocomposite, heavy metal ions, lignin-based hybrid magnetic nanoparticles, lignin nanoparticles, lignin structure, nanocellulose, ultrafast adsorption

Svensk sammanfattning

Biomassa från lignocellulosamaterial är den mest förekommande och förnybara naturliga råvaran på jorden. Biomassa anses vara ett miljövänligt och hållbart råmaterial som kan konverteras till kemikalier och biomaterial. För att lönsamt använda hela biomassan måste dess ingående huvudkomponenter, d.v.s. cellulosa, hemicellulosor och lignin, effektivt fraktioneras i en miljövänlig process. En optimal fraktioneringsprocess i en flexibel och ekonomisk lönsam integrerad bioraffineringsprocess bör dessutom vara anpassad för efterföljande förädling av de olika råmaterialströmmarna. I detta arbete utvecklades myrsyrafraktionering av bambu så att huvudkomponenterna i bambu kunde separeras. Fraktionerna som erhölls analyserades noggrant med hjälp av avancerade analysmetoder. Dessutom utarbetades metoder för att förädla lignin till nanopartiklar, lignin-baserade kompositer och hybrid-nanopartiklar för att integrera bioraffineringskonceptet med produktion av nanomaterial.

Först utvecklades en process för fraktionering av bambu (*Neosinocalamus affinis*) med myrsyra i ett steg. Processen fokuserade på selektiv isolering av lignin och hemicellulosor. Under optimala förhållanden (d.v.s. 85 % myrsyra, förhållandet koklut till fast material 7:1 och en temperatur på 145 °C i 45 min), erbjöd denna process ett högeffektivt sätt att producera 42,2 % cellulosamassa, 31,5 % lignin och 8,5 % hemicellulosor. En integrerad process som kombinerade autohydrolys och behandling med myrsyra för snabb delignifiering av bambuflis undersöktes också. Den autohydrolytiska förbehandlingen underlättade produktionen av oligosackarider, medan den efterföljande myrsyradelignifieringen, som kunde utföras med relativt korta reaktionstider och lågt förhållande mellan kokvätska och bambu, resulterade i cellulosafibrer och lignin.

Den kemiska strukturen på ligninet som erhölls från myrsyrafraktioneringen karakteriserades. Resultaten indikerade att myrsyrafraktionering under tryck var en snabb och effektiv delignifieringsmetod eftersom denna metod ökade spjälkningen av bindningar mellan ligninenheterna. Dock skedde också kondensationsreaktioner hos det utlösta ligninet. Lignin som erhållits med myrsyrafraktionering vid högt tryck, med eller utan autohydrolys, hade högre renhet och utbyte samt relativt högre halt av fenoler och karboxylsyror jämfört med lignin som producerats vid atmosfärstryck.

Det lösta ligninet processerades till nanopartiklar (lignin-NP), vilka uppvisade en sfärisk morfologi och en jämn partikelstorleksfördelning. Den erhållna cellulosan kunde dessutom lätt och relativt snabbt konverteras till cellulosananokristaller (CNC) genom TEMPO-oxidering. Blandningar av lignin-NP och CNC preparerades och filtrerades för att forma nanokomposit-membran. Lignin-nanopartiklarna dispergerades homogent i matrisen av nanocellulosa och nanokomposit-membranerna hade en väldigt jämn yta. Vid förhållandet CNC:lignin-NP 5:1, så erhölls en imponerande ökning i dragindex (44 %) och i Young's modul (47 %) jämfört med membran av enbart CNC.

Nanokompositerna uppvisade också en effektiv antibakteriell aktivitet mot *E. coli* (ATCC 11229) som kunde kopplas till närvaron av lignin-NP.

Ytterligare preparerades hybrid-nanopartiklar av lignin genom en enkel metod som inkluderade epiklorhydrin som tvärbindare mellan karboximetylerat lignin och aminofunktionaliserade magnetiska nanopartiklar. Både den speciella nanostrukturen och de rikligt förekommande aktiva centra från det karboximetylerade ligninet är fördelaktiga för att producera nanopartiklar med utmärkt prestationsförmåga att adsorbera tungmetalljoner. De syntetiserade magnetiska hybrid-nanopartiklarna kunde adsorbera 152,4 mg/l Pb^{2+} och 71,4 mg/l Cu^{2+}. Ännu viktigare var att adsorptionsjämvikten för hybrid-nanopartiklarna uppnåddes redan efter 30 s, vilket är bland det snabbaste som rapporterats för adsorbenter av bly- och kopparjoner. Bindningsmekanismen för Pb^{2+} och Cu^{2+} på hybrid-nanopartiklarna tillskrevs jonbytesreaktioner och vätebindningar.

Nyckelord

Autohydrolys, bioraffinering, myrsyrafraktionering, funktionella nanokompositer, tungmetalljoner, lignin-baserade hybrid-magnetiska nanopartiklar, lignin-nanopartiklar, ligninstruktur, nanocellulosa, ultrasnabb adsorption

List of abbreviations

2D-HSQC	two-dimensional heteronuclear single quantum coherence
2-MTHF	2-methyltetrahydrofuran
AFL	atmospheric formic acid lignin
AHFL	high-pressure formic acid lignin from autohydrolyzed residue
ALCELL	ethanol-water
APTES	3-(aminopropyl)triethoxysilane
ASAM	alkali-sulfite-anthraquinone-methanol
CNCs	cellulose nanocrystals
CNFs	cellulose nanofibrils
DMSO	dimethyl sulfoxide
DSC	differential scanning calorimetry
DTG	differential thermogravimetry
ECH	epichlorohydrin
FP	formic acid pulp
FTIR	fourier-transform infrared spectroscopy
G	guaiacyl unit
GC-MS	gas chromatography−mass spectrometry
H	*p*-hydroxyphenyl unit
HMF	5-hydroxymethylfurfural
HPFL	high-pressure formic acid lignin
HPLC	high-performance liquid chromatography
KP	Kraft pulp
LA	levulinic acid
LCC	lignin carbohydrate complex
lignin-NPs	lignin nanoparticles
MFL	modified high-pressure formic acid lignin
MWL	milled wood lignin
M_w	weight-average molar mass
M_n	number-average molar mass
NMR	nuclear magnetic resonance
p-TsOH	*p*-toluenesulfonic acid
S	syringyl unit
SEC	size exclusion chromatography
SEM	scanning electron microscopy
T_{max}	maximum temperature
TEM	transmission electron microscopy
TEMPO	2,2,6,6-tetramethylpiperidine-1-oxyl radical
TEOS	tetraethoxysilane
TG	thermogravimetry
TGA	thermal gravimetric analysis
THF	tetrahydrofuran
XPS	X-ray photoelectron spectroscopy
XRD	X-ray diffraction

1. Introduction

1.1 Biomass and biorefinery

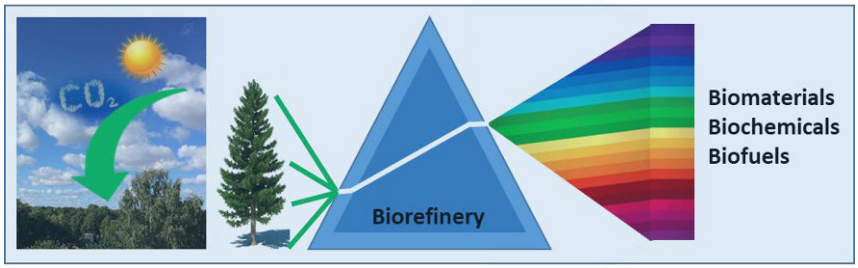

Figure 1.1. *Illustrative flow of biomass to marketable products in a biorefinery process.*

Currently, the energy requirement of human development is largely met by fossil resources, such as petroleum, coal, and natural gas. The enormous consumption of fossil fuels due to increasing industrialization has led to serious environmental problems, such as climate change, as well as air and water pollution. The urgent need to look for sustainable resources as alternatives to meet the increasing energy demand has attracted extensive attention. Biomass is one of the most promising resources to meet the challenges of sustainable and green energy systems, and contributes to over 50% of the world's renewable energy. [1] On the other hand, biomass has also enormous forthcoming potentials to deliver human needs of all useable forms of chemicals, and materials. Biomass is a plant matter, which originally comes from solar energy through the photosynthesis. Biomass includes energy crops and trees, agricultural and forestry residues, aquatic plants, industrial and municipal wastes, and other waste materials. Among various biomass resources, lignocellulosic biomass particularly attracts a great deal of attention all over the world. This is not only because its amount is abundant, but also because the integrated utilization of lignocellulosic biomass is expected to contribute to revitalizing the traditional forest products industries, such as the pulp and papermaking industry. Lignocellulosic biomass is primarily composed of cellulose, hemicelluloses, lignin and small quantities of other compounds such as pectins, proteins, extractives and ash. To overcome the disadvantages of traditional forest products industries and to achieve full utilization of lignocellulosic biomass, it is of great significance that the main components of lignocellulosic biomass are considered as a raw material to produce various bio-based chemicals and materials. [2]

A concept similar to the modern petroleum refinery defined as "biorefinery" has been proposed to produce a spectrum of marketable products and energy from biomass. [3] International Energy Agency (IEA) defines biorefinery as a sustainable processing of biomass into a spectrum of marketable food and feed ingredients, chemicals, materials and energy". [4]

Through its definition, it is clear that the most important distinguishing features of biorefinery are the numerous and various type of high-value products. Generally, an integrated biorefinery involves multi-step processes, in which the first step is conventionally referred to as fractionation of biomass. In this step the feedstock is fractionated into its main distinguished components. Afterwards, the obtained biomass components are used in further conversion processes, in which the outputs can be converted to various marketable products such as chemical intermediates, biofuels, and materials (**Figure 1.1**).

As one of the most abundant biomass feedstocks in the world, approximately 6-7 million tons of bamboo are produced annually in Asia, because of its high productivity, short regrowth period, easy propagation, and low sensitivity to disease. [5, 6] It has received increasing attention as a biomass source for numerous applications within the emerging field of biorefinery. It is important to note that the maximum utilization of the raw materials and minimum production of residues is a grand challenge for biorefinery. In order to maximize the value of the fractions obtained from lignocellulosic biomass and avoid the potential environmental pollution, establishment of an effective fractionation process is of great significance. Moreover, the sustainable valorization pathways should be further developed to convert the major components obtained from the fractionation into chemicals, materials and biofuels in future biorefinery concepts. [7-9]

1.2 Biomass fractionation processes

1.2.1 Organosolv fractionation processes

Figure 1.2. *The biorefinery platform based on organosolv fractionation of lignocellulosic biomass.*

As a typical consumer of lignocellulosic biomass, traditional pulping processes, such as conventional alkaline Kraft and acidic sulphite pulping processes, use a

lot of water and chemicals and require efficient effluent treatment to avoid serious environmental problems. Furthermore, the commercial pulping processes mainly focus on the extraction of the cellulose fraction, while the other two main components, hemicelluloses and lignin, are still underutilized. [10] For example, the majority of Kraft lignins produced by conventional chemical pulping mills are burnt to generate heat and power without considering its potential values. Only approximately 2% by mass is commercially available, ascribed to the complexity of the lignin structure formed during the pulping processes. [11] To promote full utilization of the main components of lignocellulosic biomass, it is essential to develop an efficient and environmentally friendly fractionation approach to selectively separate each component and to facilitate the subsequent valuable conversion.

Recently, new biorefinery technologies based on organosolv fractionation were developed to obtain cellulose, lignin, and hemicellulosic sugars from lignocellulosic biomass without extensive degradation and modification of those biopolymers, [12] as shown in **Figure 1.2**. Importantly, the organic solvents can easily be recovered and reused. Such an environment-friendly approach particularly also provides the possibility of exploiting the high-value applications based on the three components of lignocellulose. [13, 14]

Novel fractionation processes using organic solvents, especially alcohols and organic acids, have been proven to be promising for selective separation of lignocellulosic biomass. [15-18] During recent decades, volatile alcohols with low boiling point have been widely reported as the organic solvent to fractionate lignocellulosic biomass in organosolv processes. Among those alcohols, methanol and ethanol have been frequently used due to their low cost, [19] and ethanol is sometimes preferred because of its lower toxicity. During the fractionation processes, the reaction temperature usually exceeds 160 °C for a process times of 30-90 min. The process parameters depend on the chosen solvent, raw material, and delignification degree. The organosolv fractionation processes using ethanol and methanol are presented in **Table 1.1**. These processes can be conducted using an aqueous solution of alcohols with or without the addition of catalysts. The addition of catalysts, such as sulphuric acid, hydrochloric acid, and acetic acid, contributes to the separation of the lignicellulose, but it can also result in an excessive degradation of hemicelluloses and the enhancement of the production of furfural and HMF. The organosolv processes based on alcohols, including ASAM (alkali-sulfite-anthraquinone-methanol) and ALCELL (ethanol-water), have been implemented at a pilot-plant or industrial scale, but these processes have not succeed in replacing the Kraft process. The integrated strategies to combine ethanol fractionation and pretreatment technologies, including enzymatic pretreatment and autohydrolysis, were also applied to fractionate lignocellulose. Both pretreatment processes facilitate the subsequent delignification by enhancing cleavages of aryl-ether bonds.

Typically, the cellulose fiber is used as a raw material for papermaking and the production of dissolving pulp. It is also a feedstock for the production of

chemicals and biofuels such as glucose, ethanol, or butanol, by using enzymatic hydrolysis and fermentation. It has been proven that the ethanol-based organosolv fractionation of lignocellulosic biomass is an effective method for the subsequent enzymatic hydrolysis and fermentation of cellulose to produce glucose and ethanol. Lignin extracted from organosolv fractionation shows abundant carboxyl groups and a high purity.

Table 1.1. *Ethanol and methanol fractionation processes.*

Fractionation reagent	Raw material	Fractionation conditions	Main result	Ref.
Ethanol	*Eucalyptus globulus*	Ethanol 60%, liquid/solid ratio 6/1(v/w), 180-200 °C, and 30-120 min	Glucose yields 69-77% after enzymatic hydrolysis. Glucose to ethanol conversion 51% after fermentation	[20]
Ethanol and H_2SO_4	Pine and elm	Ethanol 75%, H_2SO_4 1%, liquor/solid ratio 8/1 (w/w), 150-180 °C, and 30-60 min	Ethanol yield 14.2-87.9 g/per kg pine and 70.1-121.2 g/kg of elm after fermentation	[21]
Ethanol and HCl	*Chamaecyparis obtusa*	Ethanol 50%, HCl 0.4%, liquor/solid ratio 5.3/1 (v/w), 170 °C, and 45 min	Glucose yield 70% after enzymatic hydrolysis	[22]
Ethanol and acetic acid	Sugarcane bagasse	Ethanol 60%, acetic acid 5%, liquor/solid ratio 8/1(v/w), 190 °C, and 45 min	Xylose yield 11.83% and cellulose conversion 93.8% after enzymatic hydrolysis	[23]
Methanol	Pressed pericarp fibers	Methanol 65%, liquor/solid ratio 8/1(v/w), 180 °C, and 75 min	Lignin removal 44.6% and glucose yields 42.5% after enzymatic hydrolysis	[24]
Methanol and H_2SO_4	Hemp hurds	Methanol 45%, H_2SO_4 3%, liquor/solid ratio 25/1(v/w), 165 °C, and 20 min	Hemicellulose removal 75%, lignin removal 75%, and cellulose-to-glucose conversion 60% after enzymatic hydrolysis	[25]
Organocell process	*Populus tomentosa Carr*	Methanol 70%, NaOH 1%, 80 °C, and 5 h	Cellulosic fraction yield 80.3% and bioethanol concentration 5.09 g/L after fermentation	[26]

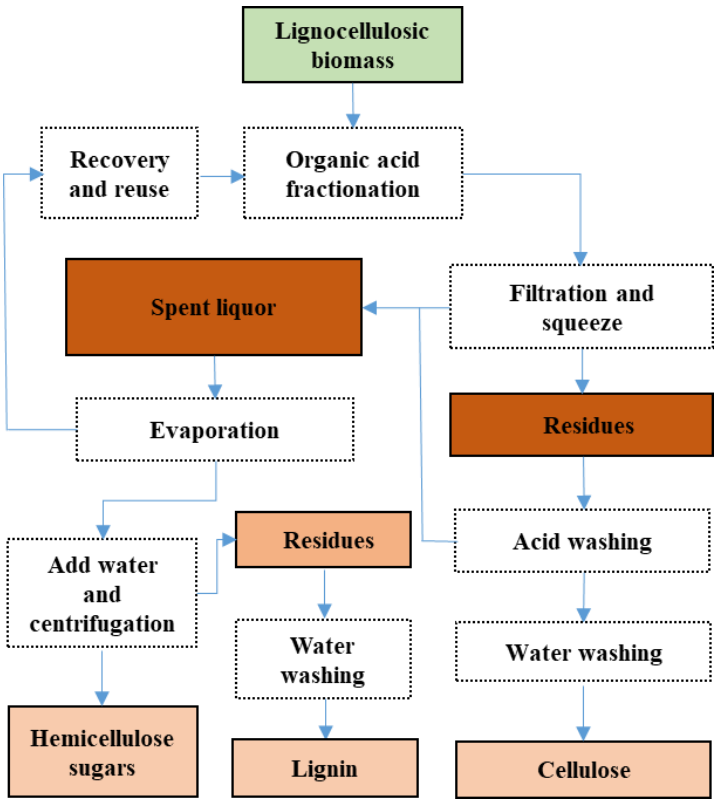

Figure. 1.3. *Overview of the organic acid-based organosolv fractionation of lignocellulosic biomass.*

Although alcohols can be used to efficiently fractionate lignocellulosic biomass for high purity cellulose and lignin, it requires a high temperature and a long holding time to achieve efficient delignification. [27] Short-chain fatty acids, acetic, and formic acids have been emerged as the fractionation agents of lignocellulosic biomass due to their good delignification selectivity. [27] As shown in **Table 1.2**, the organosolv fractionation with a high concentration of organic acid can be operated under mild conditions due to its inherent advantages, such as high acidity and its Hildebrand's solubility value is close to lignin. [19] In those processes, various catalysts, including inorganic acids (HCl and H_2SO_4) and oxidizing agents (H_2O_2), are usually added to assist the delignification during organic acid fractionation, especially in acetic acid treatment. The typical flowchart of organic acid fractionation is shown in **Figure 1.3**. After fractionation, the crude cellulose pulp and spent liquor are filtrated, and then the solids are washed with fresh organic acid and hot water, respectively, to prevent precipitation of the dissolved lignin. The high-purity cellulose is obtained by subsequent screening, which exhibited good performance in cellulose enzymatic hydrolysis. [28] Spent liquor, including the filtrate and the organic acid washings, is evaporated to recover recyclable organic solvent and concentrated residues, which is further separated into lignin

and hemicelluloses by adding water. The obtained main fractions can be further converted into a variety of chemicals and biomaterials. [29] For example, microcrystalline cellulose, which is widely used in pharmaceutical and food fields, can be produced from the cellulose fraction after organic acid fractionation. [30] Furthermore, organic acid fractionation also opens the possibility of using the lignin for high-value applications. It has been demonstrated that eucalyptus lignin obtained from the acetic acid fractionation process is an interesting candidate to produce lignin-based epoxy resin. [31]

As one of the most studied organosolv fractionation processes, organic acid fractionation has been considered as a promising alternative to traditional pulping technology, because satisfying cellulose pulp yield and effective delignification with simultaneous hemicellulose degradation can be achieved. [6] Various organic acid fractionation processes, such as the Milox, [6] Formacell, [32] and Acetosolv [33] methods, have been developed, and exhibited high efficiency on different biomass materials including hardwoods, [34, 35] softwoods, [36] and non-woods. [6] It has been reported that organosolv fractionation using acetic and formic acid (65/35 mass ratio, 85% in water) at 105 °C for 3 h resulted in efficient removal of lignin from wheat straw. [30] 85% lignin removal can be achieved by formic acid fractionation of rice straw in 90% formic acid-water solution at 100 °C for 60 min. [37] However, most of the organic acid fractionation processes are performed at atmospheric pressure with a low temperature, where the relatively mild conditions hinder efficient delignification.

To further enhance the delignification degree, the whole fractionation process requires a long reaction time or a higher proportion of solvent. It was reported that one-step formic acid fractionation of beech wood under a high pressure level at 110-130 °C resulted in higher degree of delignification than the process at atmospheric pressure. [34] A single-stage autothermal performic acid fractionation of *Miscanthus* × *giganteus* at pressures of 35 bar achieved 89% and 88% removal of lignin and hemicelluloses, respectively, in 30 min. The formic acid fractionation under pressure presents a high-efficient delignification method to produce cellulose, lignin, and hemicellulosic sugars, which could contribute significantly to achieve its industrialization.

Yet, some issues also exist in the current organosolv fractionation process. The major problem for organic acid fractionation is the corrosion risk, thus anti-corrosion equipment is required during the whole process. Organosolv fractionation aims at the full utilization of biomass based on the integrated biorefinery. To date, numerous researches focus on the enzymatic hydrolysis and fermentation of the cellulose fraction obtained from organosolv fractionation, especially ethanol-based fractionation. Other value-added utilization pathways for the obtained cellulose, such as the preparation of nanocellulose as well its derived products, are relatively less reported. Furthermore, the organosolv lignin presents great potential due to its special structural properties, it has not been developed up to a commercial level towards the new materials and chemicals yet. In order to develop organosolv biorefinery

and provide more opportunities for integrated utilization of biomass, the structure and properties of biomass lignocellulosic components should be revealed and studied more in details.

Table 1.2. *Organic acid fractionation processes.*

Fractionation reagent	Raw material	Fractionation conditions	Main result	Ref.
Formic acid	Bamboo	Formic acid 88%, liquid/solid ratio 20/1 (v/w), 101 °C, and 2 h	Pulp yield 52.8%, delignification 80.4%	[6]
Formic acid and H_2O_2	Bamboo	Step 1: Formic acid 88%, liquid/solid ratio 20/1(v/w), boiling point and 1 h; Step 2: 3% H_2O_2, 101 °C and 2 h; Step 3: boiling point and 1 h (Milox method)	Pulp yield 48.7%, delignification 88.9%	[6]
Formic acid and H_2O_2	Bamboo	Formic acid 88%, H_2O_2 3%, liquid/solid ratio 20/1 (v/w), 101 °C, and 2 h	Pulp yield 48.1%, delignification 87.9%	[6]
Formic acid and HCl	Bamboo	Formic acid 88%, HCl 1%, liquid/solid ratio 20/1 (v/w), 101 °C, and 2 h	Pulp yield 51.7%, delignification 79.1%	[6]
Formic acid and H_2SO_4	Sugarcane bagasse	Formic acid 78%, H_2SO_4 0.1%, liquid/solid ratio 10/1 (w/w), 107 °C, and 1.5 h	Pulp yield 48.2%, delignification 87.3%	[38]
Acetic acid and HCl	Empty fruit bunches from *Elaeis guineensis*	86.25% acetic acid and 0.25% hydrochloric acid by weight of liquor, boiling point, and 2 h (Acetosolv method)	Pulps with 46.56% yield and 10.3% lignin	[33]
Acetic acid and formic acid	*Miscanthus* × *giganteus*	Formic acid/acetic acid/water (30/50/20 v/v), 107 °C, and 3 h (Formacell method)	Delignification 86.5%	[32]
Acetic acid, formic acid and H_2O_2	Wheat straw	First step: acetic acid and formic acid (65/35 mass ratio, 85% in water), liquor/solid ratio 8/1(v/w), 105 °C, and 3 h; Second step: 10% H_2O_2 on dry matter raw pulp, 85 °C, 90 min	Pulp yield 48%, hemicellulose-rich fractions 27% and lignin yield 21%	[30]
Peracetic acid	Sugarcane bagasse	Peracetic acid 20-60%, liquid/solid ratio 3/1-7/1, 70-90 °C, and 2 h	Delignification over 80%	[39]

1.2.2. Autohydrolysis and acid-catalyzed hydrolysis

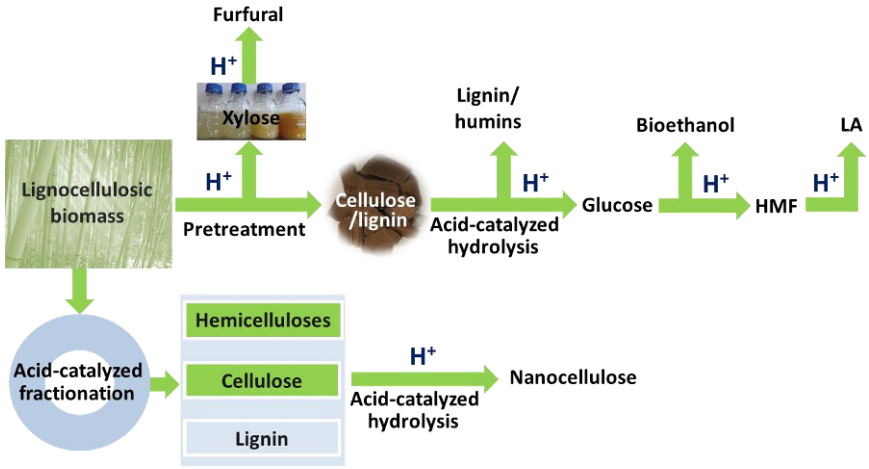

Figure 1.4. *Roadmap for acid-catalytic hydrolysis of lignocellulosic biomass for the production of high-value products.*

Autohydrolysis pretreatment and acid-catalyzed hydrolysis belong to a fractionation process in which hydronium ions break down the linkages in cellulose, hemicelluloses, and lignin. As shown in **Figure 1.4**, there are two pathways for the hydrolysis of lignocellulosic biomass for the production of high-value products, namely pretreatment and acid-catalyzed fractionation, which can be performed alone or in combination.

As an environmentally friendly and economically feasible process, autohydrolysis, in which raw material is pretreated with pure water, is applied to selectively remove hemicelluloses prior to pulping processes. [40, 41] This process is catalyzed by hydronium ions generated by water and acetic acid formed directly due to the cleavage of acetyl groups from the xylan backbone in the wood cells. [42, 43] A liquid phase rich in hemicellulose-derived products can be obtained without significant modifications to lignin and leaving cellulose in the solid material. Afterwards, sugars degraded from hemicelluloses can be recovered in a liquid phase, [44] whereas cellulose and lignin remained in solid phase can be used to further fractionation and conversion. [45, 46] Recently, it has been demonstrated that autohydrolysis pretreatment facilitates the subsequent Kraft pulping of hardwood by increasing the solubility of lignin. [47] An integrated fractionation technology combining autohydrolysis with ethanol organosolv treatment was also proposed. [48, 49]

Acid hydrolysis has been explored as a pretreatment process of lignocellulosic biomass. Pretreatment with acid hydrolysis can promote efficient saccharification of lignocellulosic biomass to fermentable sugars for the production of cellulosic ethanol. The dilute sulfuric acid pretreatment can result in removal of hemicelluloses to a high extent and significantly enhance the porosity of the substrate and accessibility of cellulose in the subsequent

enzymatic hydrolysis. [50] The released sugars from hemicelluloses by the dilute-acid pretreatment are usually recoverable. Recently developed dilute-acid hydrolysis processes usually use mild conditions to obtain a high conversion yield of xylan to xylose, which is beneficial to achieve favorable overall process economics because xylan accounts for up to one-third of the total carbohydrate content in many lignocellulosic materials. [51] Dilute sulfuric acid-based approaches are the most widely used, [52, 53] while nitric acid, [54] hydrochloric acid, [55] and phosphoric acid [56] have also been tested. However, such a mineral acid-based fractionation approach also has some inevitable drawbacks, including equipment corrosion and the recovery and recycle of the acids. [57] After acid pretreatment, the obtained hemicellulosic sugars and pretreated cellulosic solids can be further converted by acid catalytic hydrolysis. Acid catalytic hydrolysis has become a conventional technology to convert hemicelluloses and cellulose into intermediate platform chemicals, including furfural, glucose, 5-hydroxymethylfurfural (HMF) and levulinic acid (LA). [58-62] The hemicellulosic sugars, which is mainly composed of xylose, can be converted to furfural, while cellulose can be hydrolyzed to glucose, HMF, and LA. Dilute sulfuric acid has been applied to commercially manufacture furfural, which is achieved by hydrolyzing hemicelluloses to sugars and then continue to break sugars down to form furfural. [63] Jeong *et al.* proposed a two-step acid-catalyzed treatment of *Quercus mongolica* to obtain pentoses sugars and LA using dilute sulfuric acid reaction with the temperature range of 100-230 °C. [64] The pentose sugars were released from hemicelluloses through the 1st step acid-catalyzed pre-treatment, and the LA was produced through acid catalyzed hydrolysis of cellulose in solid residue under more severe conditions.

In the acid-catalyzed fractionation systems, the participation of hydronium ions is beneficial to promote the cleavage of intramolecular and intermolecular linkages of lignin and hemicelluloses. One-step fractionation process using oxalic acid-catalyzed hydrolysis in a biphasic reaction mixture comprising an aqueous phase and an immiscible 2-methyltetrahydrofuran (2-MTHF) organic phase, has been developed. Oxalic acid catalyzes the hydrolysis of hemicelluloses to soluble sugars in aqueous solution and 2-MTHF selectively dissolves lignin into the organic phase, whereas the cellulose-fibers remain mostly intact. [65] As a novel recyclable acid, *p*-toluene sulfonic acid (*p*-TsOH) can also be used to rapidly and efficiently fractionate lignocellulosic biomass under mild conditions, producing a cellulose-based water insoluble solid fraction and a lignin-based spent liquor stream, both of which are easily converted in to wood-based nanomaterials. [66]

Some of the key challenges of the acid hydrolysis process for biomass, involving environment, economy, versatility, and efficiency, limit its utilization in large-scale processes. Among most of the conventional acid hydrolysis processes, the recycling of the acid catalyst, product separation, and equipment corrosion are the main drawbacks. The use of solid acid catalysts can address some of these challenges due to efficient activity, high selectivity, long catalyst life, and mild operating conditions. [67] Several types of solid acids for biomass

hydrolysis are explored such as H-form zeolites, transition-metal oxides, cation-exchange resins, supported solid acids, and heteropoly compounds. [67] Among these solid acids, carbonaceous solid acid catalysts are considered as the most promising catalyst for cellulose hydrolysis, since they provide good access of reactants to the acidic sites of SO_3H groups. [68-70] Fukuhara *et al.* reported that a cellulose-derived and carbon-based solid acid exhibited a high catalytic performance for the hydrolysis of cellulose. [71] High glucose yields of up to 75% with 80% selectivity were achieved with the reaction conditions at 150 °C and 24 h reaction time. [71] However, solid catalysts cannot be readily separated from the un-hydrolyzed solid residues due to their similar physical and chemical properties. The use of functionalized solid catalysts designed with magnetic property is one method to improve its separation and reuse. A magnetic solid acid with mesoporous structure showed improved performance for the hydrolysis of β-1,4-glucan, producing a glucose yield of up to 96% from cellobiose, while a 50% yield of glucose was obtained from amorphous cellulose with a conventional solid acid. It also exhibited good hydrothermal stability and can be recycled when a magnetic field is applied. [72]

1.3 Plant cell wall polysaccharides

1.3.1 Cellulose and nanocellulose

The plant cell walls mainly consist of lignin and polysaccharides, which include cellulose and hemicelluloses. Cellulose is the most abundant renewable natural resource available worldwide. Approximately 10^{10}-10^{11} tons of cellulose is produced annually on earth. [73] Cellulose is found in wood, cotton, agriculture crops, and other types of sources, such as bacteria, various algae and tunicates. Cellulose is a polysaccharide comprised of unbranched beta (1-4) linked *D*-glucopyranosyl units. Its degree of polymerization (DP) is approximately 10,000-15,000. [74] Cellulose contains a large number of hydroxyl groups, which are placed at the positions C_2, C_3, and C_6, and can form intra- and intermolecular hydrogen bonds. These hydrogen bonds contribute to the formation of a relatively stable, highly ordered, and three-dimensional crystal structure. Cellulose fibrils exists as two regions: a highly-ordered (crystalline region) and a disordered (amorphous-like) region. This molecular structure of cellulose provides several characteristic properties, such as hydrophilicity, chirality, and degradability. Cellulose is typically used for manufacturing of paper, paperboard, and dissolving pulp. It can also be utilized to produce cellulose derivative products, such as cellulose ethers, rayon, and cellulose esters.

The cellulose with at least one dimension in nanoscale is named nanocellulose. Extraction of nanocellulose from natural resources includes various treatment procedures and breaking of amorphous regions of cellulose so as to extract nanocellulose in the form of cellulose nanofibrils (CNF) and cellulose nanocrystals (CNCs). For CNFs, it is produced by defibrillation of cellulose fibers using high shear forces to break the interfibrillated hydrogen bonds and

form “hair-like” particles with a diameter of 5-20 nm and a length ranging from several hundred nanometers to a few micrometers. The manufacture protocols of CNF include mechanical fibrillation, chemical treatments, and enzymatic treatments; as well as a multi-stage process combining several of those treatments. [75-77] To reduce the energy consumption of the mechanical procedures, chemical and/or enzymatic pretreatment are widely recognized methods to facilitate defibrillation. As a typical approach, the 2,2,6,6-tetramethylpiperidine-1-oxyl radical (TEMPO)-mediated oxidation can be applied to the defibrillation process, and also to introduce an increasing amount of carboxyl groups, which are beneficial to the further modification and application. CNCs, also known as cellulose nanowhiskers, are manufactured by removal of the amorphous regions in cellulose fibers to obtain “rod-like” nanocrystals with a diameter of 4-25 nm and a length of several hundred nanometers. Typical preparation procedures of CNCs involve a hydrolysis step in various acid solutions such as mineral acids, organic acids, and solid acids. [78-82] The preparation procedures have a critical role in determining the intrinsic morphology and properties of the resulted nanocelluloses. As a common method for producing CNFs, TEMPO-mediated oxidation combined with mechanical defibrillation can also be used to produce CNCs. [83, 84] Previous research successfully prepared CNCs from softwood bleached Kraft pulp using a 4.5 or 7 h TEMPO-mediated oxidation followed by a 3 h treatment process with $NaBH_4$. [84]

Nowadays, the development of nanocellulose-based composites have attracted much attention in various fields due to their unique properties, including abundance, renewability, high strength and stiffness, eco-friendliness, and low weight. The target nanocomposites can be endued with various special super-properties, such as enhanced mechanical property, antioxidant activity, water resistance and anti-UV property, etc. Both CNCs and CNFs have been employed as eco-friendly reinforcement materials for transforming from weak biopolymers to strong engineering biocomposites with excellent mechanical properties. [85] Combined with high mechanical properties, biopolymers such as chitosan, polylactic acid (PLA), starch and hemicelluloses, which itself have poor mechanical properties compared to those of synthetic polymers, have been widely used to make nanocellulose composites. [86] It is also reported that synthesized holistic nanocellulose and hemicellulose/lignin composite films exhibited significantly improved flexibility, transparencies, mechanical and moisture barrier properties. [87] Nanocellulose-based composites with various properties can be an appropriate future sustainable material for wide range applications in our daily life.

1.3.2 Hemicelluloses and their derivatives

Hemicelluloses, which account for 15-30% of the lignocellulosic biomass by weight, are branched, amorphous polysaccharides composed of different sugar units, principally xylose, mannose, arabinose, galactose, glucose, and some uronic acid depending on the raw material. Softwoods mainly contain

galactoglucomannans (approximately 20%) and arabinoglucuronoxylans (approximately 10%), while hardwoods contain mainly glucuronoxylan, which possess about 80-90% of the hardwood hemicelluloses, as well as a small amount of glucomannan. [88, 89] For example, pine and spruce usually contain about 20 wt% *O*-acetyl-galactoglucomannan and 5-10 wt% arabino-4-*O*-methyl glucuronoxylan. [90] Moreover, xylan units of hardwood glucuronoxylan are strongly acetylated, while acetyl groups in softwood hemicelluloses are attached to the glucomannan backbone. [88, 89] Due to the chemical heterogeneity and the structural positioning, hemicelluloses possess numerous interactions with other cell wall components, including lignin, and structural proteins, forming a matrix adhering to cellulose macrofibrils. It is generally believed that lignin and hemicelluloses are linked by three types of linkages in the lignocellulosic biomass, which are phenyl glycoside, benzyl ether, and ester, forming lignin-carbohydrate complex (LCC). [91, 92]

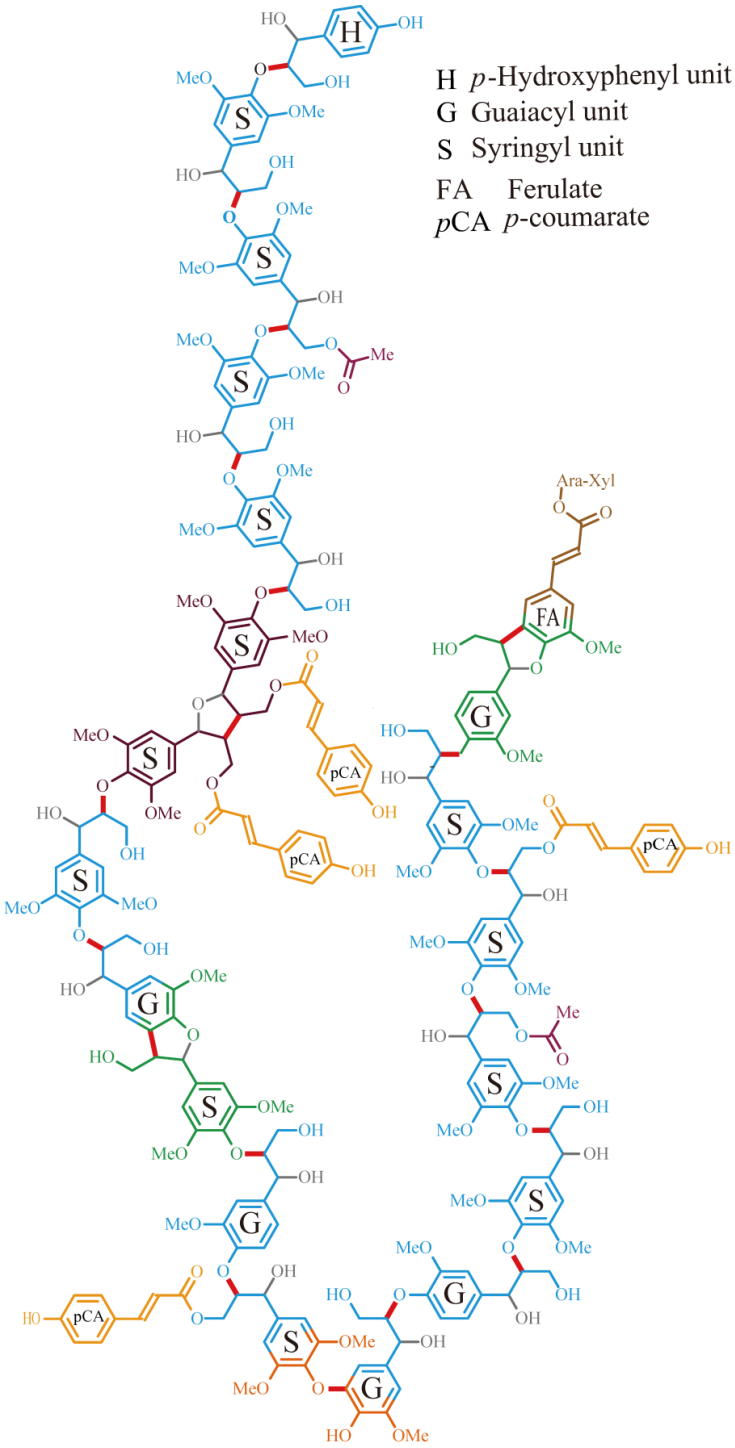

Figure. 1.5. *Chemical structures of lignin from Monocot proposed by Ralph et al. [95]*

1.4 Lignin

Lignin is an abundant natural resource, which constitutes one of the three major components of lignocellulosic biomass, together with cellulose and hemicelluloses. As one of the main sustainable bio-resource raw materials and the high content of aromatic structures, lignin opens the possibility to synthesize environmentally friendly biopolymers to replace the current fossil-based polymers. [93] Due to the structural complexity, only approximately 2% of lignin obtained from the pulp and paper industry is utilized mainly for low-value applications and the massive amounts of lignin products are burnt for heat generation. [94] The successful conversion of lignin to high-value products will require overcoming several challenges associated in lignocellulose fractionation, including characterization of lignin structure, chemical modifications of lignin, and new end-use applications.

1.4.1 Lignin chemistry and structural features

As a composite with intertwined cellulose and hemicellulose in the cell walls, lignin plays an important role in plants, composing the matrix structure of the cell wall and offering strength. [96] Lignin is a complex and amorphous biomacromolecule that typically yields high molar mass of between 1×10^3 and 2×10^4 g/mol, depending upon the extraction and measurement process used. [97, 98] The lignin structure consists of three different phenylpropane units: *p*-hydroxyphenyl (H), guaiacyl (G), and syringyl (S) units, originating from three cinnamyl alcohol monomers: *p*-coumaryl, coniferyl and sinapyl alcohols respectively (see **Figure. 1.5**). [99-101] Lignin biosynthesis is conducted *in vivo* via an enzyme-mediated dehydrogenation polymerization process. The monomers in the lignin structure are cross-linked with both ether and carbon-carbon bonds (**Figure 1.5**). [102] The main bond between monomers in lignin, the β-O-4 ether linkage, typically makes up more than 50% of the bonds formed during the biosynthesis process, which is a crucial target of the degradation mechanisms. [103, 104] Other bonds include β-5 phenylcoumaran, β-β resinol, α-O-4 ether, 4-O-5 diphenyl ether, 5-5 biphenyl, and β-1 diphenyl methane, resulting in the significantly complicated structure and difficulty of degradation due to numerous radical and C-C bond formation. [105-109] The amount of lignin varies in different lignocellulosic biomass feedstocks, and the proportion of different monolignols and chemical bonds in lignin structure is also depending on various original lignocellulosic starting material, such as hardwood, softwood, or grass sources. [110] In the case of softwoods, the lignin structure is mainly composed of guaiacyl units, whereas for hardwoods, lignin has a mixture of guaiacyl and syringyl units with equal amounts. However, the lignin obtained from grass is characterized by the three units: guaiacyl, syringyl and *p*-hydroxyphenyl units, and the *p*-hydroxyphenyl structures dominate. [111] As can be seen in **Figure 1.5**, lignin carries abundant functional groups, including aliphatic and phenolic hydroxyls, and methoxyl groups. The abundance of the chemical sites in the lignin structure open various possibilities for chemical modification and the preparation of grafted copolymers.

The properties of the lignin structure offer a number of advantages, including antioxidant, antifungal and antimicrobial activities, abundant availability as industrial waste, biodegradability, and CO_2 neutrality. [112, 113] Compared to cellulose and hemicelluloses, lignin exhibits more resistance to chemical and biological degradation and provides strength to the cell wall. [15, 114] Lignin also possesses absorption of UV-radiation and fire-retardant properties. [115] Furthermore, as an amorphous polymer, lignin offers various potential physicochemical properties, including a hydrophilic or hydrophobic feature depending on the lignin source and treatment process, viscoelastic properties, rheological characteristics, film-forming capacity, and compatibility, which make it a promising feedstock towards functional materials in a sustainable world. [98]

1.4.2 Lignin structural characterization

Native lignin in its natural states is almost colorless, but after fractionation or purification treatment it takes on a brown color due to the structural changes in the lignin macromolecular matrix. [116, 117] Moreover, the content of functional groups in the lignin structure are affected by the various fractionation processes used. [97] The complicated and changeable structure significantly hinders the subsequent high-value applications of isolated lignin. One of the most challenging issues in lignin valorization pathways is to thoroughly understand its chemical structure and physicochemical properties. [118] To address this issue, various analytical methods have been used for exploring the structures of lignin.

Three isolation lignin protocols have been widely applied prior to characterization: milled wood lignin (MWL), [119] cellulolytic enzyme lignin (CEL), [120] and enzymatic mild acidolysis lignin (EMAL), which are regarded as the representative of native lignin from the raw materials. [121] The typical protocol for the quantitative determination of the lignin content in lignocellulosic biomass is the Klason procedure. In this protocol, the acid insoluble lignin, termed as Klason lignin, is filtered, dried and weighed after the treatment of 72% concentrated sulfuric acid solution followed by dilution of the solution to 3% (TAPPI T222 om-02). The amounts of acid-soluble lignin obtained from the Klason protocol, as well as other types of lignins in solution, can be measured by the UV absorption method. [122]

One of the important physicochemical properties of lignin, *i.e.*, molar mass, including the weight-average molar mass (M_w) and the number-average molar mass (M_n), as well as the dispersity index, are important to determine. Different instruments are available to characterize the molar mass of lignin, such as gel permeation chromatography (GPC), vapor pressure osmometry (VPO), light scattering (static and dynamic), and mass spectrometry. Among the methods for molar mass determination, gel permeation chromatography (GPC), also known as size exclusion chromatography (SEC), is the most used procedure. [123] The previous SEC studies are mainly based on standard calibration through common polystyrene standards. There is a known source of error originated from the

structural differences between linear polymer standards and branched lignin macromolecules, which can result in the underestimation of the true molar mass. [124, 125] The utilization of molar mass sensitive detectors, such as viscosimetric [124], and laser light scattering detectors can provide a much more precise picture of the lignin macromolecule.[125, 126] However, fluorescence, which is found in many types of macromolecules and nanoparticles, including lignin and proteins, could interfere the detectors designed to measure scattered light due to the fluorescent emission. The multi angle light scattering (MALS) detector with fluorescence-blocking filters presents an available technology for most types of lignin (except Kraft lignin) to overcome the challenges of fluorescence. In addition, to improve the solubility of lignins in SEC eluents, the derivatization of lignin is usually required.

Nuclear magnetic resonance (NMR) spectroscopy has long been regarded as one of the key techniques for structural characterization of lignin due to its versatility in exploring structural features and structural transformation of lignin. [127, 128] Among NMR analytical technologies, ^{1}H NMR can be used for conventional examination to provide some key lignin functionalities, such as carboxylic acids, -CH_3 groups, aliphatic and phenolic hydroxyl, methoxyl group, β-O-4 linkages, and type of structure units in lignin. However, ^{13}C NMR has been primarily used to investigate lignin chemical structure and its functional groups, including methoxyl, aromatic condensed and non-condensed carbons, β-O-4 linkages, aldehyde end groups, and ratio of structural units in lignin. [129] Both qualitative and quantitative ^{13}C NMR spectra can be performed to elucidate the lignin characterization. Compared to ^{1}H NMR and ^{13}C NMR, ^{31}P NMR has been extensively utilized to quantitative measurement of various hydroxyl and carboxylic groups in the lignin structure, including aliphatic and phenolic hydroxyls. These functional groups are critical structural features since they have a prominent role in affecting the physical and chemical properties of lignin. [130] Importantly, as one of the most promising diagnostic techniques, two-dimensional heteronuclear single quantum coherence ^{1}H-^{13}C correlation NMR (2D-HSQC) is currently the most commonly applied method for the structural characterization of lignin, which may increase the sensitivity of ^{13}C nuclei and avoid signal overlaps that occur in one-dimensional spectra. The application of 2D-HSQC NMR significantly improves the apparent resolution as a very efficient tool due to it can conduct reliable assignments of proton and carbon nuclei signals in lignin structures. The 2D-HSQC NMR not only is powerful for structural identification but also can offer the estimation of relative abundance of various interunit linkages and monolignol ratios in lignin. [131] It has been widely employed as a quantitative approach to provide the structural features by calculating the relative percentage of each respective interunit linkage, such as β-O-4, β-5, β-β, α-O-4, 4-O-5, 5-5 and β-1 linkages, and the ratio of various monolignol units in lignin. With the development of modern NMR techniques, HSQC has become popular as a powerful tool for the structural characterization of lignin.

In addition, Fourier-transform infrared spectroscopy (FTIR) is recognized as a versatile, rapid technique for lignin characterization and has been extensively utilized for identifying the structural unit composition and the characteristic absorption bands of the chemical groups in lignin, such as -OH, -CH_2-, and -COOH. [132, 133] Thermal characterization techniques are important techniques to reveal the physical properties of lignin. [134] thermal gravimetric analysis (TGA) and differential scanning calorimetry (DSC) techniques can be used to determine the mass loss of samples due to the temperature treatment, as indicative of thermal stability and thermal decomposition of a compound. In addition, the pyrolysis behavior of lignin is important to evaluate the possibility of their potential use in commercial materials or high-value chemicals. In DSC, the differences in heat flow are recorded as a function of temperature and depend on the behavior of endothermic or exothermic events of the sample during the treatment. Other characterization methods, such as gas chromatography-mass spectrometry (GC-MS), electron microscopy, UV-visible absorption spectroscopy and Raman spectroscopy, are used to access the chemical and physical properties of lignin. [135]

1.4.3 Lignin modification

Currently, lignin has exhibited huge potential and numerous opportunities for multiple applications due to its versatility. Without chemical modification, lignin can be directly incorporated into a polymeric matrix as UV-light stabilizer, antioxidant, surfactant, flame retardant, filler, and additive to increase plasticity and flow properties of the target products. [93, 136-139] Lignin can reduce production costs and improve some special properties. However, unmodified lignin still limits its large-scale applications due to the poor properties, such as the weak mechanical properties and thermal instability. To circumvent this limitation and promote the wide applications of lignin, lignin can be chemically modified to be used as a starting material for synthesizing polymers or for the conversion into chemicals and fuels. [93, 140] Due to the abundant functional groups, especially the phenolic and aliphatic hydroxyl groups, lignin structure has relatively high reactivity and can be easily modified for exploring novel materials. The chemical modification of lignin can be classified into three main categories: (1) lignin depolymerization; (2) modification of lignin by introducing new chemically active sites; (3) chemical modification of hydroxyl groups in the lignin structure.

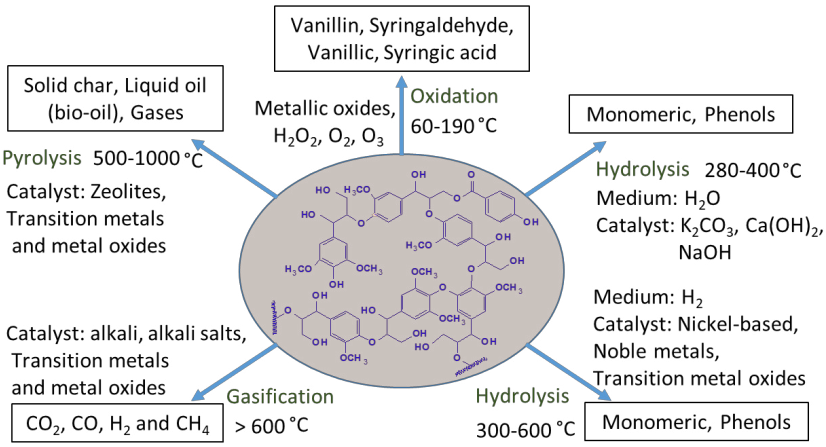

Figure. 1.6. *Summary of main processes for lignin depolymerization.*

Lignin has been recognized as an appropriate feedstock for producing low molar mass compounds, including vanillin, hydroxylated aromatics, aliphatic acids, and many other chemical compounds, which can be further converted into fuels and basic chemicals or oligomers. [141, 142] A great number of thermochemical methods have been proposed for lignin depolymerization, such as pyrolysis, oxidation, hydrogenolysis, hydrolysis, and gasification. [143] **Figure 1.6** gives a brief overview of the range of reaction temperature, processing catalyst, and the main products produced from these depolymerization methods. The main aims of these processes can be summarized as two aspects: (i) the elucidation of the composition and structure of lignin, and (ii) the production of high-value chemicals from lignin.

Functional groups, such as hydroxyls, methoxyls, carbonyls and carboxyls, allow lignin to be modified for different applications. The most studied modifications include sulfonation, sulfomethylation, hydroxyalkylation, amination, and nitration as shown in **Figure 1.7**. [93, 144] Sulfonation of lignin is a common reaction to introduce sulfonate groups in the lignin structure by using sulfuric acid. [145] Sulfomethylation of lignin is performed to introduce methylene sulfonate groups into the lignin structure. The increasing of the number of sulfonate groups in the obtained lignin product can dramatically improve its tanning capacity. This reaction is achieved using equal moles of methanol, alkali metal sulfite salt, and reactive phenolic repeating units of lignin dissolved in water at 100 °C under neutral conditions. [145, 146] The sulfomethyl products of lignin with various degrees of substitution of aromatic rings and side-chains can also be achieved by changing the conditions and ratios of reagents used in this reaction. [147] These sulfomethylation products are usually used as a dye dispersant due to their good dispersibility. [148] Sulfonated lignin is also a good dispersant for the cement matrix because the high zeta-potential value can contribute to the strong electrostatic repulsion forces between cement particles. [145, 149] Currently, the development of lignin-based phenolic adhesives has attracted attention due to their properties of

being renewable and biodegradable. The synthesis of lignin-phenol-formaldehyde resins is expected to provide an alternative for the preparation of phenol-formaldehyde resins. The chemical reactivity of lignin molecules can also be increased through the modifications, such as demethylation, phenolation, and methylolation. To introduce methylol groups in the lignin structure, the reaction of lignin with formaldehyde is typically a prerequisite, and then the lignin methylolation modification process can take place. [93, 150] Hydroxyalkylation of lignin can be performed to improve the strength of an adhesive with a low free formaldehyde content. [93, 150] The amine functional group can be introduced into the lignin structure by using several amination methods. Among these methods, the Mannich reaction of lignin can be easily conducted under alkaline, neutral, or acidic conditions. A Mannich reaction is typically achieved selectively and completely at the C-5 position on the guaiacyl aromatic rings of lignin under acidic conditions using secondary amines. [150] The nitration of lignin is commonly achieved in non-aqueous medium by using nitrating agents, including nitric acid with sulfuric acid, acetic acid, or acetic anhydride.

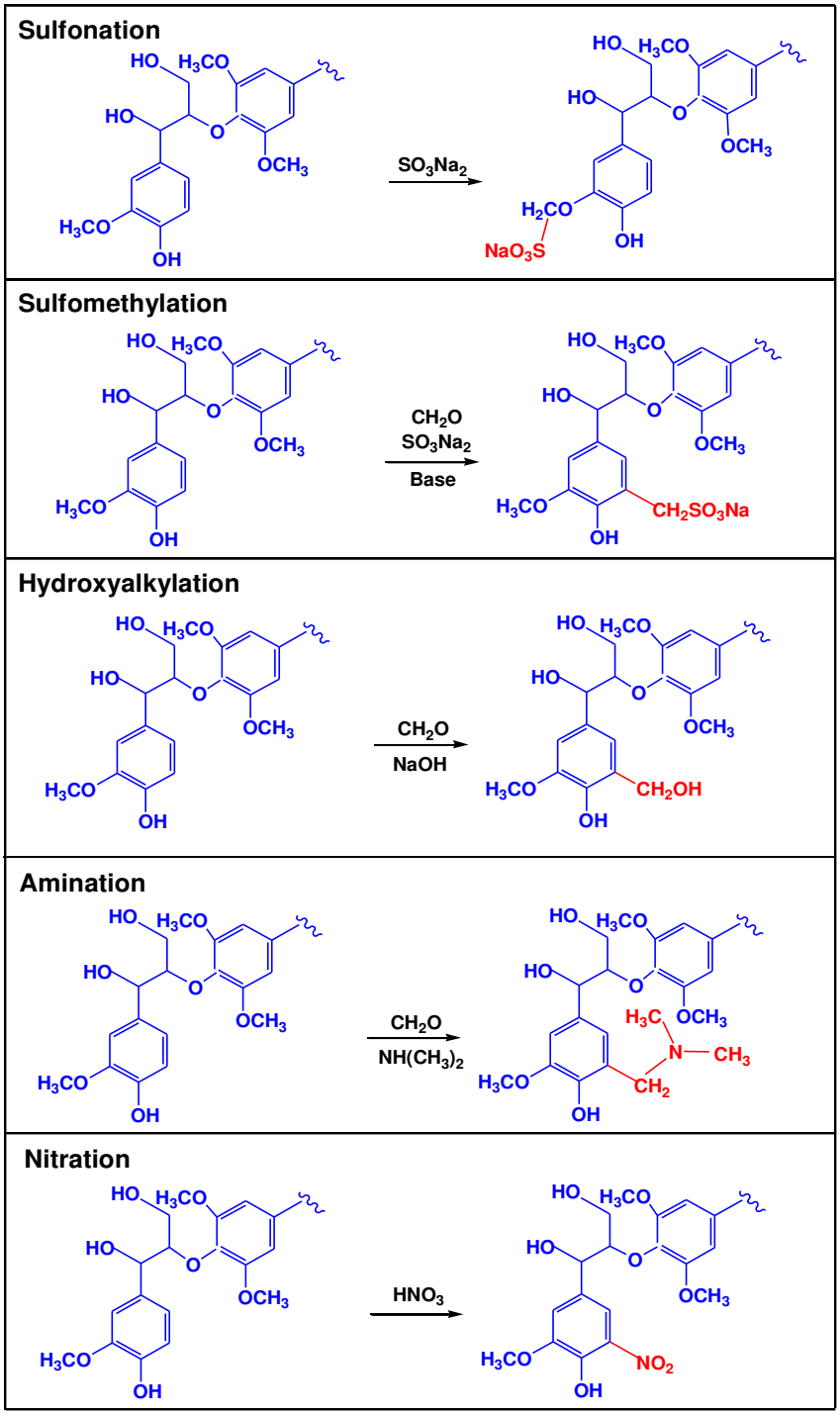

Figure. 1.7. *Overview of some chemical modifications of lignin for the introduction of new chemically active sites.*

As described above, phenolic hydroxyl groups and aliphatic hydroxyl groups at the C-α and C-γ positions on the side chain are present in lignin. As one of the most reactive functional groups, the phenolic hydroxyl groups can influence the chemical reactivity of the formed products. Modifications on hydroxyl groups in lignin structure play an important role on the formation of polyol derivatives of lignin. For this purpose, numerous reactions, such as carboxymethylation, alkylation, esterification, etherification, phenolation, and carbamination can be used, as shown in **Figure 1.8**. [93]

As an effective modification approach, carboxymethylation can yield a carboxymethylated lignin with controlled charge density as a natural adsorbent for heavy metals or dyestuff from aqueous solutions of wastewater and as a dispersant in various areas due to its solubility in water and its effects as a surfactant, respectively. [151] Esterification, including dehydration polymerization with dicarboxylic acids, condensation polymerization with carboxylic acid chloride, and ring opening reactions using cyclic esters can be used to prepare lignin-based polyesters. Lignin-based polyethers can also be produced by one or combined procedures, including polymerization using the alkylene such as ethylene oxide and propylene oxide, polymerization with cross-linkers such as epichlorohydrin and diglycidyl ethers, and solvolysis with ethylene glycol. [152] The oxypropylation of lignin is the most used etherification approach to produce lignin-based epoxy resins through modification using propylene oxide in alkaline solution. The phenolation of lignin is known as phenolysis, by which the lignin modification is conducted by the reaction with phenols in organic solvents (*e.g.,* methanol and ethanol) under acidic conditions. [93] Thus the increased content of phenol groups may improve the chemical reactivity of the lignin structure. [93, 153] The phenolation is commonly used for the synthesis of phenol-formaldehyde resins, which can be achieved at 70 °C for a few hours after lignin is mixed with the phenol-ethanol solution. The natural phenols, such as cardanol, can also be used to modify lignin to produce lignin-based polyurethane films with an improved flexibility. The carbamination of lignin can be performed by forming a urethane link between the lignin hydroxyl groups and isocyanate groups. Polyurethanes produced from polyols and diisocyanates provides versatile products, including low temperature elastomers and flexible or rigid adhesives with high tensile strength. To improve the mechanical properties of lignin-based polyurethanes, chemical modifications can be performed by hydroxyalkylation to introduce soft segments, or by adding other polyols (e.g., polyethylene glycol and other diols).

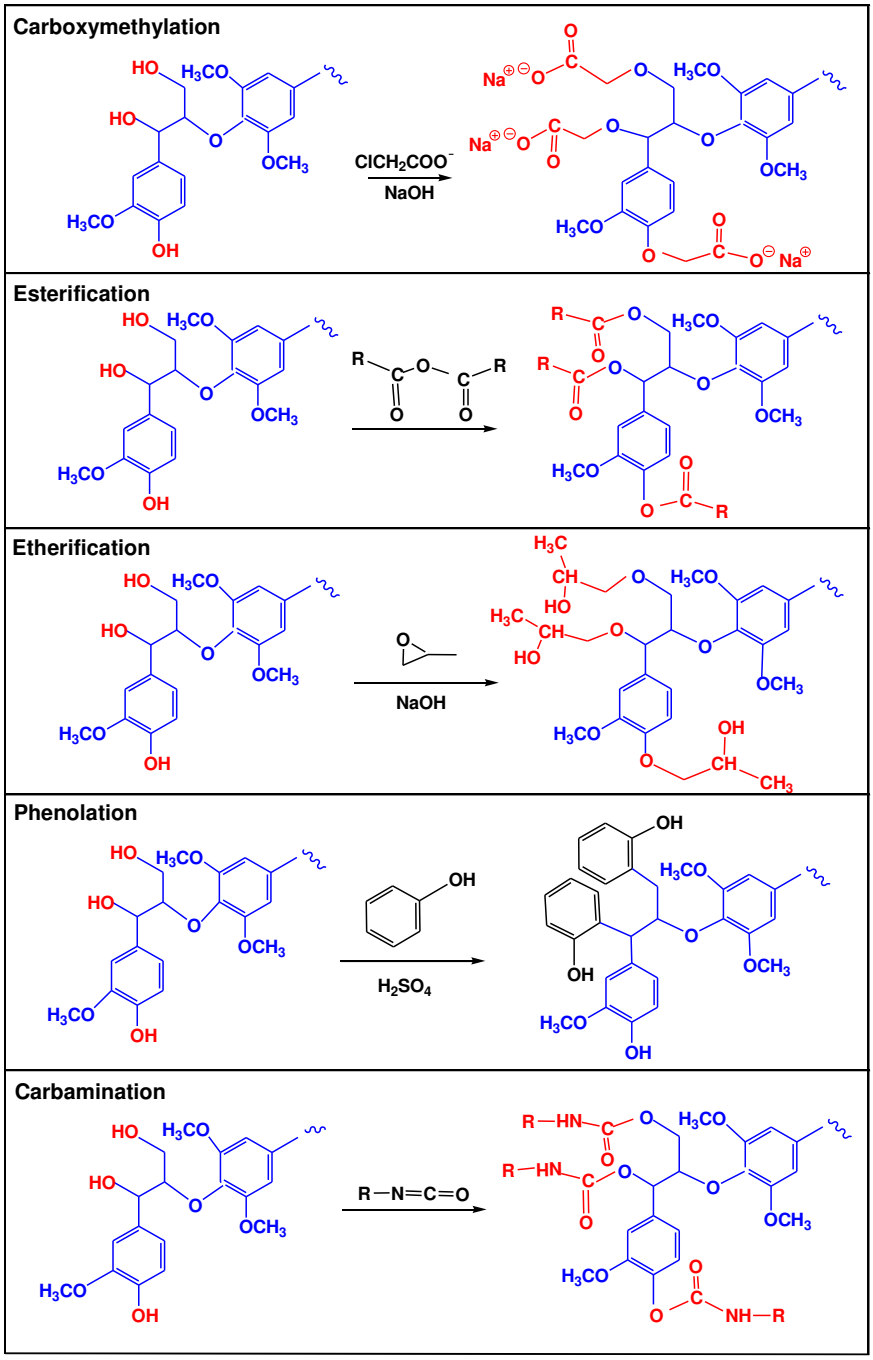

Figure. 1.8. *Overview of some chemical modifications of lignin for the functionalization of the hydroxyl groups.*

1.4.4. Lignin nanoparticles (lignin-NPs) and nanocomposites

Modification and further valorization of low-value but high-volume lignin is important for achieving an integrated lignocellulosic biorefinery. The application of lignin is limited due to its structural complexity and inhomogeneity. To overcome this limitation, nanotechnology offers an alternative approach to build a promising versatile lignin-based material platform. [154] Recently, manufacturing of nanostructured lignin-based materials, such as nanoparticles, nanotubes, and nanocomposites, is the latest and emerging trend and opens the possibility to the full exploitation of lignin in high-value applications. [94, 114, 155]

Lignin-NPs have been fabricated by different approaches, such as precipitation methods initiated with acids, [156] CO_2 saturation, [157] solvent exchange, [158] and dialysis, [159] as well as by sonication [160] and a water-in-oil microemulsion method. [161] All of these lignin-NPs have characteristically different sizes and shapes. More specifically, Frangville *et al.* reported the preparation of lignin-NPs by gradually adding HCl to the lignin solutions. [156] The particle size decreased from the micrometer scale down to less than 100 nm depending on the adding dosage of HCl. The obtained nanoparticles were found to be stable for up to a month under a wide pH range (from 1 to 9) through crosslinking using glutaraldehyde. [156] The development of lignin-NPs presented several important advantages, such as non-cytotoxicity, antioxidativity, biocompatibility, degradability, and biodegradability. [162-164] Yearla and Padmasree prepared dioxane lignin-NPs with an average size of approximately 104 nm using a solvent exchange method and the resulting lignin-NPs presented higher antioxidant and UV-protection properties than the bulk lignin. [163]

Lignin-based nanoparticles have been prepared and applied as vehicles for different applications. Due to its low cost and eco-friendly properties, lignin-based nanoparticles are recognized as one of the potential filler components in polymer matrix and composites for the improvement of thermal and mechanical properties. [165] Furthermore, lignin-NPs can be chemically modified through their various functional groups, which significantly broaden their application field. It was reported that lignin-NPs can be incorporated into the traditional polymeric (vinyl alcohol) matrix to prepare lignin-NPs/PVA (polyvinyl alcohol) composite films. The addition of lignin-NPs presents a great potential to produce a transparent nanocomposite film with additional UV-shielding efficacy and antioxidant properties. [166] Furthermore, abundant phenolic hydroxyl groups on the surface of the lignin-NPs improve the interfacial adhesion with the PVA matrix through the formation of a hydrogen bonding network, which further results in the improvement of the mechanical and thermal performances of the fabricated nanocomposite films. [166] Moreover, lignin-NPs have the potential to be used for the encapsulation of various compounds for pharmaceutical applications. Lignin-based nanoparticles could be infused with silver ions and coated with poly (diallyldimethylammonium

chloride), which significantly promote the adhesion of synthesized nanocomposites to the bacteria films. [167] The prepared nanocomposite exhibits good performance to efficiently kill a wide-range of bacteria. Figueirêdo *et al.* prepared three types of spherical lignin-based nanoparticles: pure lignin-NPs, [159] iron(III)-complexed lignin-NPs, [168] and iron oxide nanoparticle infused lignin-NPs. The introduced Fe_3O_4 in nanoparticles present super magnetic property, which makes the synthesized nanoparticles a promising material for cancer therapy and diagnosis. [169] The obtained pure lignin-NPs could be used to encapsulate hydrophobic drugs, which contributed to the improvement of their release profiles and anticancer activity. Therefore, these synthesized nanoparticles provided important features for drug delivery and biomedical applications. [169]

1.4.5 Lignin-based adsorbents for heavy metal removal

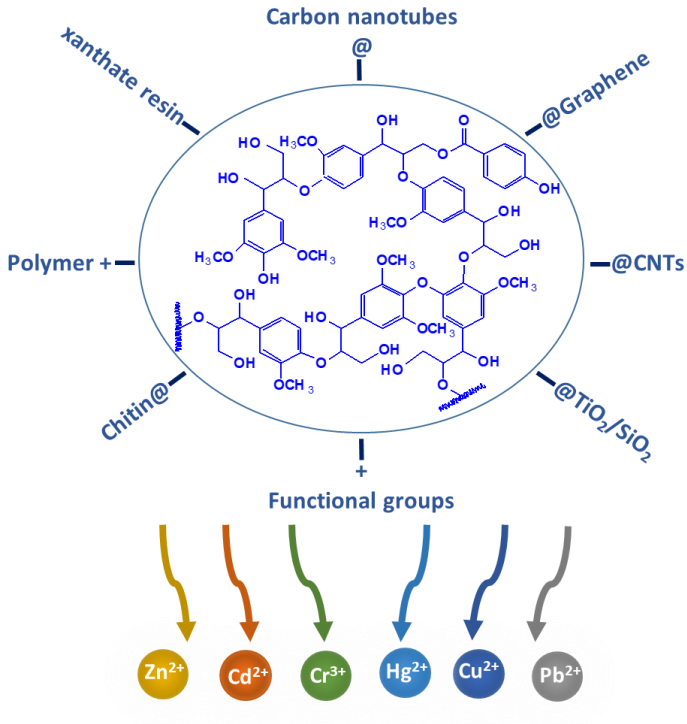

Figure. 1.9. *Lignin-based adsorbents for the adsorption of heavy metal ions in water.*

Lignin and lignin-derived products present a good performance for the adsorption of heavy metal ions and organic dyes as a potential renewable, low cost, and sustainable adsorbents for wastewater treatment. The adsorption performance strongly depends on the lignin structure, which is mainly determined by the feedstock and the extraction conditions. [170] Generally, unmodified lignin usually provides poor adsorption capacity for heavy metals ions. [170] However, lignin-based composite materials have been demonstrated

to have high selectivity and adsorption capacities for a wide range of adsorbents. Carbonization, carboxymethylation, activation, and other modifications of lignin are essential and contributes to enhance adsorption capacity and selectivity. [171] As shown in **Figure 1.9**, numerous approaches have been exploited to manufacture lignin-based composites as novel adsorbents for wastewater treatment, such as lignosulfonate-modified graphene hydrogel, [172] poly (ethyleneimine)-graft-lignin, [173] lignin-based resin [174] and lignin-grafted biopolymers. [175, 176] Most importantly, lignin-based adsorbents can confer high environmental benefits due to its unique properties. The adsorption of lignin-based materials is highly pH-dependent since the deprotonation of acidic groups at high pH contributes to the adsorption of metal ions and the adsorption capacity achieves a plateau above pH 5-6. [177-179]

2. Hypothesis and objectives of the work

The main hypothesis of this thesis was to fractionate each component of the lignocellulose and thereafter to convert them into high-value products based on a novel biomass fractionation approach using recyclable formic acid under pressure. This could greatly contribute to the development of a green pathway to the valorization of formic acid lignin.

The first objective was to optimize the fractionation process conditions, such as reaction temperature and time especially for bamboo. In order to increase the recovery yield of the main components of bamboo, especially for hemicelluloses, a combined fractionation process of autohydrolysis and formic acid induced rapid-delignification was also developed. Different analysis techniques, including FTIR, NMR and GPC were applied to thoroughly reveal the structural features of the fractionated lignin.

The second objective was to valorize of the different fractions, especially cellulose and lignin. The cellulose fraction was used to prepare nanocellulose by TEMPO-mediated oxidation. The sulfur-free lignin fraction was to be used to produce lignin-NPs through a pH adjustment method from basic to acidic aqueous medium. In an attempt to achieve multifunctional nanomaterials, a nanocomposite based on nanocellulose and lignin-NPs, as well as lignin-based hybrid magnetic nanoparticles, were to be synthesized to demonstrate the feasibility of the combined process to integrate production of nanomaterials. We envision this research could open the door for building an integrated nanomaterials production platform based on formic acid fractionation of lignocellulosic biomass.

3. Materials and methods

3.1 Materials

Bamboo (*Neosinocalamus affinis*) chips (20-30 mm long, 10-20 mm wide, and 3-4 mm thick) were collected from Sichuan Province in China and used as raw material. The main chemical composition of the bamboo chips were detailed as follow: Klason lignin 25.56%, acid-soluble lignin 1.87%, xylan 21.96%, glucan 39.63%, ethanol-toluene extractives 2.10%, and ash 2.2%.

All solvents, chemicals, and reagents were purchased from Sigma-Aldrich, MERCK, or VWR and used without further purification.

3.2 Fractionation and preparation approaches

3.2.1 Formic acid fractionation (Paper I)

Approximately 100 g of bamboo chips was utilized in a fractionation process using 85% (v/v) formic acid at a liquid-to-solid ratio of 7:1. The reaction was carried out in a 3 L Hastelloy alloy sealed container, which includes an outer jacket containing electrical wires and intelligent temperature control system. The mixtures was heated to a pre-determined maximum temperature (T_{max}) and held for a certain time without stirring. Afterwards, the obtained solid fraction (mainly cellulose) was separated from the reacted liquid by filtration and squeezed to remove the largest possible amount of liquor. The crude pulp was then washed with 85% formic acid and deionized water (85 °C), respectively, for three times each. The yield of the obtained pulp was determined gravimetrically after the pulp was thoroughly dried to a constant weight in an oven at 105 °C. The determination of Kappa number and intrinsic viscosity of the pulp were conducted according to Tappi T236 om-99 and T230 om-04, respectively.

The obtained pulp was bleached by a $D_1E_PD_2P$ sequence in sealed polyethylene bags immersed in a thermostatic water bath. Handsheets with 60 g/m^2 grammage of the bleached pulp were made in a standard handsheet-making apparatus (Blattbildner-Sheet Former, RK-3A, Austria PTI Company).

The filtrates from the reacted liquid and the above-mentioned formic acid washing liquids were combined as spent liquor, and further evaporated to near dryness to recover the formic acid with a rotary evaporator. Then, 10 volumes of distilled water were poured into the concentrated spent liquor to precipitate the dissolved lignin, while the hemicellulose fraction was contained in liquid phase. The crude lignin was obtained by centrifugation at a speed of 3000 rpm for 10 min and then washed with distilled water twice at room temperature. The yield of crude lignin was measured gravimetrically after freeze-drying. The supernatant was concentrated using a rotary evaporator to obtain hemicellulose fraction, which was heavily degraded. The crude lignin was further purified according to the method proposed by Abdelkafi *et al*. [180]

3.2.2 Autohydrolysis (Paper III)

The autohydrolysis process was carried out in a 15-liter electrically heated and thermostatically controlled rotary digester (Xianyang Tongda Light Industrial Equipment Co. Ltd., China). 200 g of bamboo chips and distilled water were mixed with a solid-to-liquid-ratio of 1:6, and then added in the digester. Based on the optimal condition, the mixture was heated to 170 ℃ in 30 min, and then kept at this temperature for 60 min. After autohydrolysis, the mixture of autohydrolyzed bamboo chips and the autohydrolysis liquor was rapidly cooled down to about 80 ℃. The autohydrolysis residue was separated by filtration with a 120-mesh nylon screen and thoroughly washed with distilled water.

3.2.3 Milled wood lignin (MWL) extraction (Paper II)

It is well recognized that MWL is a typical representative of native lignin in the wood cell wall. Although lignin could undergo structural change somehow during the milling process, but a relatively complete picture of native lignin could still be demonstrated. Thus, MWL as a representative of native lignin was isolated for comparison, according to the method of Björkman. [181] Briefly, the extractive-free raw material was dried, transferred to a porcelain jar, and then ground in a rotary ball mill for 72 h. The ball-milled sample (20 g) was extracted twice with dioxane-water (200 mL; 96:4, v/v) for 24 h. The extracted mixture was centrifuged, and the collected supernatant was concentrated using a rotary evaporator under reduced pressure. The concentrated solution was then freeze-dried, and the crude lignin was obtained. The crude lignin was dissolved in acetic acid-water (20 mL; 9:1, v/v) and precipitated into deionized water (400 mL). The precipitated lignin was separated by centrifugation and then freeze-dried. For further purification, the dried sample was dissolved in 1,2-dichloroethane-ethnol (10 mL; 2:1, v/v), and precipitated into diethyl ether (200 mL). Subsequently, the mixture was centrifuged and the obtained solid was washed (twice) with diethyl ether and petroleum ether, respectively. After further vacuum-drying, the milled wood lignin based on various materials was obtained.

3.2.4 Preparation of cellulose nanocrystals (CNCs) (Paper IV)

The bleached pulp was used as the starting material to prepare nanocellulose using a TEMPO-mediated oxidation process according to the literature. [182] Briefly, 2 g of bleached cellulose fibers from bleached bamboo pulp were dispersed in 100 mL of distilled water and stirred for 4.0 h at room temperature. Subsequently, 32 mg of TEMPO (0.1 mmol/g fiber) and 200 mg of NaBr (1.0 mmol/g fiber) were dissolved into 100 mL of distilled water, and then the solution was mixed with the dispersed fiber suspension and stirred at 300 rpm. Next, the pH of the slurry was adjusted to 10.0 by dropwise addition of 0.5 M NaOH. The oxidation was started by the addition of the desired amount of the 10% NaClO dropwise (10 mmol/g fiber). The total volume of the NaClO was added within about one-third of the designated reaction time, and the pH was maintained at 10.5 by dropwise addition of 0.5 M NaOH. When the desired

reaction time (0.5-24 h) was reached, the reaction mixture was poured into 3 volumes of ethanol to precipitate the TEMPO oxidized cellulose. After the centrifugation (3500 rpm, 10 min) the obtained cellulose gel was thoroughly washed with deionized water, and the residual ethanol was removed by rotary evaporation. The oxidized cellulose was diluted to a consistency of 0.5%, and then fibrillated by a domestic blender (OBH Nordica 6658, Denmark) for 2 min at an output of 300 W. Finally, the obtained nanocellulose was stored at 4.0 °C for further analysis. The carboxylate content of nanocellulose products was determined according to the published method. [182]

3.2.5 Preparation of lignin-NPs (Paper IV)

1.0 g of dried lignin was mixed with 150 mL of distilled water, and then the pH was increased stepwise to reach the target pH value of 12.00 by adding 0.1 M NaOH under constant stirring (500 rpm). The sample was equilibrated for 5 min. Finally, lignin-NPs were formed by adding 0.1 M HCl to hit the final pH value of 5.00.

3.2.6 Preparation of nanocomposite films based on nanocellulose and lignin-NPs (Paper IV)

Nanocomposite films were prepared by mixing the obtained nanocelluloses and lignin-NPs suspension above, followed by dilution to 0.1% (w/v) during constant stirring (500 rpm) at room temperature for 30 min. The total amount of dry substance in each sample was kept constantly at 300 mg with different compositional weight ratios of nanocellulose/lignin-NPs. 300 mL of the suspension was filtered through a 0.1 μm nylon membrane with 90 mm diameter (Sterlitech, USA). A nanocomposite film was obtained after drying in vacuum desiccator at 40 °C under a pressure of 88 mbar for 4.0 h.

3.2.7 Preparation of lignin-based magnetic hybrid nanoparticles (Paper V)

Modified lignin-based magnetic hybrid nanoparticles were synthesized through a three-step procedure. Firstly, 100 mg of Fe_3O_4 particles, which were prepared by the combination of an oxidation-coprecipitation method and a chemical coprecipitation method, [183] were dispersed in a mixture solution containing 400 mL ethanol and 100 mL water with 30 min sonication. Subsequently, the mixture was stirred for 30 min at room temperature, and then the pH was adjusted to 10 by adding $NH_3 \cdot H_2O$. Tetraethoxysilane (TEOS, 1 mL) was added dropwise into the mixture and then stirring for 6 h. The obtained product was collected by magnetic separation and washed with ethanol and water several times, and then redispersed in dry toluene (300 mL). 3-(aminopropyl)triethoxysilane (APTES, 2 mL) was added dropwise and stirred for 24 h at room temperature. The resulting product, which was denoted as $Fe_3O_4@SiO_2$-NH_2, was separated through a magnet, washed three times with ethanol and dried using vacuum freeze-drying.

Secondly, carboxymethylated lignin was prepared from the obtained formic acid lignin according to the literature with a slight modification. [184] Briefly, 5 g of lignin was added into 135 mL of methanol (72%), and then 13.5 mL of NaOH solution (30% w/v) was added dropwise under continuous stirring. After stirring for 90 min at room temperature, 6.0 g monochloroacetic acid was gradually added, and then the mixture was heated to 55 °C and stirred for 210 min. The mixture was filtered and placed into dialysis membranes, sealed, and then put into deionized water for 2 days while water was replaced twice a day. Finally, the modified formic acid lignin (MFL) was obtained after freeze-drying.

Thirdly, as a typical procedure, 1.2 g carboxymethylated lignin was dissolved in 12 mL of NaOH solution (12% w/v) under mechanical stirring to form a clear solution. Next, the Fe_3O_4@SiO_2-NH_2 nanoparticles (0.4 g) were dispersed into 200 mL toluene with 30 min sonication, and then the suspension was added in the above solution. 8 mL epichlorohydrin (ECH) solution was dropwise added into the above dispersion and reacted at 70 °C for 3 h. Finally, the resulting modified lignin-based hybrid magnetic nanoparticles (Fe_3O_4@SiO_2-NH-MFL) were separated by a magnet, rinsed with ethanol, and dried using vacuum freeze-dryer.

As a control experiment, non-silica coated modified lignin-based hybrid magnetic nanoparticles (Fe_3O_4-NH-MFL) and non-modified lignin-based hybrid magnetic nanoparticles (Fe_3O_4@SiO_2-NH-FL) were also prepared according to the same procedure.

3.3 Characterization methods

3.3.1 Composition analysis (Paper I, II & III)

Carbohydrate analysis of the pulp, lignin, and hemicellulose-rich fractions was conducted by gas chromatography (GC) according to a previous publication. [185] Briefly, the dried solid sample was hydrolyzed using acidic methanol at 100 °C for 5 h. After the acid methanolysis process was finished, 1 mL of 0.1 mg/mL sorbitol and resorcinol was added as the internal calibration and then the sample was evaporated by nitrogen flow in a 50 °C water bath. After drying, the sample was silylated and then transferred to GC vials. The silylated sample was analyzed by GC-FID.

The degradation by-products of carbohydrates in the spent liquors, including acetic acid, furfural, and hydroxymethyl furfural (HMF), were determined according to a previous method as described by Wang *et al*. [61] A Shimadzu LC-20T high-performance liquid chromatography (HPLC) system equipped with a Waters C18 symmetry column (4.6 × 150 mm, 5 μm) and a UV detector was used. Samples were run at 30 °C and eluted at 1.0 mL/min^{-1} with the mobile phase A and B for elution. Mobile phase A was a mixture of 0.02 mol/L NaH_2PO_4 and acetonitrile with a volume ratio of 95:5 at pH 2.8 adjusted by H_3PO_4. Mobile phase B was a mixture of acetonitrile and methanol with a volume ratio of 50:50.

3.3.2 Characterization (Paper II, III, IV & V)

*Molar mass determination (**Paper II & III**)*

The molar mass of lignin samples was determined after the acetylation by acetic anhydride. [186] The acetylated lignin was dissolved in tetrahydrofuran (THF) with a concentration of 1 mg/mL, and then the molar mass and dispersity index were determined using a Shimadzu HPLC system, including system controller SCL-10AVP on-line degasser DGU-14A, low-pressure gradient valve FCV-10ALVP, HPLC pump LC-10ATVP, autosampler SIL-20AHT and column oven CTO-10ACVP), equipped with a sequentially connected guard column (50 mm × 7.8 mm) and two Jordi Gel DVB 500A (300 mm × 7.8 mm) columns in series. The column was operated at 40 °C and the eluent was THF with 1% acetic acid at a flow rate of 0.8 min^{-1}. 50 µL solution was injected by the autosampler. A LT-ELSD detector (SEDERE SEDEX 85 LF Low-Temperature Evaporative Light Scattering Detector) was performed using the following parameters: HPLC nebulizer, 40 °C, air pressure: 3.4 bar, gain 3, no-split mode.

*FTIR spectroscopy (**Paper II, III, IV & V**)*

FTIR spectra were recorded on an FTIR spectrophotometer (IRPrestige-21, Shimadzu, Japan). 64 scans were taken for each sample recorded from 4000 to 400 cm^{-1} with a resolution of 0.5 cm^{-1}. The fingerprint region was baseline corrected between 1900 and 750 cm^{-1}.

*X-ray diffraction (XRD) analysis (**Paper V**)*

The XRD patterns were recorded using a Bruker Discover D8 (Bruker-AXS, Karlsruhe, Germany) with a Ni-filtered Cu K_α radiation generated with an operating voltage of 45 kV and a filament current of 40 mA. The XRD patterns were collected with the changing scattering angle (2 θ) from 0 to 80 ° (Scanning rate = 2 s/step, step size = 0.002 °).

*X-ray photoelectron spectroscopy (XPS) (**Paper V**)*

XPS of nanomaterials was performed using an ESCA Lab220i-XL electron spectrometer with the following parameters: Monochromatized Al K_α-radiation with 50 W and 15 kV. The spectrometer pass energy was 117.4 eV and low energy Ar-ions and electrons were used for charge compensation. The diameter of the analyzed area was 200 µm and the X-ray take off angle was 45 °.

*NMR analysis (**Paper II & III**)*

The ^{1}H- and ^{13}C NMR spectra of the lignin samples were recorded with a 500 MHz Bruker Advance instrument, fitted with a 5-mm broadband probe with a gradient field in the Z-direction at room temperature in deuterated dimethyl sulfoxide (DMSO-d_6) as the solvent. For 2D HSQC spectra, a standard Bruker HSQC pulse sequence, "hsqcedegpsisp2.3," was used. The lignin (80 mg) was placed into a 5-mm NMR tube and dissolved in 0.75 mL of DMSO-d_6. The ^{1}H NMR spectrum was recorded on the spectrometer with a minimum of eight scans, a sweep width of 400 MHz, an acquisition time of 2.0 s, and a relaxation

delay time of 3 s, while the ^{13}C NMR spectrum was acquired with a minimum of 20,000 scans, a sweep width of 400 MHz, an acquisition time of 0.4 s, and a relaxation delay of 1.5 s. All experiments were carried out at 25 °C.

Quantitative ^{31}P NMR spectra of the lignin samples were obtained according to a published method. [187] Lignin (40 mg) was accurately weighted and dissolved in 650 μL anhydrous pyridine/$CDCl_3$ (1.6:1, v/v). 50 μL internal standard solution (N-hydroxynaphthalimide, 80 mg/mL, in anhydrous pyridine/$CDCl_3$ (1.6:1, v/v)) and 50 μL relaxation reagent (chromium (III) acetylacetonate, 11 mg/mL, in anhydrous pyridine/$CDCl_3$ (1.6:1, v/v)), and 100 μL 2-chloro-4,4,5,5-tetramethyl-1,3,2-dioxaphospholane (TMDP) were added successively into the above solution, and then the mixture was kept for 10 min. The final phosphorylated lignin was then subsequently determined. The acquisition time and the relaxation delay parameter were 1.5 s and 2.0 s, respectively. A high signal/noise ratio of approximately 1000 transients was acquired. Chemical shifts were relative to the signal of the phospholane hydrolysis product at 152.0 ppm. The integral value of the internal standard was used for the calculations of the absolute amount of each functional group.

3.3.3 Thermal property (Paper IV)

Thermogravimetry (TG) and differential thermogravimetry (DTG) analyses were conducted through a thermal gravimetric analyzer (TGA Q50, TA instruments, USA). The test samples of 4-6 mg, which were vacuum dried at 40 °C for 48 h before measurement, were heated in an aluminum crucible from ambient temperature up to 1000 °C at a heating rate of 10 °C/min, while using a constant nitrogen flow as an inert atmosphere during the experiment.

3.3.4 Morphological property

*Transmission-electron-microscopy (TEM) (**Paper IV & V**)*

The TEM images were obtained using a JEM-1400 Plus TEM microscope (JEOL Ltd., Japan) with an accelerating voltage of 80 kV. The samples were dispersed by placing them in a sonicator for 5 min. 5 μL of dilute sample suspension (0.1 mg/mL) was dropped onto a carbon supported copper grid, and then the sample was stained with 5 μL uranyl acetate solution (1 wt%) for 40 s. Afterwards, the excess liquid was carefully absorbed using filter paper, and the remaining solution formed an even layer on grid. The samples were completely air dried prior to the measurements.

*Scanning electron microscopy (SEM) (**Paper IV & V**)*

The SEM images were obtained using a LEO Gemini 1530 instrument with a Thermo Scientific UltraDry Silicon Drift Detector (SDD) (LEO, Oberkochen, Germany). For the measurement of composite film, the cross-sections were prepared by cryo-fracturing of the films after dipping in liquid N_2. The nonconductive samples were sputter-coated with carbon before imaging.

3.3.5 Particle size and zeta-potential (Paper IV & V)

The particle size distribution and zeta-potential of the obtained nanoparticles were analyzed by a Zetasizer Nano ZS instrument (Malvern Instruments Ltd., UK). All the samples suspensions with a concentration of 0.1 wt % were dispersed by ultrasonic bath (VMR, 80 W) for 30 min prior to the measurements. All the measurements were conducted in triplicates and runs of 10 and 13 were performed. The average data was reported after the analyses.

3.3.6 Mechanical property (Paper IV)

Mechanical properties of the nanocomposite films were studied determining their tensile strength, elongation at break, and Young's modulus. Each film was cut into a rectangular shape measuring 5 × 30 mm. The test were performed using an Instron universal testing machine [Instron-33R4465, (Instron Corp., High Wycombe, England)] equipped with a static load cell of 100 N and a 20 mm gauge length at a constant strain rate of 5 mm/min. The mechanical testing was conducted at 23 °C and 50% RH in a climate room. The prerun was first conducted at a rate of 2 mm/min until 0.1 N load was reached before the main run at 5 mm/min, in order to eliminate the error, which is caused by loosely attached samples. The thickness and width of the specimen were determined through a micrometer (Lorentzen & Wettre, Kista, Sweden, precision 1 μm) and a digital caliper (Mahr GmbH 16ER, Germany, precision 10 μm), respectively. Each sample was tested in at least ten specimen from three replicate films.

3.3.7 Antibacterial property (Paper IV)

The antibacterial activity of the prepared nanocomposites against Escherichia coli (*E. coli*) ATCC 11229 was studied. The specific procedures are as follows: First, 0.2 mL of bacterial culture (106 CFU/mL) of Gram negative bacterium *E. coli* was spread on the LB agar plates, and then round pieces of nanocomposite samples were plated on the surface. After 12 h of cultivation in the incubator at 37 °C, the nonleaching effect was evaluated by examining the inhibition zone (ring) around the film sample.

3.3.8 Adsorption measurements (Paper V)

The adsorption capacities of the synthesized lignin-based nanoparticles were evaluated by the adsorption of Pb^{2+} and Cu^{2+}. The Pb^{2+} and Cu^{2+} aqueous solutions with a desired concentration (50 mg/L for pH and contact time influence, while 10-150 mg/L with an increment of 10 mg/L for isotherms study) were prepared by dissolving a certain amount of $Pb(NO_3)_2$ and $CuSO_4 \cdot 5H_2O$ in deionized water, respectively. Generally, the experiments were carried out in a batch model described as follows: 20 mg of freeze-dried adsorbent was added into 40 mL metal ion solution and continuously stirred at 180 rpm. The initial solution pH values ranging from 2.0 to 6.0 were adjusted by adding 2.0 mol/L of HNO_3 or 1.0 mol/L of NaOH aqueous solution and measured with a pH meter. For pH influence and isotherms study, the mixture was stirred for 12 h to reach

adsorption equilibrium. After quick filtration through a 0.22 mm membrane, metal ion concentrations of the filtrate were quantitatively determined using an atomic absorption spectrometer (AAS6300 Shimadzu). The adsorbed amount of metal ions was calculated according to the following Eq. (1),

$$q_t = (C_0 - Ct)V/m \quad (1)$$

where q_t is the adsorbed amount after time t; C_0 (mg/L) and C_t (mg/L) are initial concentration and concentration of the adsorbate after time t, respectively; V (L) is the volume of the solution, and m (g) is the weight of the adsorbent material used.

The adsorption isotherms were further investigated by Langmuir (eqn (2)), Freundlich (eqn (3)) and Sips (eqn (4)) adsorption models, which were given by the following equations: [188-190]

$$q_e = q_m K_L C_e/(1+K_L C_e) \quad (2)$$

$$q_e = K_F C_e^{1/n} \quad (3)$$

$$q_e = q_s K_s C_e^m/(1+K_s C_e^m) \quad (4)$$

where C_e (mg/L) and q_e (mg/g) are metal ion concentration and adsorption capacity at equilibrium, respectively. q_m represents the maximum adsorption capacities of metal ions (mg/g). K_L is the Langmuir adsorption constant. K_F is the Freundlich constant indicating the adsorption capacity, n is the heterogeneity factor representing the adsorption intensity. In the Sips model, q_s is the specific adsorption capacity at saturation, mg/g, K_S is Sips isotherm constant, mL/mg, and m is the heterogeneity factor.

4. Results and discussion

4.1 Overview of the thesis work

The thesis work aimed at comprehensively fractionating lignocellulosic biomass, especially bamboo, into its main components including cellulose, hemicelluloses, and lignin by using a green fractionation procedure, and developing subsequent value-added applications for the obtained fractions. As shown in **Figure 4.1**, formic acid fractionation under pressure presented rapid and selective separation of bamboo, which can be combined with autohydrolysis pretreatment to recover hemicellulosic sugars *(Paper I, III)*. Furthermore, the chemical composition and structural characterization of the various fractions were thoroughly investigated, especially for lignin, thus promoting the subsequent valorization of the obtained fractions (*Paper II*). Multi-functional nanocomposites based on lignin-NPs and CNCs from fractionated streams were developed (*Paper IV*), and modified lignin-based hybrid magnetic nanoparticles presented excellent performance for the adsorption of heavy metal ions (*Paper V*). We envision this work could open the door for building an integrated biorefinery platform based on formic acid fractionation.

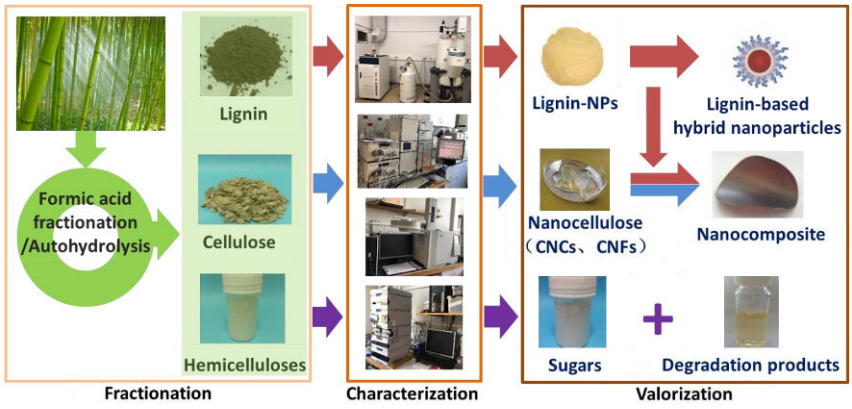

Figure 4.1. *Overview of the thesis work.*

4.2 Fractionation of bamboo

To profitably use the three dominant components of biomass, including cellulose, hemicelluloses, and lignin, lignocellulosic biomass must be fractionated effectively. A fractionation process should result in the selective separation of the lignocellulosic biomass and allow an easy and high-yield recovery of various fractions. [25] As a promising organosolv fractionation process, formic acid fractionation has attracted an increasing interest. [6] However, most of the fractionation procedures using formic acid are performed at atmospheric pressure, and therefore the relative mild conditions at a low temperature could hinder the improvement of delignification efficiency, which

significantly limits its industrialization. [33] Currently, formic acid fractionation under a higher pressure achieved through a higher temperature has presented excellent performance in efficiently separating lignocellulosic biomass. In order to promote the development of one-step formic acid fractionation under high pressure on an industrial scale, first and foremost, the effect of operational variables on the properties of obtained fractions should be assessed for the process optimization.

4.2.1 One-step fractionation of the main components of bamboo using formic acid (Paper I)

Table 4.1. *Effects of operational variables on the delignification of bamboo and the properties of cellulose pulp. (Paper I)*

No.	T_{max}/pressure (°C/MPa)	Holding time (min)	Yield (%)	Kappa number	Intrinsic viscosity (mL/g)
1	130/0.10	30	46.7	53.9	1080.2
2	130/0.10	45	45.5	46.4	1046.0
3	130/0.10	60	44.4	42.4	985.0
4	135/0.15	30	45.6	45.6	1078.1
5	135/0.15	45	44.2	41.1	1010.1
6	135/0.15	60	43.2	39.1	998.5
7	140/0.20	30	44.6	39.8	1133.9
8	140/0.20	45	43.7	36.7	1057.9
9	140/0.20	60	42.7	33.7	987.7
10	145/0.30	30	42.6	30.4	1002.1
11	145/0.30	45	42.2	28.5	979.3
12	145/0.30	60	40.5	29.4	899.1

Table 4.1 summarizes the effect of operational variables in formic acid fractionation of bamboo, including reaction time and temperature, on the Kappa number, yield, and intrinsic viscosity of the cellulose pulp. A higher temperature and a longer process time led to a lower Kappa number. The Kappa number decreased significantly with an increase of the T_{max} from 130 °C to 145 °C, indicating that a higher temperature contributes predominantly to accelerating the delignification. A longer reaction time was required for sufficient delignification in formic acid fractionation at a lower reaction temperature. Previous research proved that lignin was degraded by the cleavage of α-ether and β-ether bonds during organic acid delignification. [191] Higher temperatures and longer holding times could contribute to the cleavage of the

aryl ether bonds and facilitate the lignin degradation. [35] However, it was found that the organosolv fractionation under harsh conditions for a long reaction time may not be beneficial to the lignin depolymerization due to the condensation and re-precipitation of the dissolved lignin fragments onto the fibers. [192] This hypothesis is verified by the results shown in **Table 4.1**. The Kappa number of the obtained pulp increased slightly with the increasing of the holding time at 145 °C, but this accelerated the degradation of carbohydrates and resulted in a significant decrease in cellulose yield. This is in consistent with the report by Vázquez *et al.* [191] Dapía *et al.* also reported that the major delignification stage for beech chips occurred in the first 30 min of the formic acid treatment. [35] The intrinsic viscosity of the cellulose pulp gradually decreased with an increase in the holding time. As expected, formic acid fractionation at high T_{max} led to satisfactory intrinsic viscosities of 899.1-1133.9 mL/g. Therefore, it can be concluded that the optimal conditions for formic acid delignification of bamboo chips are T_{max} of 145 °C and holding time of 45 min, as at these conditions a low Kappa number, a satisfactory viscosity and a high pulp yield could be achieved.

Under the optimized conditions, the yield and chemical compositions of the fractions were studied. As described in **Figure 4.2**, 43.3 g of cellulose pulp was produced from 100.0 g of bamboo chips and approximately 48% of the mass fraction was dissolved into the process liquid. Only approximately 8% of the biomass was lost during the process. The yield of the purified pulp decreased from 43.3 g to 42.2 g after the cellulose pulp was screened with an 8-cut plate screen, and 2.5% of the screening reject, which primarily consisted of coarse fiber bundles, was obtained. This result proved that the raw materials could be sufficiently disintegrated during formic acid fractionation process under the optimized conditions. It was found that only 0.49% HMF (w/w on bamboo), 0.62% oligo-glucose, and 1.93% glucose were found in the spent liquor, demonstrating that the cellulose fraction in the bamboo remains intact to a large extent during formic acid fractionation under a high pressure.

Moreover, 31.5 g of lignin could be recovered from the spent liquor, while the raw material only contains 27.43% of original lignin. The increase of the lignin content may be partially attributed to the condensation of lignin with the degradation products of carbohydrates (*e.g.*, furfural), proteins, and extractives. [19, 193] The decreased amount of the identified hemicellulose derivatives in the spent liquor further indicated that the derivatives of hemicelluloses, such as furfural, have reacted with lignin at high temperature. A previous study also reported similar results. [194]

As shown in **Figure 4.2**, about 8.5 g of total sugars (monosaccharides and oligosaccharides) could be produced, indicating that approximately 22% of the hemicelluloses in the bamboo was dissolved in the form of sugars during the fractionation process. Mass fractions of 3.56% furfural and 3.80% acetic acid were generated by the degradation of hemicelluloses. These results indicate that the formic acid fractionation under the harsh conditions resulted in severe degradation reactions of the dissolved hemicellulosic sugars. Most sugars were

degraded into other chemical compounds, such as furfural and acetic acid, which also could be commercialized as value-added products. Monosaccharides predominated in the carbohydrate part, and only approximately 12% of the total carbohydrates were present in oligomeric form. The main constituents of the monosaccharides were xylose (59.5%) and glucose (25.7%), but other sugars, such as arabinose (7.4%), galactose (5.0%), and mannose (2.4%), were also present.

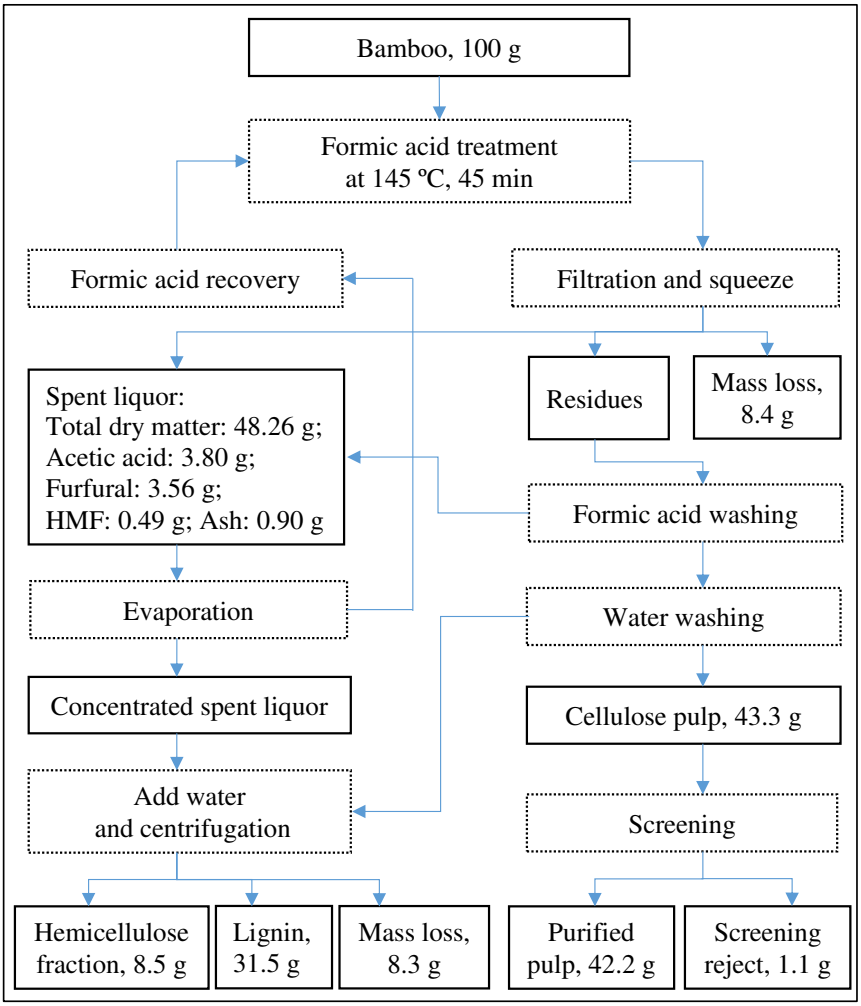

Figure 4.2. *Simplified flowchart and overall mass balance of the organosolv fractionation process based on formic acid. (Paper I)*

4.2.2 Integrated fractionation by combining autohydrolysis and formic acid hydrolysis (Paper III)

One-step formic acid fractionation was proven to be an efficient and rapid process to separate bamboo into its individual major fractions. However, under

the harsh conditions, most of the hemicelluloses were severely degraded into monosaccharides and other low molar mass compounds, such as acetic acid, furfural, and HMF, which are difficult to be effectively separated and recovered.

In order to promote the high value-added applications of hemicelluloses, the combined fractionation approach based on the autohydrolysis and formic acid rapid-delignification was developed, and the scheme of the whole process is shown in **Figure 4.3**. As it can be seen, 36.8 g cellulose fibers, 25.9 g lignin, and 7.0 g hemicellulosic sugars were produced from 100.0 g dried bamboo chips through the combined fractionation process, indicating that the combined process exhibited an effective fractionation approach. Importantly, approximately 89.6% of the extracted hemicellulosic sugars through the autohydrolysis process were present in an oligomeric form, and 85.8% of oligosaccharides were oligo-xylose.

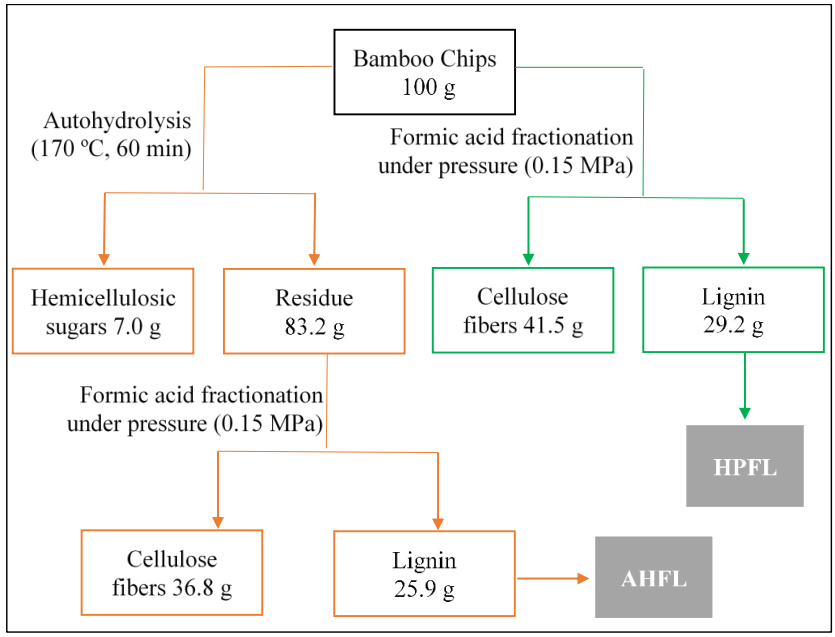

Figure 4.3. *Scheme of the combined fractionation process based on the autohydrolysis and formic acid rapid-delignification (HPFL: high-pressure formic acid lignin; AHFL: high-pressure formic acid lignin from autohydrolyzed residue). (Paper III)*

4.3 Structural characterization of lignins obtained by formic acid fractionation (Paper II & III)

Formic acid fractionation under pressure, in both the one-step process and the integrated procedure combining the autohydrolysis and formic acid rapid-delignification, has been proven highly efficient and selective in separating bamboo into its main components. In order to verify the superiority of this procedure as compared to conventional fractionation using formic acid at atmosphere pressure, the delignification mechanism at different pressure levels

was thoroughly revealed. Therefore, the detailed structural characterization of the obtained formic acid lignins at a higher pressure (high-pressure formic acid lignin, HPFL) and at atmosphere pressure (atmospheric formic acid lignin, AFL), as well as the high-pressure formic acid lignin from autohydrolyzed residue after the integrated process (AHFL), were investigated by chromatographic and spectroscopic techniques, including FTIR, GPC, and NMR (^{1}H-, ^{13}C-, ^{31}P-NMR and 2D-HSQC). As contrast, lignin from bamboo in native form (MWL), which can be regarded as the representative of native lignin in the raw materials due to the relatively mild process, was prepared and subsequently analyzed. Furthermore, following the integral biorefinery concept, more in-depth knowledge on the characteristics of the obtained formic acid lignin could provide important information for its further application potential.

4.3.1 FTIR spectra

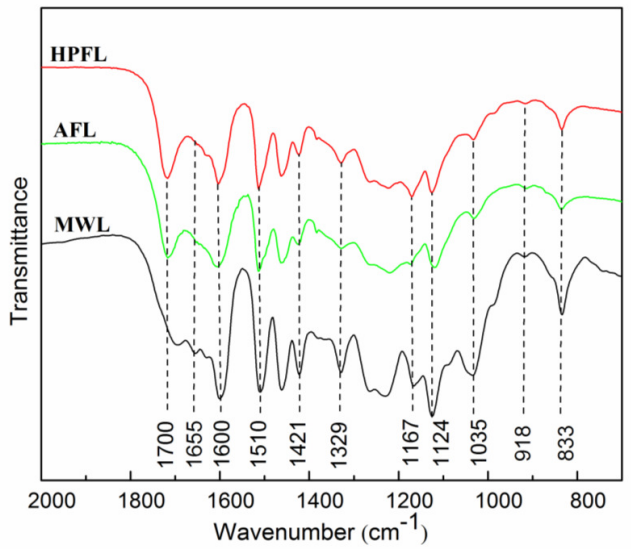

Figure 4.4. *FTIR spectra of bamboo formic acid lignins (AFL, HPFL) compared to MWL (MWL: milled wood lignin; AFL: atmospheric formic acid lignin; HPFL: high-pressure formic acid lignin). Image was adapted from Paper II with Copyright (2017) ELSEVIER.*

FTIR spectra of MWL, AFL, and HPFL are presented in **Figure 4.4**. The assignments of the characteristic bands of lignin skeleton and functions were identified according to literature. [6, 180] As can be seen, the FTIR spectra present different bands of aromatic ring vibrations at 1600, 1510, and 1421 cm^{-1}, which are typical lignin patterns. The band at 1167 cm^{-1}, which is assigned to C=O in conjugated structure, presents a typical signal of lignin. The signal at 833 cm^{-1} corresponds C-H out of plane in positions of 2 and 6 of S and in all position of *p*-hydroxyphenyl (H) units. Moreover, the signals at 1035 and 918 cm^{-1} are assigned to guaiacyl (G) units, and at 1329 and 1124 cm^{-1} correspond to syringyl (S) units. The bands and their relative intensities of the fingerprint region in the three lignin samples were rather similar (**Figure 4.4**), indicating

that the formic acid delignification process did not lead to significantly different modification for the chemical structures of lignin. Similar results have been reported in a previous study of organosolv lignin extracted using ethanol from *Miscanthus* × *gigant*. [195] However, formic acid lignin samples (AFL and HPFL) presented strong signals at 1700 cm^{-1} corresponding to the formate ester, which is attributed to the esterification of part of the alcohol and phenol functional groups of lignin by the formic acid in the delignification process.

4.3.2 ^{1}H NMR spectra

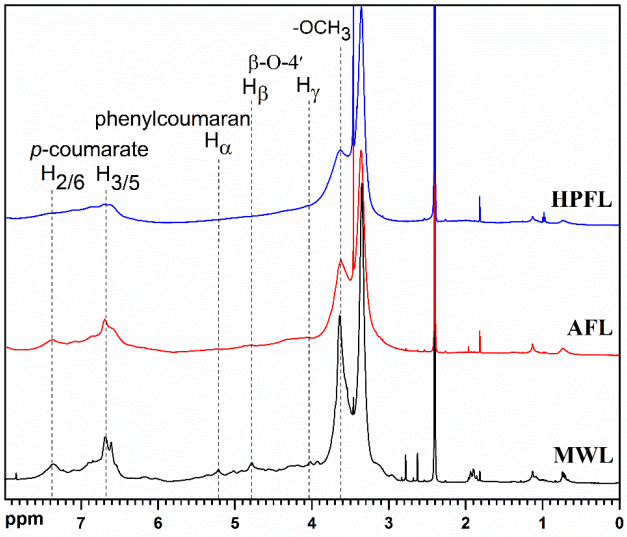

Figure 4.5. *^{1}H NMR spectra of bamboo formic acid lignins (AFL, HPFL) and MWL (MWL: milled wood lignin; AFL: atmospheric formic acid lignin; HPFL: high-pressure formic acid lignin). Image was adapted from Paper II with Copyright (2017) ELSEVIER.*

The ^{1}H NMR spectra of lignin samples were used to understand the structural characteristics of lignin. ^{1}H NMR spectra of MWL, AFL, and HPFL exhibit the classic patterns of lignin (**Figure 4.5**). The signals between 6.00 and 8.00 ppm originated from the aromatic protons in syringyl (S), guaiacyl (G), and *p*-hydroxyphenyl (H) units, p-coumarate and ferulate. [196] A comparison of the spectra of MWL and formic acid lignin allows the evaluation of the effect of the formic acid fractionation on lignin structure. It is noteworthy that a weak peak at 5.32 ppm corresponding to phenyl coumaran structures was observed in the MWL spectrum, while this peak was no longer detected in the formic acid lignin spectra, indicating that this structure might be destroyed during formic acid fractionation. Moreover, the signal at 4.85 ppm corresponding to H_{β} of the β-O-4 structure could only be found in the spectra of MWL, suggesting the cleavages of beta-aryl ether bonds during formic acid fractionation. All lignin samples exhibit a sharp signal at 3.7 ppm corresponding to methoxyl protons ($-OCH_3$). This signal in the ^{1}H spectrum of formic acid lignins was significantly lower

than that of MWL, and that of HPFL was lower than AFL. This means that more severe demethoxylation reactions occurred during formic acid fractionation, especially under harsh reaction conditions. In addition, the signals in ^{1}H spectrum of AFL and HPFL did not show a distinct difference.

4.3.3 ^{13}C NMR spectra

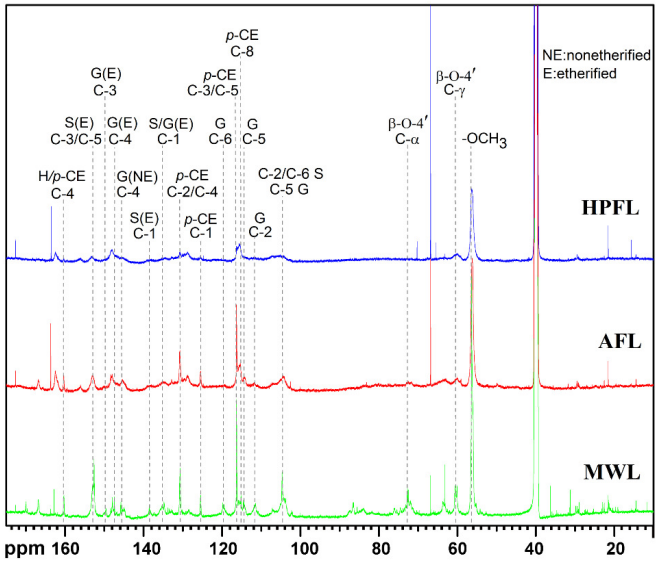

Figure 4.6. *^{13}C NMR spectra of bamboo formic acid lignins (AFL, HPFL) and MWL (MWL: milled wood lignin; AFL: atmospheric formic acid lignin; HPFL: high-pressure formic acid lignin). Image was adapted from Paper II with Copyright (2017) ELSEVIER.*

To further investigate the structural characterization of formic acid lignin, formic acid lignins and MWL were analyzed with ^{13}C NMR spectroscopy, as presented in **Figure 4.6**. In the aromatic region, ^{13}C NMR spectra exhibited several moderately strong signals originated from syringyl units, guaiacyl units and *p*-hydroxyphenyl units. It can be found that the intensities of signals for syringyl units were higher than those of the guaiacyl units, implying that the obtained lignin contains a higher proportion of syringyl moieties. In addition, the signals originated from *p*-CE (*p-coumarates*) were also identified. As compared to MWL, the signals in the regions of 173–168 ppm corresponding to aliphatic -COOR and 168-166 ppm to conjugated C=O in -COOR from coumaric and ferulic acids disappeared in HPFL, indicating that the -COOR structures have been hydrolyzed in the formic acid fractionation under the severe acidic conditions. In the region of aliphatic carbons, the signals in the ^{13}C NMR spectra of both AFL and HPFL at 72.7 and 60.3 ppm attributed to side chain carbons C-α and C-γ in β-O-4' linkages are rather weak compared to MWL, further confirming the cleavage of beta-aryl ether bonds during formic acid fractionation. Additionally, the intensity of the signal of HPFL at 56.2 ppm

attributed to methoxy carbons showed a significant decrease as compared to MWL, further indicating that the formic acid lignins occurred extensive demethoxylation under severe acidic conditions.

4.3.4 2D-HSQC NMR spectra of the lignin samples

Table 4.2. *Quantification of the lignin samples (MWL, AFL, HPFL and AHFL) isolated from bamboo by quantitative 2D-HSQC NMR (MWL: milled wood lignin; AFL: atmospheric formic acid lignin; HPFL: high-pressure formic acid lignin; AHFL: high-pressure formic acid lignin from autohydrolyzed residue). (Paper II & III)*

	MWL	AFL	HPFL	AHFL
β-Aryl-ether units (β-O-4, A)[a]	54.0	17.4	ND[b]	ND[b]
Resinol substructures (β-β, B)[a]	6.4	2.4	ND	ND
Phenylcoumaran (β-5, C)[a]	3.3	0.4	ND	ND
Spirodienone (β-1, D)[a]	2.0	ND	ND	ND

[a] Results expressed per 100 Ar based on quantitative 2D-HSQC spectra.
[b] ND, not detected

The HSQC spectra of MWL, AFL, HPFL, and AHFL are presented in **Figure 4.7,** and the corresponding substructures are depicted in **Figure 4.8**. [197, 198] As shown in the **Figure 4.7**, the HSQC spectrum of MWL exhibits strong and relatively complete signals as compared to AFL, HPFL and AHFL. In the side-chain region, it can be found that the main substructures in MWL of bamboo are the β-O-4 alkyl-aryl ether linkages, including β-O-4 substructures (A), γ-acylated β-O-4 alkyl-aryl ether linkages (A′) and oxidized (C_α=O) β-O-4 substructures (A″). Other signals attributed to resinol (β-β, B) and the phenyl coumaran substructures (β-5′, C) were also observed. However, the HSQC spectrum of these lignin samples exhibit different signal intensities. As shown in **Table 4.2**, as compared to MWL, a lower signal intensity corresponding to β-O-4 linkage was found in the HSQC spectrum of formic acid lignin samples, and this signal in the spectra of HPFL and AHFL was not detected. It can be concluded that the cleavage of β-O-4 linkages in lignin structure was the major mechanism of lignin degradation during formic acid delignification under pressure, which is in agreement with the results as reported earlier. [195, 198] The reaction scheme of the cleavages of β-O-4 linkages is shown in **Figure 4.9**, the reaction led to the formation of the structures of the Hibbert ketone type together with a new phenolic compound. Moreover, as compared to AFL, the spectra of HPFL and AHFL was observed that the resinol substructures (β-β, B), the phenylcoumaran substructures (β-5′, C) and spirodienone substructures (β-1, D) in the side chains occurred modification. This result further proved a more effective delignification in the formic acid fractionation under high pressure level. In addition, as compared to MWL and AFL, the disappearance of signals for carbohydrates in HPFL and AHFL indicates a relatively high purity of HPFL.

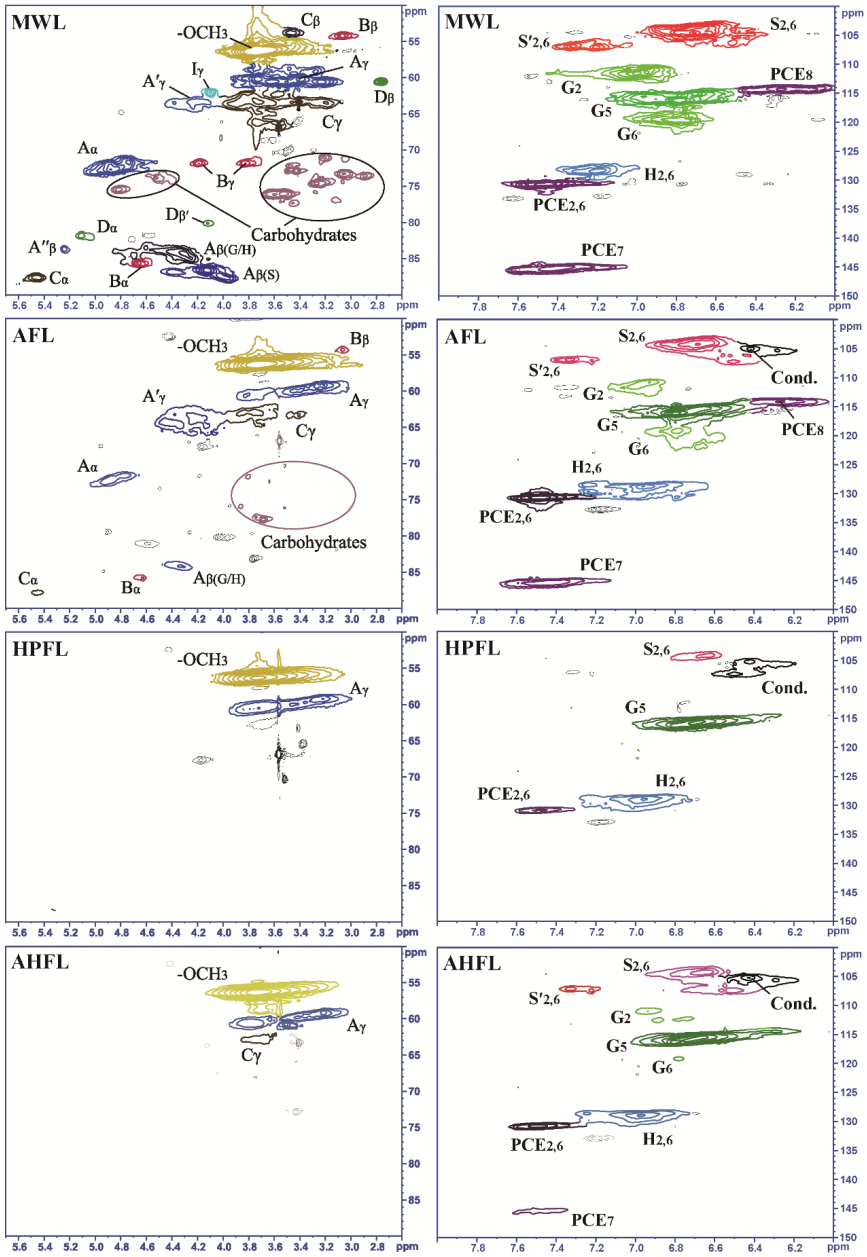

Figure 4.7. *Side-chain regions (left column) and aromatic regions (right column) in the HSQC spectra of bamboo MWL and AFL and HPFL (MWL: milled wood lignin; AFL: atmospheric formic acid lignin; HPFL: high-pressure formic acid lignin; AHFL: high-pressure formic acid lignin from autohydrolyzed residue). (Paper II & III)*

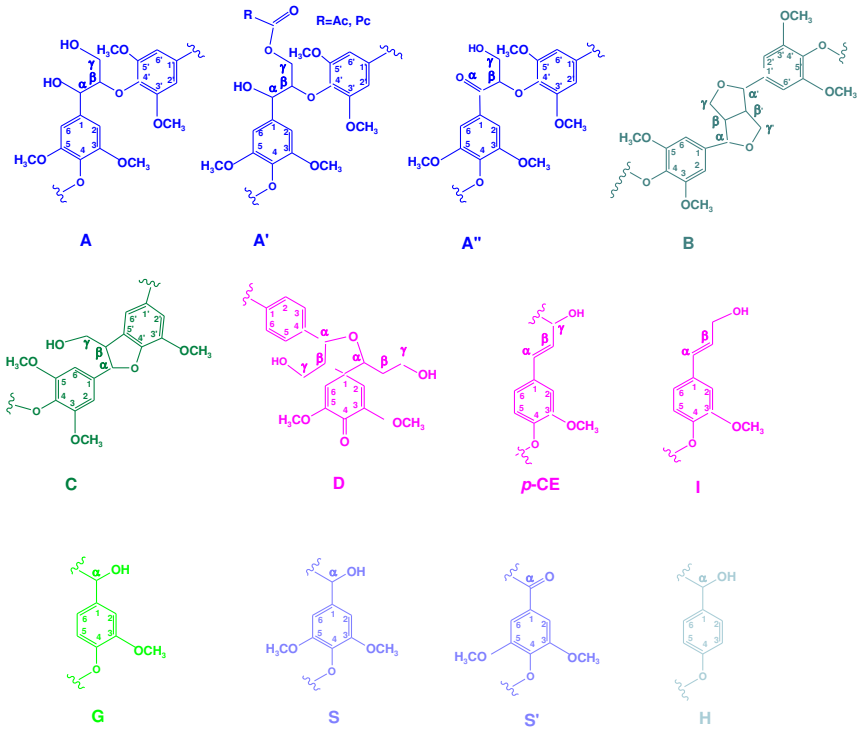

Figure 4.8. *Main substructures of bamboo lignin samples involving different side-chain linkages and aromatic units identified by HSQC. (**A**) β-O-4 aryl ether linkages with a free -OH at the γ-carbon; (**A'**) β-O-4 aryl ether linkages with acylated γ-OH with p-coumaric acid; (**A''**) C_α-oxidized β-O-4 substructures; (**B**) resinol substructures formed by β-β, α-O-γ, and γ-O-α linkages; (**C**) phenylcoumarane substructures formed by β-5 and α-O-4 linkages; (**D**) spirodienone substructures formed by β-1 and α-O-α linkages; (**p-CE**) p-coumarates; (**I**) p-hydroxycinnamyl alcohol end groups; (**G**) guaiacyl units; (**S**) syringyl units; (**S'**) oxidized syringyl units with a C_α ketone; (**H**) p-hydroxyphenyl units. (Paper II & III)*

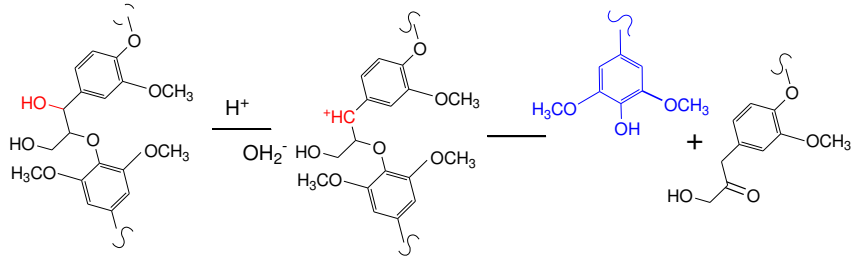

Figure 4.9. *Reaction scheme showing the depolymerization of lignin model compounds by the cleavages of β-O-4 linkages in formic acid.*

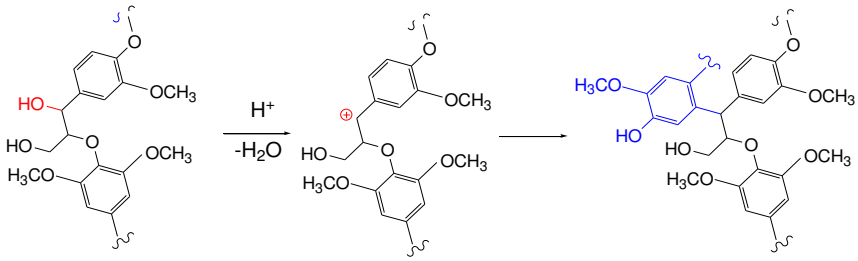

Figure 4.10. *Reaction scheme showing the condensation of lignin model compounds in formic acid.*

In the aromatic region, H, G, and S units could be easily identified by their strong typical signals (**Figure 4.7**). Several relatively intense signals attributed to *p*-coumarate (*p*-CE) were found in both MWL, AFL and AHFL, while only signals corresponding to the *p*-$CE_{2,6}$ could be observed in HPFL. After formic acid fractionation, condensed structures were observed in the HSQC spectra of AFL, HPFL and AHFL, suggesting that the cleavage of β-O-4 linkages and condensation reaction occurred simultaneously in lignin structures during formic acid fractionation, which was also reported in recent publications. [17] Under acidic conditions, the acid-catalyzed condensation between the aromatic C_6 or C_5 and a carbonium ion could be the predominant reaction pathway during formic acid fractionation under high pressure, as shown in **Figure 4.10**. On the other hand, the formed phenolic compounds from the cleavage of β-O-4 linkages were further reacted with the carbonium ions at C_α of the side chain, and formed the new stable carbon-carbon linkage between two lignin units. [199, 200] Both the depolymerization and condensation have a common intermediate, a carbonium ion (**Figure 4.9** and **Figure 4.10**), and therefore they occur more or less simultaneously. The condensation of the lignin structure not only leads to a negative influence on the delignification of raw materials, but also dramatically affects its subsequent upgrading, such as catalytic depolymerization.

According to the quantitative analysis the lignin samples through in HSQC spectra, the schematic representations of the bamboo milled wood lignin structures, which show the common linkages, are depicted in **Figures 4.11**. The structure is merely pictorial and does not imply a particular sequence. Since most of the linkages in side chain of the HPFL were broken during the formic acid fractionation under high pressure, the condensed lignin linkages could not be fully accessed by current analytical methods.

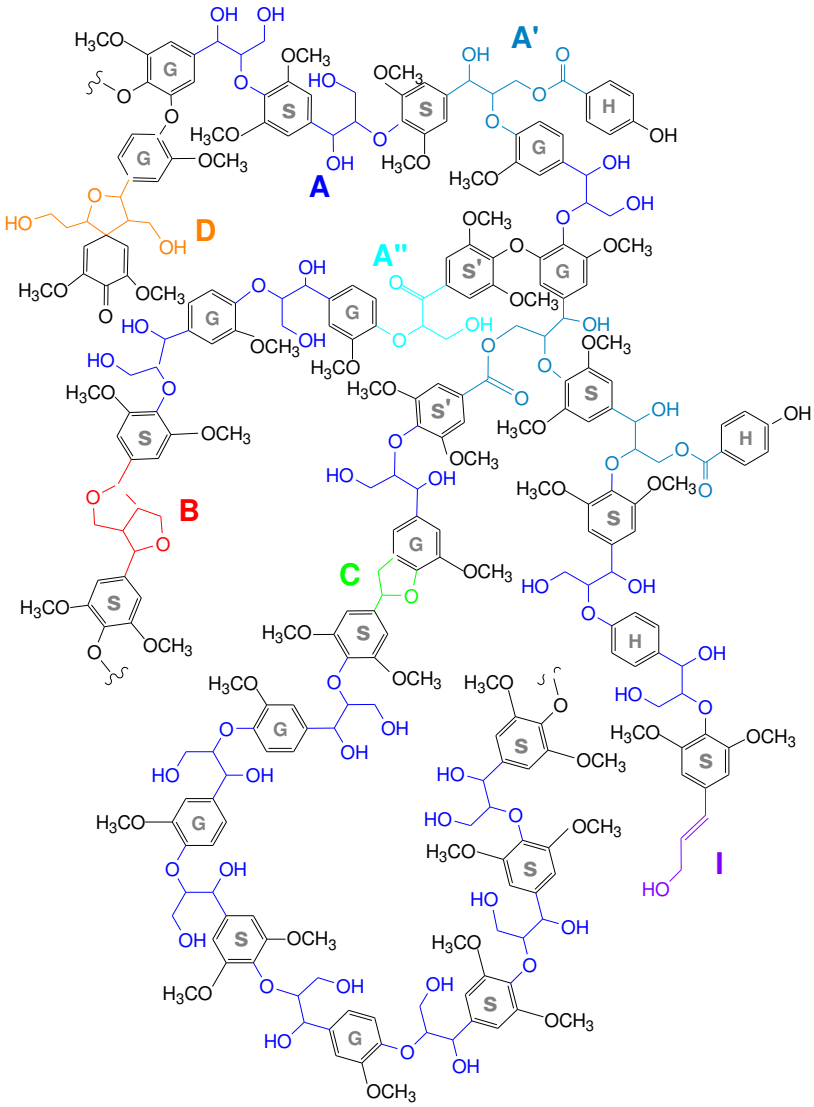

Figure 4.11. *Representation of the lignin polymer from bamboo milled wood lignin, as predicted from NMR-based lignin analysis.*

4.3.5 ^{31}P NMR spectra of the lignin samples

^{31}P NMR analysis results of lignin samples are summarized in **Table 4.3**. As it can be seen, all the four lignin samples contained S/G/H structures with various proportions of S/G/H phenol structures. In general, formic acid fractionation led to the decrease of the content of aliphatic hydroxyl groups and the increase of the content of phenolic and carboxylic groups. The observed trends are in agreement with the *B. davidii* organosolv lignin reported by Hallac *et al.* [201] The decrease of aliphatic hydroxyl groups suggested that modification occurred on the aliphatic -OH groups during formic acid fractionation, such as the *in vitro* acetylation and the acid-catalyzed elimination reactions, while the high content

of the phenolic hydroxyl could be explained by the cleavage of β-O-4 linkages. [195, 198] As compared to AFL, the content of phenolic hydroxyl groups in HPFL (3.51 mmol/g) and AHFL (3.62 mmol/g) was significantly higher than that of AFL (2.95 mmol/g), suggesting formic acid fractionation under a high pressure exhibited a significant impact of the delignification. Obviously, the condensed phenolic hydroxyl groups content in HPFL was 1.02 mmol/g which was significantly higher than that of AHFL (0.63 mmol/g), suggesting that the autohydrolysis pretreatment was contributed to reduce the condensation of lignin structure during the subsequent formic acid hydrolysis. In addition, the content of *p*-hydroxyphenyl -OH in the formic acid lignins increased, suggesting that formic acid fractionation also resulted in the demethoxylation reactions.

Table 4.3. *Quantification of the lignin samples (MWL, AFL, HPFL and AHFL) isolated from bamboo by quantitative ^{31}P NMR method (mmol/g) (MWL: milled wood lignin; AFL: atmospheric formic acid lignin; HPFL: high-pressure formic acid lignin; AHFL: high-pressure formic acid lignin from autohydrolyzed residue). (Paper II & III)*

Lignin samples	Aliphatic OH	Phenolic OH					Carboxylic acid
		Syringyl		Guaiacyl		*p*-Hydroxyl	
		C[a]	NC[b]	C	NC		
MWL	4.52	0.05	0.23	0.14	0.48	0.74	0.24
AFL	1.50	0.30	0.59	0.44	0.59	1.03	0.29
HPFL	0.77	0.31	0.85	0.71	0.75	0.89	0.42
AHFL	1.45	0.26	1.15	0.37	0.81	1.03	0.34

[a] C, condensed.
[b] NC, non-condensed

4.3.6 Molar mass

Table 4.4. *Weight-average (M_w) and number-average (M_n) molar masses and dispersity (M_w/M_n) of lignin samples (MWL: milled wood lignin; AFL: atmospheric formic acid lignin; HPFL: high-pressure formic acid lignin; AHFL: high-pressure formic acid lignin from autohydrolyzed residue). (Paper II & III)*

Sample	MWL	AFL	HPFL	AHFL
M_w(g/mol)	9420	8075	10571	9404
M_n(g/mol)	7458	5026	5958	5137
M_w/M_n	1.263	1.607	1.774	1.527

The molar mass values and the dispersity of the four lignin samples are summarized in **Table 4.4**. As compared to MWL, both the weight-average molar mass (M_w) and the number-average molar mass (M_n) of AFL were lower due to the depolymerization reaction of lignin. However, for HPFL and AHFL, a higher M_w and a lower M_n were obtained in comparison to MWL and AFL. It was further confirmed that formic acid fractionation under high pressure caused condensation reactions of the lignin, which is in accordance with that of discussion in the NMR section. The molar mass of AHFL (9404 g/mol) is slightly lower than that of HPFL (10571 g/mol), indicating that the autohydrolysis process enhanced the depolymerization of lignin during the subsequent formic acid rapid-delignification process under pressure. Besides, the formic acid lignin samples had a fairly analogous dispersity, and were slightly higher than that of WML.

Overall, it can be summarized that formic acid fractionation under pressure, in both the one-step process and the integrated procedure combining the autohydrolysis and formic acid rapid-delignification, presents a quick and efficient delignification method by enhancing the cleavage of interunitary bonds in lignin, as compared to atmospheric formic acid fractionation. The condensation reaction also occurred simultaneously during the delignification process. High-pressure formic acid lignins, both HPFL and AHFL, showed higher purity, and had relatively higher contents of phenolic and carboxylic groups. From the perspective of industrialization, we selected HPFL to use as the raw material for the subsequent valorization of formic acid lignin.

4.4 Multifunctional nanocomposites of nanocellulose and lignin-NPs (Paper IV)

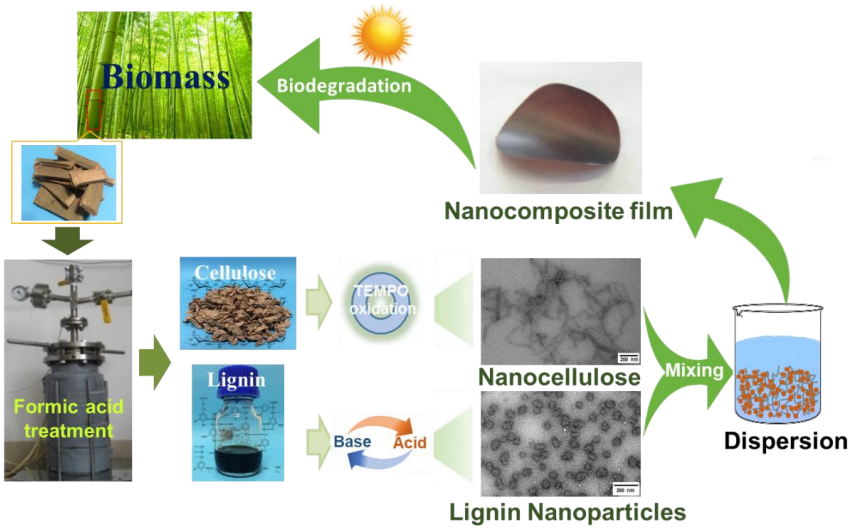

Figure 4.12. *A schematic process flow diagram illustrating the preparation of nanocellulose and lignin-NPs based on formic acid rapid-fractionation for producing multifunctional nanocomposite films. Image was adapted from Paper IV with Copyright (2019) American Chemical Society.*

Based on the aforementioned thorough analysis for the chemical compositions and structural features, the valorizations of the obtained fractions from formic acid fractionation under high pressure were further explored. Therefore, the fabrication of novel biodegradable lignin-NPs and nanocellulose, as well as nanocomposites from bamboo based on formic acid rapid-fractionation were conducted. As shown in **Figure 4.12**, the obtained lignin was directly applied for producing lignin-NPs and the produced cellulose pulp was subjected to a TEMPO-mediated oxidation process to prepare nanocellulose. Furthermore, a multifunctional nanocomposite was prepared through the dispersions of nanocellulose and lignin-NPs followed by filtration. From an industrial viewpoint, the direct preparation of all-bamboo-based nanocomposite film enables the full utilization of the fractioned streams, and is of great significance for the large-scale production of lignocellulosic nanocomposite.

4.4.1 Preparation and characterization of lignin-NPs

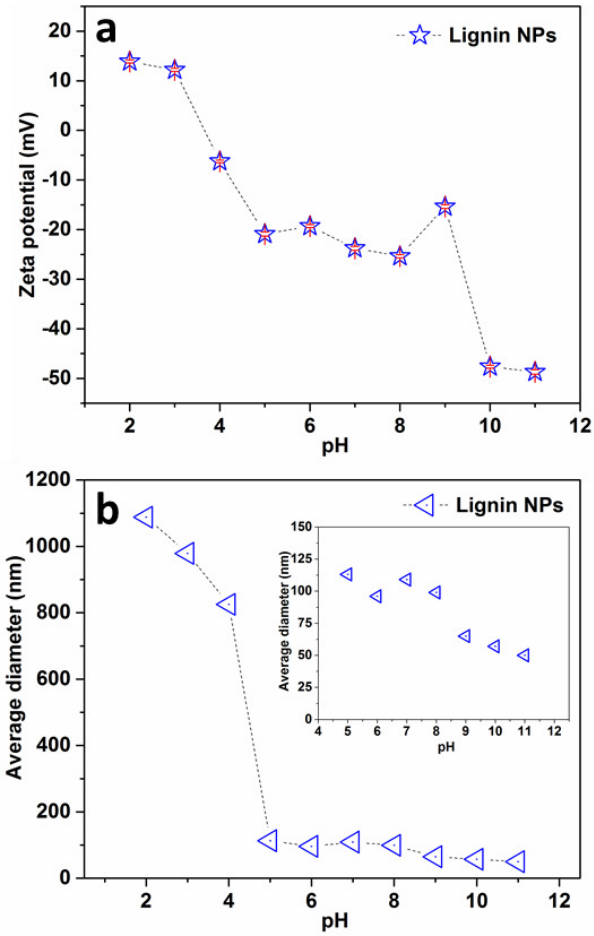

Figure 4.13. *Surface charge related properties of lignin-NPs: (a) zeta-potentials of the lignin-NPs as a function of pH. (b) Effect of pH on average hydrodynamic diameter of lignin-NPs. (Paper IV)*

As described in **Figure 4.13**, the lignin fractions were further used for preparing lignin-NPs based on a solubility change method by adjusting the pH value from basic to weakly acidic. The particle size, zeta-potential, and morphology of the obtained lignin-NPs were analyzed. The variation of the zeta-potentials and hydrodynamic diameter with an increase in pH is shown in **Figure 4.13a** and **Figure 4.13b**, respectively. The lignin-NPs dispersions exhibited a stable state in the pH range 5.0-8.0, with a diameter of about 100 nm and zeta-potentials of around -25 mV. At pH < 5.0, the magnitude of the electrical double layer repulsion decreased significantly due to the protonation of charged functional groups, resulting in the aggregation of lignin-NPs. When the pH > 9, the particle size decreased to about 50 nm, which can be attributed to the onset of the disassembly of the particle toward dissolution, and the complete dissolution occurred at pH > 12.0.

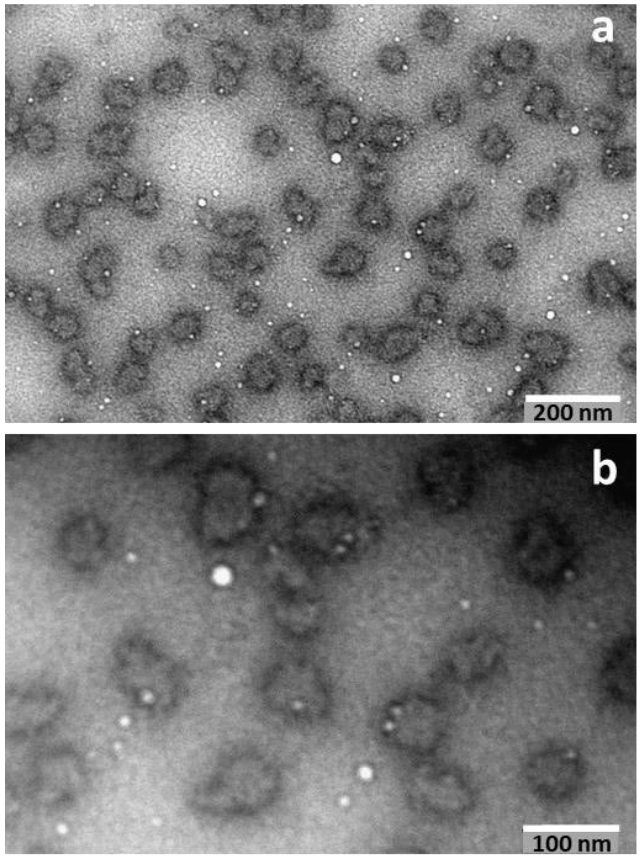

Figure 4.14. *TEM images of lignin-NPs with different magnifications. Image was adapted from Paper IV with Copyright (2019) American Chemical Society.*

Figure 4.14a and b show TEM micrographs of lignin-NPs. It is clear that uniform particles in the range of 60-80 nm, which exhibited clear boundaries and a spherical morphology, were formed under neutral conditions in water.

Meanwhile, the hydrodynamic diameter of the lignin-NPs measured by DLS analysis was larger than the particle size indicated in the TEM images, which was attributed to a hydration sphere formed around the lignin-NPs in water. Thus, the uniform particle size, spherical morphology, and high stability of the lignin-NPs indicated a promising candidate for producing lignin-NPs based nanomaterials.

4.4.2 Preparation and characterization of nanocellulose

Cellulose pulp obtained from formic acid rapid-fractionation of bamboo was subjected to a bleaching treatment prior to nanofibrillation. A commercial bleached Kraft pulp (KP) was selected as a reference. Both reference KP and bleached formic acid pulp (FP) were used to prepare nanocellulose through TEMPO-mediated oxidation at different reaction times (5 h or 24 h). The obtained products were coded as (KP-CNFs, 24 h), (FP-CNCs, 5 h), and (FP-CNCs, 24 h), depending on their original material and oxidation time. The obtained nanocelluloses were diluted and further characterized by TEM. As shown in **Figure 4.15a,** the sample of (KP-CNFs, 24 h) exhibited a spaghetti-like nanofibrous structure, consisting of CNFs with lengths below 1 µm and widths between 5-9 nm. Meanwhile, the nanocellulose samples of (FP-CNCs, 5 h) and (FP-CNCs, 24 h) showed a morphology more similar to individual rods rather than fibrils, as seen in the **Figure 4.15b** and **Figure 4,15c**, respectively. Both nanocelluloses of (FP-CNCs, 5 h) and (FP-CNCs, 24 h) presented a length range of 80-300 nm and widths of 5-9 nm, which are similar to the dimensions of CNCs commonly produced by sulfuric acid hydrolysis, [202] indicating that formic acid rapid-fractionation contributed to the subsequently nanofibrillation of the obtained cellulose fractions through TEMPO-mediated oxidation. The CNCs samples originated from FP were dispersed well in water due to their high surface charge density and no fiber bundles were observed. It also suggested that almost all individual particles were peeled off from original formic acid fiber bundles during a 5 h oxidation time.

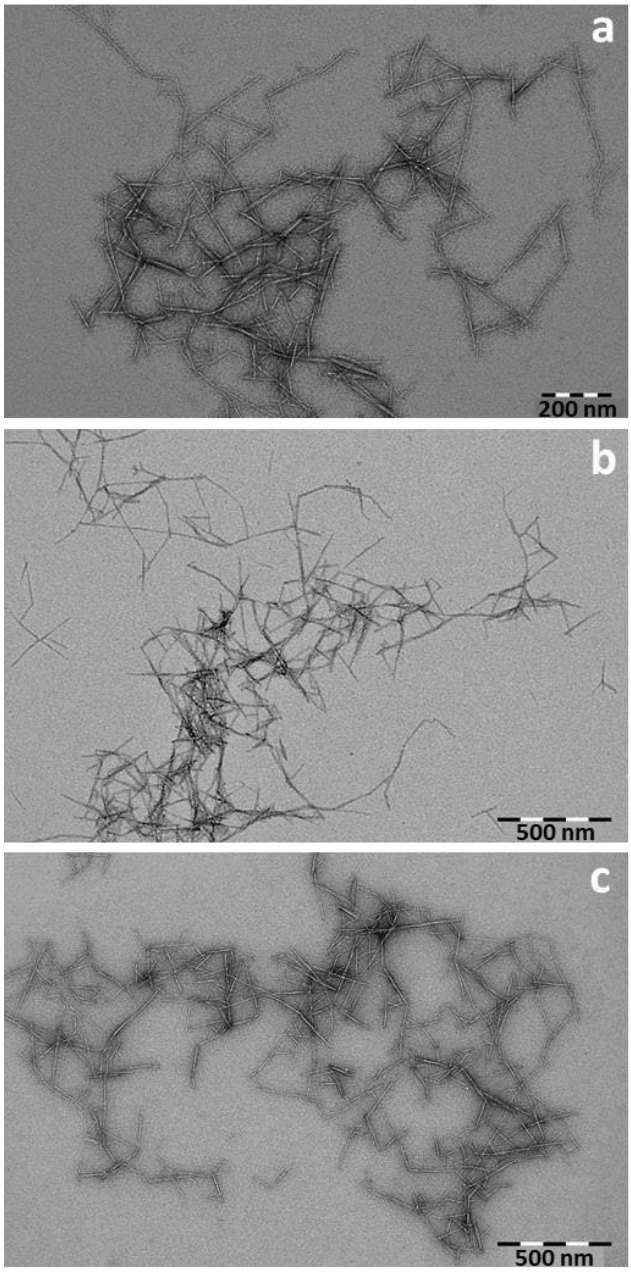

Figure 4.15. *TEM images of nanocellulose prepared from different types of fibers though TEMPO-mediated oxidation. (a) (KP-CNFs, 24 h); (b) (FP-CNCs, 5 h); (c) (FP-CNCs, 24 h). Image was adapted from Paper IV with Copyright (2019) American Chemical Society.*

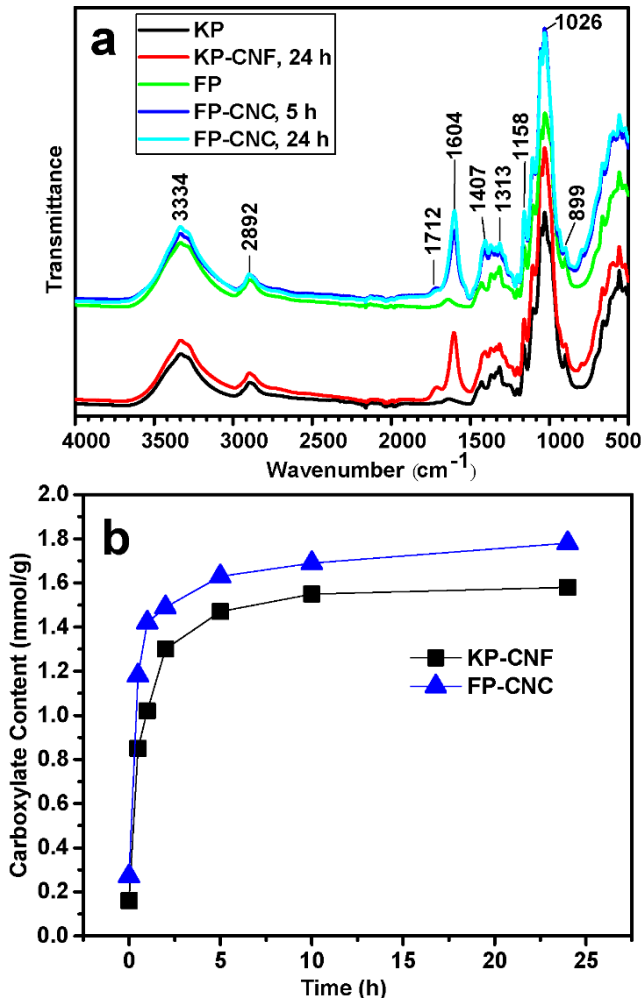

Figure 4.16. *(a) FTIR and (b) carboxylate contents of nanocelluloses compared with that of the original fiber. (Paper IV)*

Figure 4.16a shows the FTIR spectra of the obtained nanocellulose samples, and their original fibers. As it can be seen, a strong band at 1604 cm^{-1} corresponding to the antisymmetric stretching of $-COO^-$ in carboxylate salts appeared in the spectra of all three nanocelluloses, while this band was very weak in the spectra of their original fibers. This suggests that the carboxyl groups were introduced on the nanocellulose surface after TEMPO-mediated oxidation of KP and FP. The carboxylate content in the nanocellulose was quantified with respect to the reaction time in TEMPO-mediated oxidation. As displayed in **Figure 4.16b**, FP and KP original fibers contained 0.27 and 0.16 mmol/g of carboxyl group, respectively. The content of carboxyl groups in both KP and FP fibers exhibited a rapid rise within the initial reaction period of 5 h, followed by a slight increase up to 24 h and then leveled off. Furthermore, the carboxylate content of nanocellulose originated from FP could reach 1.63

mmol/g with a 5 h reaction time, while that of the KP-CNF reached to only 1.58 mmol/g after 24 h reaction time. The lower carboxylate content of KP-CNF is probably attributed to a higher hemicellulose content of the original fiber. [182] The high carboxylate content of nanocellulose is a crucial factor determining the dispersibility of the resultant nanocellulose in the suspension, [203] which is in good agreement with the TEM analysis.

4.4.3 Properties of nanocomposite films

Morphology of the nanocomposite films

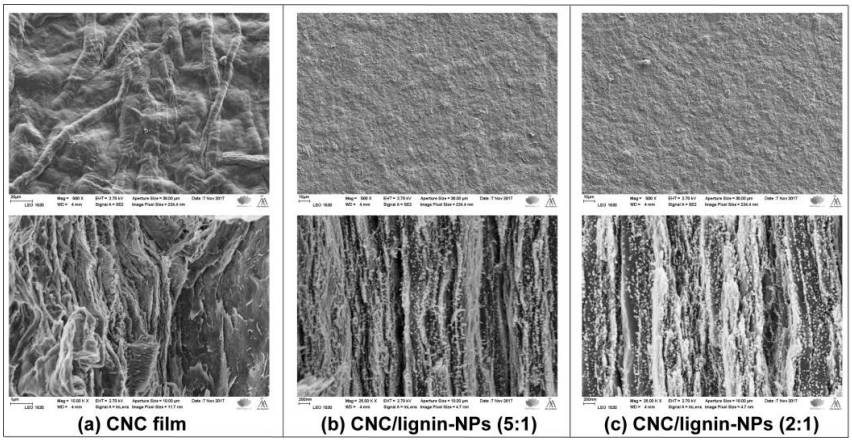

Figure 4.17. *SEM images of nanocomposite film: surface (top row) and cross section (bottom row). Image was adapted from Paper IV with Copyright (2019) American Chemical Society.*

Nanocomposite films were prepared from aqueous dispersions with various proportions of cellulose nanocrystals (FP-CNCs, 5 h) and lignin-NPs. The SEM images of the selected nanocomposite films are shown in **Figure 4.17**. The cross-sections of selected nanocomposite films exhibited a multilayer network surrounded by lignin-NPs, as compared to the pure CNC film. This architecture indirectly suggested the lignin-NPs were homogeneously dispersed in the CNCs matrix without any visible aggregation. The top-view SEM images of pure CNC film showed a rather rough topography, while that of composite film presented a very smooth and homogenous surface due to the interspaces in the CNCs network were filled by the lignin-NPs. It can be inferred that the homogenous dispersity of lignin-NPs in the CNCs network may be attributed to the strong interactions between CNCs and lignin-NPs, which mainly arise from the hydrogen bonds formed among the abundant hydroxyl groups. [204]

Mechanical properties

Mechanical properties are essential for expanding the utilization of the obtained nanocomposite films to meet various application requirements. The tensile strength, the elongation at break, the Young's modulus, and thickness for the nanocomposite films were determined and are summarized in **Table 4.4**. The

incorporation of lignin-NPs contributed to an increase in the tensile strength and Young's modulus of the nanocomposite films, and the highest value of tensile strength was obtained as the CNCs/lignin-NPs film with a compositional ratio of 5, which was much higher than those of the pure CNC film. It can be concluded that the lignin-NPs reinforced the CNC films by the formed strong hydrogen bonds, which allow strong interfacial adhesion between CNCs and lignin-NPs. [204]

Table 4.4. *Young's modulus, tensile strength, elongation at break, and thickness of composite films with different ratios of CNCs/lignin-NPs. (Paper IV)*

CNC/lignin -NPs	Tensile strenth (MPa)	Elongation at break (%)	Young's modulus (GPa)	Thickness (μm)
100:0	63.15±4.2	2.52±0.2	4.94±0.01	95.9±2.1
10:1	82.70±0.3	2.62±0.2	6.53±0.02	70.6±1.9
5:1	91.84±0.3	2.86±0.3	7.24±0.01	70.2±1.2
2:1	69.70±4.3	1.39±0.3	6.23±0.1	69.6±1.1
1:1	66.03±3.7	1.62±0.1	5.62±0.02	67.1±1.4

Thermal properties

As shown in **Figure 4.18a**, the thermal stability of the nanocomposite films was significantly improved, especially with a higher content of the incorporated lignin-NPs, as compared to that of the pure CNC film. The enhanced thermal stability of these nanocomposites can be attributed to the formed molecular interactions between CNCs and lignin-NPs, such as hydrogen bonds. [205] The derivative TG curves showed that the degradation of all the samples occurred in two stages and presented similar decomposition profiles, as indicated in **Figure 4.18b**. The first (T_1) and second (T_2) decomposition temperature are around 260 °C and 315 °C, respectively, both of which correspond to the degradation of the polymer backbone.

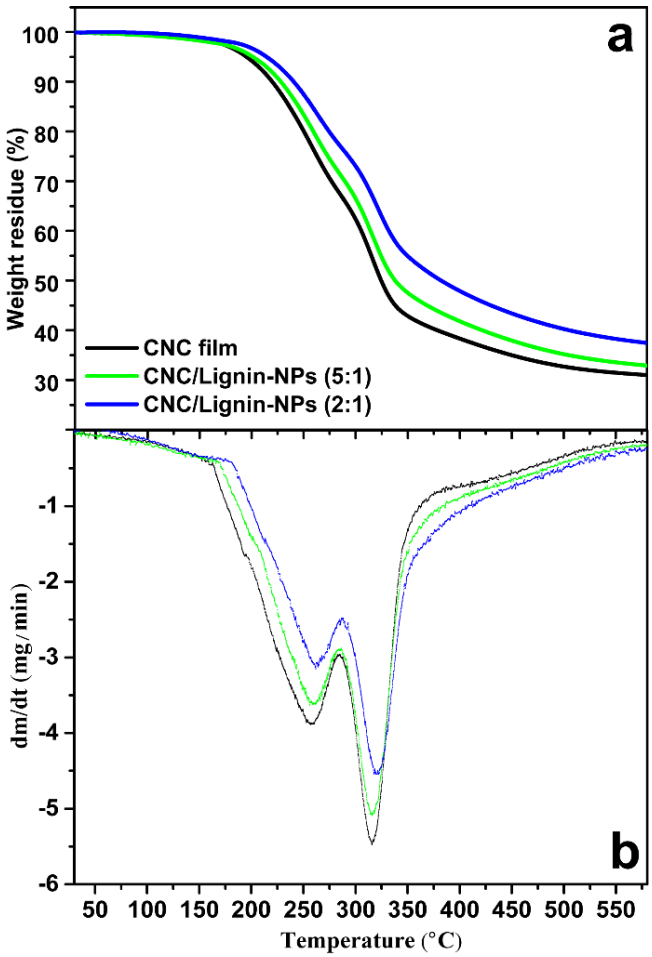

Figure 4.18. *Thermal stability of different nanocomposites produced under the various CNCs/lignin-NPs ratio: (a) TGA weight loss; (b) TGA temperature derivative weight loss. Image was adapted from Paper IV with Copyright (2019) American Chemical Society.*

Antibacterial activity

The inhibition of the nanocomposites against *E. coli* is visually displayed in **Figure 4.19**. It is clear that all the nanocomposite film formed inhibitive holes with the diameters ranged in 9-16 mm, while the pure CNC film showed no clear inhibition zones. The incorporation of lignin-NPs significantly imposed the nanocomposites with antibacterial activity against *E. coli*. A previous study reported that lignin exhibited excellent antibacterial performance and could be used as an innovative antimicrobial natural material due to its original structure, including phenolic compounds and the presence of certain functional groups with oxygen. [206] Therefore, the nanocomposite films produced from a direct and low-cost processing procedure have exhibited functionality, and have the

potential to substitute for petrochemical-based polymers in such cases as packaging applications.

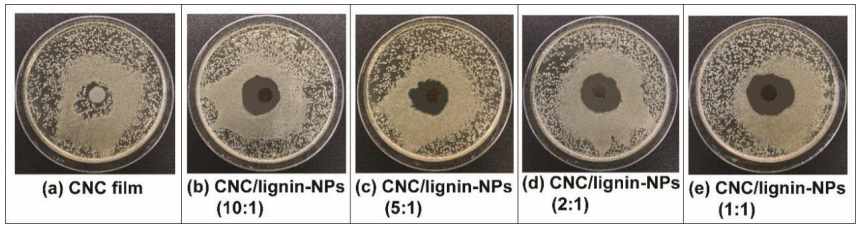

Figure 4.19. *Inhibition halos measured and spot diffusion assay of nanocomposites tested toward E. coli. Image was adapted from Paper IV with Copyright (2019) American Chemical Society.*

4.5 Lignin-based hybrid magnetic nanoparticles for ultrafast removal of heavy metal ions (Paper V)

Various materials have been explored for the adsorption of heavy metal ions from aqueous solutions. [207, 208] In an up-to-date research context, nanomaterials, especially nanoparticles, exhibit unprecedented opportunities for the adsorption of heavy metals ions in high efficiency due to their unique physical and chemical properties. [209-211] Among various types of nanoparticles, magnetic hybrid nanoparticles have drawn considerable interest for the adsorption of heavy metal ions due to their intriguing features, such as being easy to separate, large surface area, and diversity in surface functionalization. [212, 213] The magnetic nanoparticles can be used as magnetic cores, which can be modified or cross-linked with other functional polymers to enhance their chemical stability and their performance in the adsorption of heavy metal ions. [214, 215] As one of the main fraction obtained from formic acid fractionation, the valorization of formic acid lignin is considered as an important part of the integrated biorefinery platform. The unique structural features of formic acid lignin, which contains numerous functional groups including -OH and $-COO^-$ groups, can be regarded as a promising raw material for preparing lignin-based magnetic hybrid nanoparticles for the adsorption of heavy metal ions. It may open windows of opportunity for the valorization of the obtained lignin.

4.5.1 Synthesis of lignin-based hybrid nanoparticles

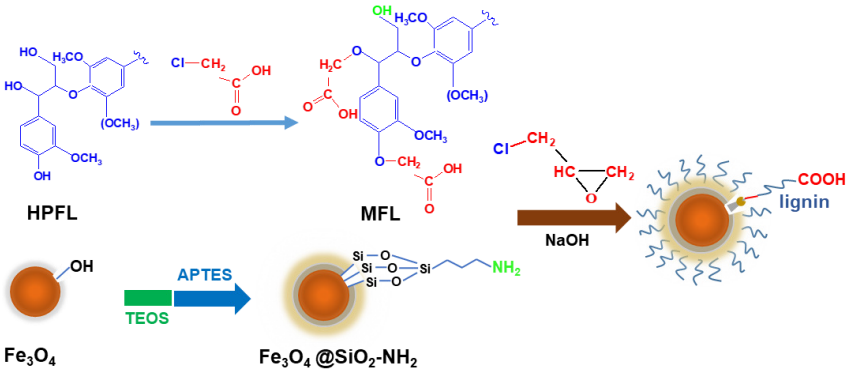

Figure 4.20. *A schematic process flow diagram illustrating the synthesis of the lignin-based hybrid magnetic nanoparticles (HPFL: high-pressure formic acid lignin; MFL: modified high-pressure formic acid lignin). (Paper V)*

As shown in **Figure 4.20**, formic acid lignin-based hybrid magnetic nanoparticles were synthesized through a chemical cross-linking reaction between the amine-functionalized Fe_3O_4@SiO_2 and modified lignin. To improve the active sites of the synthesized materials, the lignin structure was modified via carboxymethylation to introduce carboxylate group.

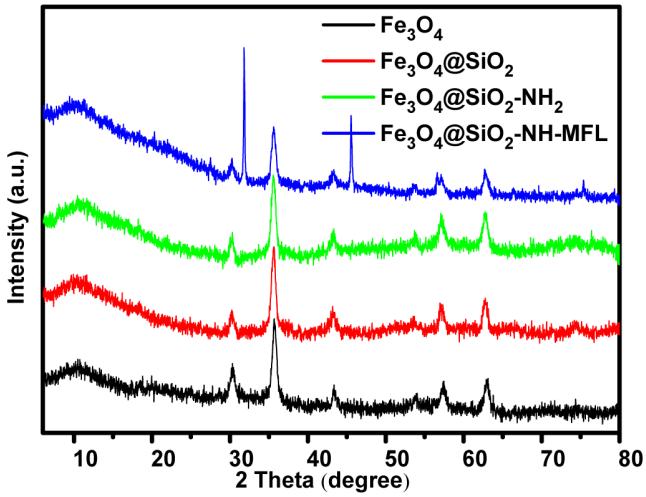

Figure 4.21. *XRD patterns of synthesized nanoparticles (Fe_3O_4: magnetic nanoparticles; Fe_3O_4@SiO_2: silica coated magnetic nanoparticles; Fe_3O_4@SiO_2-NH_2: silica coated magnetic nanoparticles with amine groups; Fe_3O_4@SiO_2-NH-MFL: modified lignin-based hybrid magnetic nanoparticles). (Paper V)*

The XRD pattern was recorded by from 5° to 80° 2θ (**Figure 4.21**). The presence of magnetic nanoparticles as a core was identified by the characteristic

diffraction peaks at 30.3°, 35.7°, 43.3°, 53.5°, 57.4° and 62.9° 2θ (JCPDS card No. 19-0629), respectively, which also revealed the hexagonal phase structure of the Fe_3O_4 nanoparticles. [216] These above-mentioned peaks were all observed in the amine-functionalized Fe_3O_4@SiO_2 and as-synthesized Fe_3O_4@SiO_2-NH-MFL, indicating that the silica coating, further modification and cross-linking reaction did not lead to any significant change in terms of the size and crystal structure of the Fe_3O_4 nanoparticles.

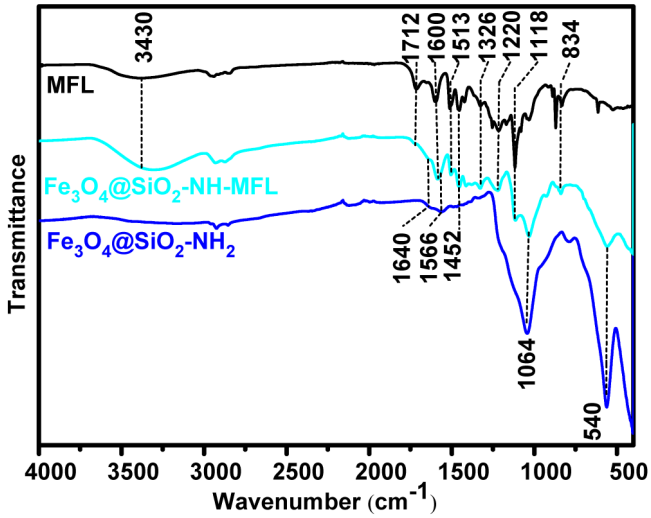

Figure 4.22. *FTIR spectra of synthesized nanoparticles (MFL: modified formic acid lignin; Fe_3O_4@SiO_2-NH_2: silica coated magnetic nanoparticles with amine groups; Fe_3O_4@SiO_2-NH-MFL: modified lignin-based hybrid magnetic nanoparticles). (Paper V)*

FTIR spectra are illustrated in **Figure 4.22**. The typical characteristic peaks of the carboxymethylated lignin at 3430 and 1600 cm^{-1} are ascribed to hydroxyl groups and carboxylate groups (asymmetric stretching), respectively. [80] The spectra also showed characteristic "lignin bands" at 1513 and 1452 cm^{-1}, which are due to aromatic rings, and the peaks at 1220 cm^{-1} ascribed to phenolic C-O groups. [173] Furthermore, the typical absorption peak at 540 cm^{-1} is attributed to the stretching vibration of Fe-O bond, and the strong absorption peaks at 1064 cm^{-1} resulted from Si-O vibrations, which highlighted the formation silica network surrounded the Fe_3O_4 nanoparticle core. [217] Two weak peaks at 1640 and 1566 cm^{-1} are attributed to the deformation vibration of amide I and amide II, respectively, indicating the successful amine modification of Fe_3O_4@SiO_2 nanoparticles. [173] After chemical cross-linking, these above-mentioned peaks are clearly found in the end target product (Fe_3O_4@SiO_2-NH-MFL), indicating the successfully synthesis of the magnetic hybrid nanoparticles.

4.5.2 Surface properties of the synthesized nanoparticles

It is important to reveal the surface properties of synthesized nanoparticles in order to understand their suitability for adsorption of heavy metal ions. As shown in **Figure 4.23a-d**, the morphology of the synthesized nanoparticles was investigated by TEM and SEM equipped with an EDX system. All the obtained nanoparticles present an approximate diameter of 10-20 nm and a nearly spherical shape. As the final synthesized products, the Fe_3O_4@SiO_2-NH-MFL nanoparticles display a relatively similar spherical morphology and size as its precursor nanoparticles. The morphology of these nanoparticles was also examined by SEM, as displayed in **Figure 4.23a$_1$-d$_1$**, which is in agreement with the result found by TEM. Representative morphology of the as-synthesized Fe_3O_4@SiO_2-NH-MFL nanoparticles structures, as revealed by SEM (**Figure. 4.23d$_1$**), exhibits a coarse and polydisperse mesoporous structure, which enables the synthesized hybrid nanoparticles to achieve a high adsorption capability for heavy metal ions owing to a larger exposed specific surface area.

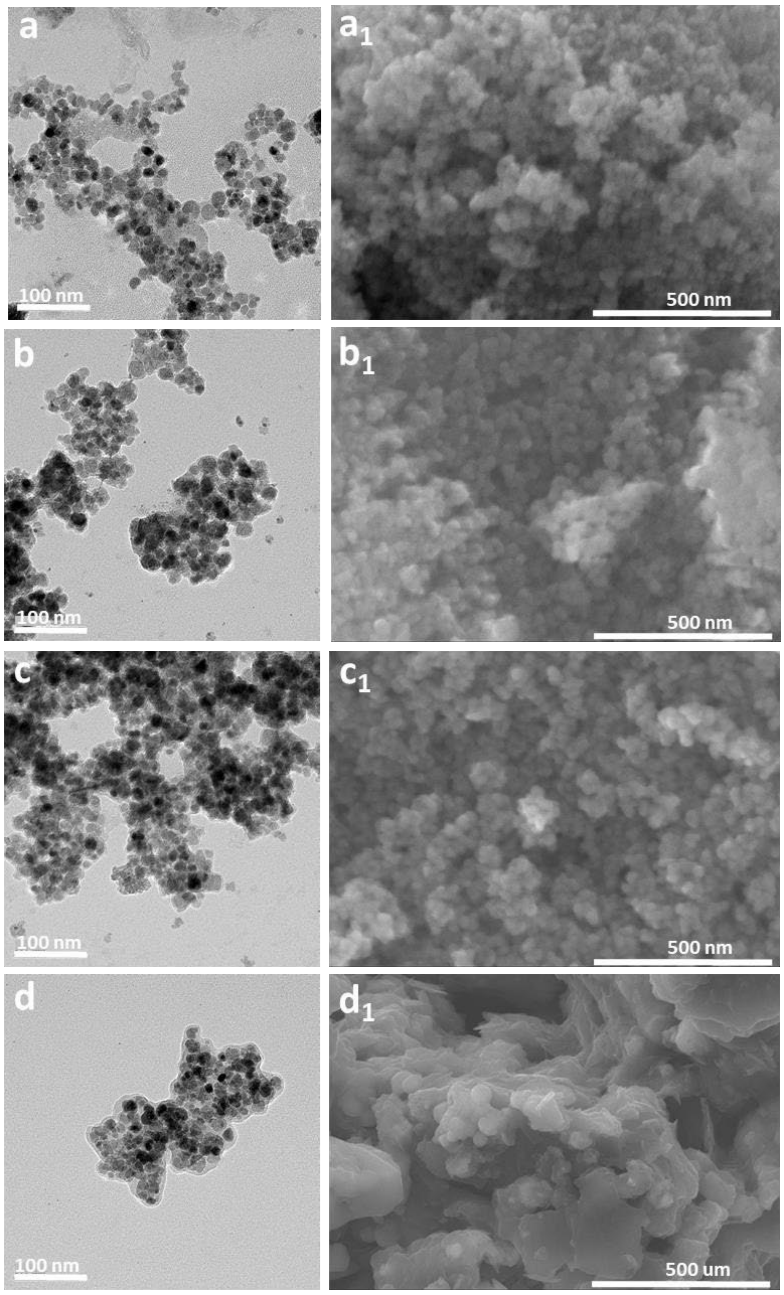

Figure 4.23. *Representative TEM images (left column) and SEM images (right column) of Fe_3O_4 (a and a_1), $Fe_3O_4@SiO_2$ (b and b_1), $Fe_3O_4@SiO_2$-NH_2 (c and c_1) and $Fe_3O_4@SiO_2$-NH-MFL (d and d_1) (Fe_3O_4: magnetic nanoparticles; $Fe_3O_4@SiO_2$: silica coated magnetic nanoparticles; $Fe_3O_4@SiO_2$-NH_2: silica coated magnetic nanoparticles with amine groups; $Fe_3O_4@SiO_2$-NH-MFL: modified lignin-based hybrid magnetic nanoparticles). Image was adapted from Paper V with Copyright (2019) ELSEVIER.*

In order to reveal the stability of liquid dispersions of the synthesized nanoparticles, zeta-potential was measured at different pH values. As shown in **Figure 4.24**, the zeta-potential of synthesized Fe_3O_4@SiO_2-NH-MFL decreased with an increase in pH, and the isoelectric point was reached at pH 2.4. At pH > 3, the hybrid nanoparticles possess a negative surface charge of below -30 mV. In comparison, the isoelectric point of Fe_3O_4@SiO_2-NH-FL and Fe_3O_4@SiO_2-MFL shifted to 3.5 and 3.1, respectively, and then the surface charge was transformed to a negative charge with large fluctuations. These results indicate that the synthesized Fe_3O_4@SiO_2-NH-MFL dispersion exhibited excellent stability over a wide pH range. The presence of coated silica and linked carboxymethylated lignin exhibited a clear effect on the zeta-potential of Fe_3O_4@SiO_2-NH-MFL nanoparticles. [218]

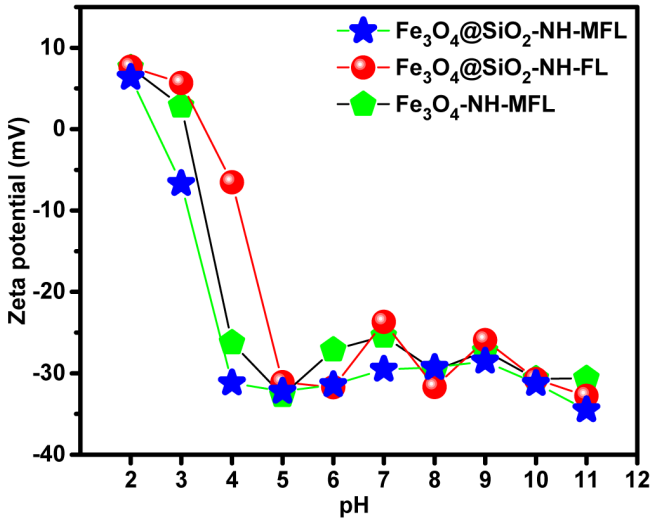

Figure 4.24. *Zeta-potential of the synthesized nanoparticles as a function of pH (Fe_3O_4-NH-MFL: non-silica coated modified lignin-based hybrid magnetic nanoparticles; Fe_3O_4@SiO_2-NH-FL: non-modified lignin-based hybrid magnetic nanoparticles; Fe_3O_4@SiO_2-NH-MFL: modified lignin-based hybrid magnetic nanoparticles). (Paper V)*

4.5.3 Adsorption of heavy metal ions using synthesized lignin-based hybrid nanoparticles

Adsorption performance

We selected an initial pH of 5.0 to further investigate the adsorption efficiency and isotherm of hybrid nanoparticles (Fe_3O_4@SiO_2-NH-MFL). **Figure 4.25a and b** show the removal of Pb^{2+} and Cu^{2+} ions by the synthesized Fe_3O_4@SiO_2-NH-MFL as a function of contact time. Impressively, the adsorption of Pb^{2+} and Cu^{2+} ions showed an ultra-fast process and the equilibrium was reached within 30 s under an initial metal ions concentration of 50 mg/L. Such an ultrafast adsorption of heavy metal ions by the synthesized Fe_3O_4@SiO_2-NH-MFL presents a great potential for the large-scale applications. This superior performance of the adsorbent can be attributed to the following synergistic effects: (1) the cross-linked carboxymethylated lignin provides numerous active sites; (2) the porous structure of the synthesized Fe_3O_4@SiO_2-NH-MFL offers a large surface area; (3) the highly negative charge on the nanoparticle surface (zeta-potential < -30 mV in the pH range of 3-11) accelerates the diffusion and enrichment of metal ions towards the adsorbent surface.

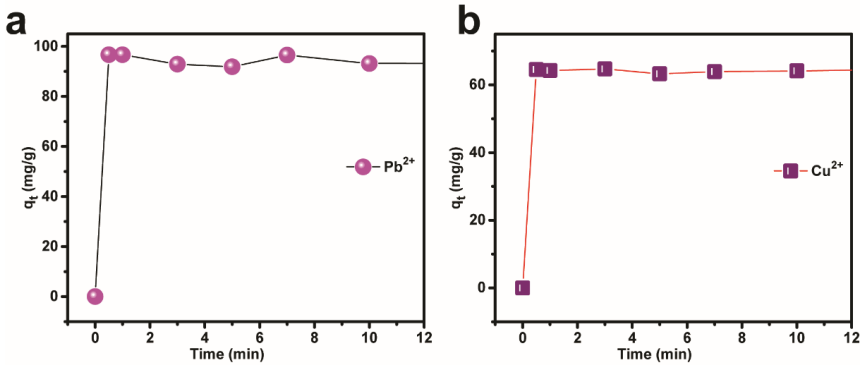

Figure 4.25. *(a) Effect of contact time on the adsorption capacity of Pb^{2+} and (b) Cu^{2+} by Fe_3O_4@SiO_2-NH-MFL (Fe_3O_4@SiO_2-NH-MFL: modified lignin-based hybrid magnetic nanoparticles). (Paper V)*

The Pb^{2+} and Cu^{2+} adsorption isotherms were investigated as described in **Figure 4.26a and b**. The adsorption capacities of the as-synthesized Fe_3O_4@SiO_2-NH-MFL at first increased rapidly at low metal ion concentration, and then reached a plateau with the maximum adsorption capacity of 152.4 and 71.4 mg/L for Pb^{2+} and Cu^{2+}, respectively. As shown in **Figure 4.26a and b**, it can be concluded that the Sips model fits the experimental data well with a higher correlation coefficient as compared to Langmuir and Freundlich isotherm model. This offers the best description for the adsorption of both Pb^{2+} and Cu^{2+} onto the synthesized Fe_3O_4@SiO_2-NH-MFL nanoparticles. Under the utilization of Sips model, the maximum adsorption capacity was predicted to be 150.33 and 70.69 mg/g for Pb^{2+} and Cu^{2+} ions, respectively.

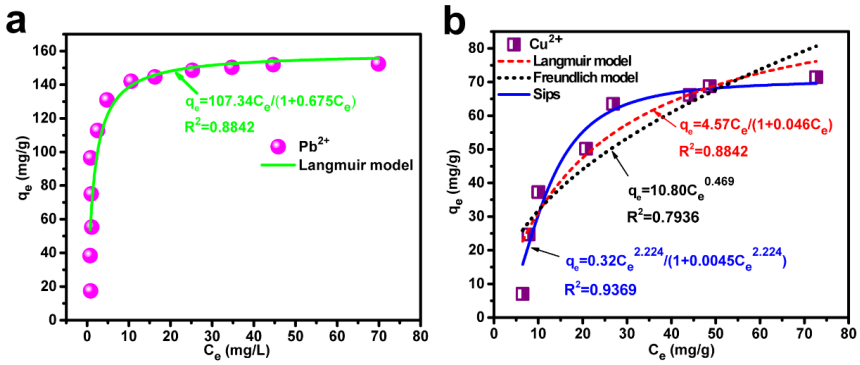

Figure 4.26. *(a) Adsorption isotherms for Pb^{2+} and (b) Cu^{2+} adsorption on Fe_3O_4@SiO_2-NH-MFL and the corresponding Langmuir, Freundlich and Sips models (Fe_3O_4@SiO_2-NH-MFL: modified lignin-based hybrid magnetic nanoparticles). (Paper V)*

Adsorption mechanism

It is essential to understand the adsorption mechanism of the heavy metal ions onto the Fe_3O_4@SiO_2-NH-MFL nanoparticles. As shown in **Figure 4.27a**, the FTIR spectra was recorded before and after adsorption by Fe_3O_4@SiO_2-NH-MFL. It is observed that the stretching vibration of the -OH group shifted from 3369 to 3302 cm^{-1} after adsorption of Pb^{2+}, indicating that strong -OH interactions are developed due to the formation of hydrogen bonding between -OH groups. Furthermore, the C=O stretching vibration in the $-COO^-$ groups occurred a slight shift from 1712 to 1706 cm^{-1} and the relative intensity of the C=O absorption band decreased after Pb^{2+} adsorption.

XPS was also applied to reveal the adsorption mechanism of heavy metal ions. After adsorption of Pb^{2+}, the relative area ratio of the peak attributed to Na 1s decreased, instead some characteristic peaks for Pb were observed in the XPS spectra (**Figure 4.27**), indicating the ion exchange between -COONa and Pb^{2+}. According to the high-resolution XPS scan (**Figure 4.27c and d**), the C-O signal occurred a shift from 286.06 eV to a lower binding energy at 285.89 eV after metal ions adsorption, which was probably caused by the interaction of Pb^{2+} ions with C-OH. While the peak for the $-COO^-$ signal shifted to higher binding energy from 287.33 eV to 287.72 eV due to the binding of Pb ions to $-COO^-$. [219] After the metal ions adsorption, the peak attributed to -OH shifted to lower binding energy from 532.77 eV to 532.27 eV and the peak of the $-COO^-$ signal shifted to higher binding energy due to the decreased electron density, which was feasibly caused by the interaction of Pb^{2+} ions with oxygen atoms. These results further confirmed that the -OH and $-COO^-$ groups on the surface of Fe_3O_4@SiO_2-NH-MFL nanoparticles play a significant role in the ultrafast adsorption process. Therefore, based on the above discussions, the adsorption mechanism of heavy metal ions by the synthesized Fe_3O_4@SiO_2-NH-MFL is mainly attributed to ion exchange and hydrogen bonding.

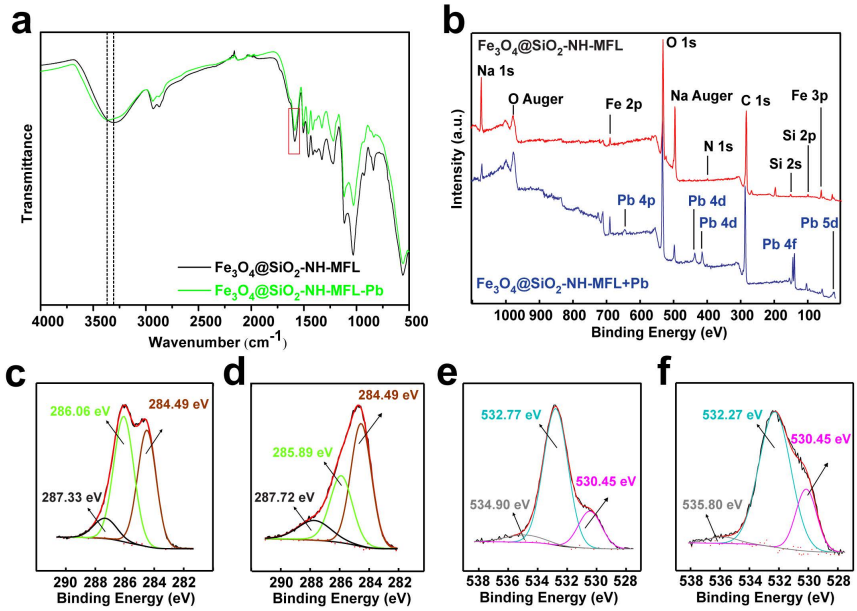

Figure 4.27. *FTIR analysis (a), XPS survey spectra (b), O 1s spectra (c and d) and C 1s spectra (e and f) of Fe_3O_4@SiO_2-NH-MFL before and after the adsorption of Pb^{2+} ions (Fe_3O_4@SiO_2-NH-MFL: modified lignin-based hybrid magnetic nanoparticles). Image was adapted from Paper V with Copyright (2019) ELSEVIER.*

5. Concluding and future remarks

5.1 Summary of the thesis

With the aim of building an integrated biorefinery platform, based on formic acid fractionation of bamboo, a full value chain of the fractions with integration of nanomaterials production was explored. Based on the thorough understanding of the chemical compositions and structural features of various streams, especially for lignin, valorization processes for the production of lignin-NPs, a lignin-based composite, and hybrid nanoparticles were exploited.

As the basis of this thesis work, formic acid fractionation of bamboo under pressure was firstly investigated for converting the lignocellulose into its main components. Lignin and hemicelluloses were selectively dissolved, while cellulose remained without being obviously degraded. Under the optimized conditions, this process provided a high efficient way to fractionate bamboo into 42.2% cellulose pulp, 31.5% lignin, and 8.5% hemicellulose fractions. In order to promote the recovery and high-value applications of hemicelluloses, a combined fractionation process based on autohydrolysis and subsequent formic acid rapid-delignification was also successfully explored. The autohydrolysis facilitated oligosaccharide production, and the subsequent formic acid rapid-delignification further fractionated autohydrolyzed bamboo into lignin and cellulose.

Furthermore, the obtained formic acid lignin was subjected to comprehensive structural characterization. The results confirmed that formic acid fractionation under high pressure presents a quick and efficient delignification method by enhancing the cleavage of interunitary bonds in lignin. The condensation reaction also occurred simultaneously during the delignification process. As compared to atmospheric formic acid lignin, high-pressure formic acid lignin showed higher purity and yield, and had relatively higher contents of phenolic and carboxylic groups.

Moreover, the dissolved lignin in spent liquor was processed into nanoparticles (lignin-NPs), which exhibited spherical morphology and a uniform particle size distribution. The bamboo-originated cellulose can be easily converted into cellulose nanocrystals (CNCs) using TEMPO oxidation in a relatively short time. Importantly, nanocomposite films were prepared based on the dispersions of CNCs and lignin-NPs. The nanocomposite films exhibited a very smooth surface and homogeneous structure. Most impressively, at the CNCs/lignin-NPs ratio of 5, the tensile strength and Young's modulus were improved by 44% and 47%, respectively, compared to the pure CNC film. Owning to the presence of lignin-NPs, and the nanocomposites exhibited an effective antibacterial activity against *E. coli*.

Additionally, as a highly efficient and effective bio-degradable adsorbent for heavy metal ion removal, novel lignin-based hybrid nanoparticles (Fe_3O_4@SiO_2-NH-MFL) were prepared through a facile method using

epichlorohydrin as a cross-linker between amino-functionalized magnetic nanoparticles and carboxymethylated lignin. Taking the advantages of their special mesoporous structure and numerous active sites, the as-synthesized lignin-based hybrid nanoparticles were found to be exceptionally effective and efficient in the removal of heavy metal ions from aqueous solutions, with ultrafast adsorption equilibrium (within 30 s) and a relatively high adsorption capacity, respectively. The ion exchange and hydrogen bonding mainly contribute to the ultrafast and high capacity removal of heavy metal ions by Fe_3O_4@SiO_2-NH-MFL nanoparticles. All of these superior properties suggest that the Fe_3O_4@SiO_2-NH-MFL nanoparticles could become eco-friendly hybrid materials for the ultrafast removal of heavy metal ions from wastewater on a large scale.

Overall, this thesis work explored an efficient fractionation approach to overcome the highly recalcitrant nature of lignocellulose and to facilitate the subsequent valuable conversion based on the integrated biorefinery. Formic acid fractionation provides a green pathway to separate lignocellulosic biomass, as in this thesis exemplified for bamboo, and the obtained fractions, especially for lignin, offer various possibilities for their valorization. It is believed that the full transformation of lignocellulosic components from materials based on formic acid fractionation opens a window for the building of a promising versatile material platform to meet the green chemistry principles and the commercial cost target.

5.2 Future remarks

Formic acid fractionation is a promising protocol to overcome the recalcitrance of lignocellulosic biomass, achieving a full separation in an environmentally-friendly way. The fractionated streams allow a holistic valorization based on the integrated biorefinery system, whereas some challenges still exist in the current fractionation process:

(a) A certain amount of condensation structure exists in the structure of formic acid lignin. The condensation of lignin structure not only leads to a negative influence on the delignification of raw materials, but also dramatically affects its subsequently upgrading. How to effectively prevent the formation of condensation structure during formic acid fractionation is worth to consider.

(b) The complex structure of lignin, including various types of bonds, functional groups, and molar mass, limits its high-value applications. There is still a knowledge gap in the structural analysis of the lignin molecular structure. Therefore, in order to overcome the current technological challenges, the development of innovative analytical techniques and combined analysis methods should gain more attention.

(c) The valorization of lignin is still in the developing stage, and challenges are yet to be overcome to realize large-scale operation. The high-value products based on lignin, such as new materials and chemicals, are in urgent need for the integrated utilization of lignocellulosic materials. Research efforts could be

intensified on the further functionalization of lignin nanomaterials for their high-value use as solid catalysts, biomedical materials and adsorbents. Furthermore, the accurate gradation of lignin according to its special features may bring us a better choice to improve the performance of the end products.

6. Acknowledgements

This doctoral thesis was carried out during the time of 09.2016-10.2019 in the Research Group of Wood and Paper Chemistry at the Faculty of Science and Engineering of Åbo Akademi University. The main funding support was from China Scholarship Council, Graduate School of Chemical Engineering at Åbo Akademi University and Fortum Foundation in Finland. The travel grants from Magnus Ehrnrooth foundation, Puunjalostusinsinöörit (Finnish Forest Products Engineers' Association), as well as funding from Department of Chemical Engineering during my research visit in the Lakehead University, are gratefully acknowledged.

First and foremost I would like to express my deep sense of gratitude to my supervisors, Professor Stefan Willför and Docent Chunlin Xu, for their supervision and all the support during these past three years. I appreciate Professor Stefan Willför who offered me this opportunity to expand my research career and gave me the freedom to pursue various projects without objection. Docent Chunlin Xu is especially acknowledged for being my guiding light, for encouraging me, and for making me who I am today. It seems like he's always online whenever you'd like to have a discussion. It is always a pleasure to work with him as well-motivated as he is. He is a tremendous mentor for me, a role model for moving forward and a big brother to both my research and life. Thanks!!! I am also hugely appreciative to Dr. Xiaoju Wang, especially for sharing her professional knowledge and research experience so willingly, and for being so dedicated to her role as my co-supervisor. I would also like to thank Academy lecturer, Docent Anna Sundberg for all the help and valuable suggestions in my studies.

I greatly appreciate to Professor Menghua Qin from Taishan University (Taian, China) for introducing me to Åbo Akademi University. You taught me so much and brought me into the scientific world. Your encouragement and constant motivation pushed me to heights I never thought possible. Special thanks go to Professor Qingxi Hou from Tianjin University of Science and Technology (TUST, Tianjin, China), for your supervision with carefulness and continuous support. You taught me how to become a competitive researcher with rigorous attitude towards science. I also very grateful to the teachers and friends in Qilu University of Technology (Jinan, China) and TUST, especially Professor Yingjuan Fu, Professor who have inspired me all these years.

Many thanks also to Assistant Professor Pedram Fatehi for giving me the opportunity to visit his group at Department of Chemical Engineering of Lakehead University, Canada. His supervision with motivation and patience was very helpful to my research career. All the colleagues and friends in Canada are acknowledged gratefully.

I thank all the present and former colleagues at Research Group of Wood and Paper Chemistry, for making such a pleasant working environment. Especially Andrey Pranovich, Jarl Hemming, Annika Smeds, Jun Liu, Wenyang Xu,

Ekaterina Korotkova, Weihua Zhang, Huanfei Xu, Luyao Wang, Qingbo Wang and Yury Brusentsev, for their assistance, valuable scientific discussions, laughs and joys. I also would like to thank all the co-authors, the research work cannot be finished without your contributions.

I would like to express my deep gratitude towards my friends in Finland for providing support and friendship that I needed and all the wonderful time together. Too many to list here but you know who you are!

I would also like to say a heartfelt thank you to my loving family for their endless love, support and encouragement. My dear parents, sister and my beloved, thank you all. I love you all!

7. References

1. Maity, S.K., 2015. Opportunities, recent trends and challenges of integrated biorefinery: Part I. *Renewable and Sustainable Energy Reviews*, **43**, 1427-1445.
2. Fernando, S., Adhikari, S., Chandrapal, C., Murali, N., 2006. Biorefineries: current status, challenges, and future direction. *Energy & Fuels*, **20**(4), 1727-1737.
3. Morais, A.R., Bogel-Lukasik, R., 2013. Green chemistry and the biorefinery concept. *Sustainable Chemical Processes*, **1**(1), 18.
4. Bioenergy, I., 2014. Sustainable and synergetic processing of biomass into marketable food & feed ingredients, chemicals, materials and energy (fuels, power, heat). *Wageningen, The Netherlands*.
5. Li, M.F., Fan, Y.M., Xu, F., Sun, R.C., 2010. Characterization of extracted lignin of bamboo (*Neosinocalamus affinis*) pretreated with sodium hydroxide/urea solution at low temperature. *Bioresources*, **5**(3), 1762-1778.
6. Li, M.F., Sun, S.N., Xu, F., Sun, R.C., 2012. Formic acid based organosolv pulping of bamboo (*Phyllostachys acuta*): Comparative characterization of the dissolved lignins with milled wood lignin. *Chemical Engineering Journal*, **179**, 80-89.
7. Posada, J.A., Rincón, L.E., Cardona, C.A., 2012. Design and analysis of biorefineries based on raw glycerol: Addressing the glycerol problem. *Bioresource Technology*, **111**, 282-293.
8. Moncada, J., El-Halwagi, M.M., Cardona, C.A., 2013. Techno-economic analysis for a sugarcane biorefinery: Colombian case. *Bioresource Technology*, **135**, 533-543.
9. Demirbas, A., 2009. Biorefineries: current activities and future developments. *Energy Conversion and Management*, **50**(11), 2782-2801.
10. Vila, C., Santos, V., Parajó, J.C., 2003. Simulation of an organosolv pulping process: Generalized material balances and design calculations. *Industrial & Engineering Chemistry Research*, **42**(2), 349-356.
11. Bugg, T.D.H., Rahmanpour, R., 2015. Enzymatic conversion of lignin into renewable chemicals. *Current Opinion in Chemical Biology*, **29**, 10-17.
12. Delmas, M., 2008. Vegetal refining and agrichemistry. *Chemical Engineering & Technology*, **31**(5), 792-797.
13. Jahan, M.S., Chowdhury, D.A.N., Islam, M.K., 2007. Atmospheric formic acid pulping and TCF bleaching of dhaincha (Sesbania aculeata), kash (Saccharum spontaneum) and banana stem (Musa Cavendish). *Industrial Crops and Products*, **26**(3), 324-331.
14. Bozell, J.J., Black, S.K., Myers, M., Cahill, D., Miller, W.P., Park, S., 2011. Solvent fractionation of renewable woody feedstocks: Organosolv generation of biorefinery process streams for the production of biobased chemicals. *Biomass & Bioenergy*, **35**(10), 4197-4208.
15. Pan, X., Kadla, J.F., Ehara, K., Gilkes, N., Saddler, J.N., 2006. Organosolv ethanol lignin from hybrid poplar as a radical scavenger: relationship between lignin structure, extraction conditions, and antioxidant activity. *Journal of Agricultural and Food Chemistry*, **54**(16), 5806-5813.
16. Reisinger, M., Tirpanalan, Ö., Huber, F., Kneifel, W., Novalin, S., 2014. Investigations on a wheat bran biorefinery involving organosolv fractionation and enzymatic treatment. *Bioresource Technology*, **170**, 53-61.
17. Villaverde, J.J., Li, J., Ek, M., Ligero, P., de Vega, A., 2009. Native lignin structure of *Miscanthus x giganteus* and its changes during acetic and formic acid fractionation. *Journal of Agricultural and Food Chemistry*, **57**(14), 6262-6270.
18. Villaverde, J.J., Li, J.B., Ligero, P., Ek, M., de Vega, A., 2012. Mild peroxyformic acid fractionation of *Miscanthus x giganteus* bark. Behaviour and structural characterization of lignin. *Industrial Crops and Products*, **35**(1), 261-268.

19. Zhao, X.B., Cheng, K.K., Liu, D.H., 2009. Organosolv pretreatment of lignocellulosic biomass for enzymatic hydrolysis. *Applied Microbiology and Biotechnology*, **82**(5), 815-827.
20. Muñoz, C., Baeza, J., Freer, J., Mendonça, R.T., 2011. Bioethanol production from tension and opposite wood of Eucalyptus globulus using organosolv pretreatment and simultaneous saccharification and fermentation. *Journal of Industrial Microbiology & Biotechnology*, **38**(11), 1861.
21. Amiri, H., Karimi, K., 2015. Improvement of acetone, butanol, and ethanol production from woody biomass using organosolv pretreatment. *Bioprocess and Biosystems Engineering*, **38**(10), 1959-1972.
22. Hideno, A., Kawashima, A., Endo, T., Honda, K., Morita, M., 2013. Ethanol-based organosolv treatment with trace hydrochloric acid improves the enzymatic digestibility of Japanese cypress (*Chamaecyparis obtusa*) by exposing nanofibers on the surface. *Bioresource Technology*, **132**, 64-70.
23. Zhang, H.D., Wu, S.B., 2014. Efficient Sugar Release by Acetic Acid Ethanol-Based Organosolv Pretreatment and Enzymatic Saccharification. *Journal of Agricultural and Food Chemistry*, **62**(48), 11681-11687.
24. Hii, K.L., Yeap, S.P., Mashitah, M.D., 2012. Pretreatment of pressed pericarp fibers (PPF) using alcohols as solvent to increase the accessibility of cellulose for cellulase production. *Journal of the Korean Society for Applied Biological Chemistry*, **55**(4), 507-514.
25. Gandolfi, S., Ottolina, G., Consonni, R., Riva, S., Patel, I., 2014. Fractionation of hemp hurds by organosolv pretreatment and its effect on production of lignin and sugars. *ChemSusChem*, **7**(7), 1991-1999.
26. Wang, K., Yang, H., Guo, S., Tang, Y., Jiang, J., Xu, F., Sun, R.-C., 2012. Organosolv fractionation process with various catalysts for improving bioconversion of triploid poplar. *Process Biochemistry*, **47**(10), 1503-1509.
27. Li, M.F., Yang, S., Sun, R.C., 2016. Recent advances in alcohol and organic acid fractionation of lignocellulosic biomass. *Bioresource Technology*, **200**, 971-980.
28. Vila, C., Santos, V., Parajo, J.C., 2014. Manufacture of microcrystalline cellulose from eucalyptus globulus wood using an environmentally friendly biorefinery method. *Journal of Wood Chemistry and Technology*, **34**(1), 8-19.
29. Kupiainen, L., Ahola, J., Tanskanen, J., 2012. Distinct effect of formic and sulfuric acids on cellulose hydrolysis at high temperature. *Industrial & Engineering Chemistry Research*, **51**(8), 3295-3300.
30. Snelders, J., Dornez, E., Benjelloun-Mlayah, B., Huijgen, W.J.J., de Wild, P.J., Gosselink, R.J.A., Gerritsma, J., Courtin, C.M., 2014. Biorefining of wheat straw using an acetic and formic acid based organosolv fractionation process. *Bioresource Technology*, **156**, 275-282.
31. Feng, P., Chen, F.G., 2012. Preparation and characterization of acetic acid lignin-based epoxy blends. *Bioresources*, **7**(3), 2860-2870.
32. Vanderghem, C., Richel, A., Jacquet, N., Blecker, C., Paquot, M., 2011. Impact of formic/acetic acid and ammonia pre-treatments on chemical structure and physico-chemical properties of *Miscanthus x giganteus* lignins. *Polymer Degradation and Stability*, **96**(10), 1761-1770.
33. Ferrer, A., Vega, A., Rodriguez, A., Jiménez, L., 2013. Acetosolv pulping for the fractionation of empty fruit bunches from palm oil industry. *Bioresource Technology*, **132**, 115-120.
34. Dapía, S., Santos, V., Parajó, J.C., 2002. Study of formic acid as an agent for biomass fractionation. *Biomass & Bioenergy*, **22**(3), 213-221.

35. Dapía, S., Santos, V., Parajó, J.C., 2000. Formic acid-peroxyformic acid pulping of *Fagus sylvatica*. *Journal of Wood Chemistry and Technology*, **20**(4), 395-413.
36. Obrocea, P., Cimpoesu, G., 1998. Contribution to sprucewood delignification with peroxyformic acid I. The effect of pulping temperature and time. *Cellulose Chemistry and Technology*, **32**(5-6), 517-525.
37. Lam, H.Q., Le Bigot, Y., Delmas, M., Avignon, G., 2001. Formic acid pulping of rice straw. *Industrial Crops and Products*, **14**(1), 65-71.
38. Zhao, X., Liu, D., 2012. Fractionating pretreatment of sugarcane bagasse by aqueous formic acid with direct recycle of spent liquor to increase cellulose digestibility-the Formiline process. *Bioresource Technology*, **117**, 25-32.
39. Zhao, X.B., Wang, L., Liu, D.H., 2007. Effect of several factors on peracetic acid pretreatment of sugarcane bagasse for enzymatic hydrolysis. *Journal of Chemical Technology & Biotechnology: International Research in Process, Environmental & Clean Technology*, **82**(12), 1115-1121.
40. Ligero, P., de Vega, A., van der Kolk, J.C., van Dam, J.E., 2011. Gorse (*Ulex europæus*) as a possible source of xylans by hydrothermal treatment. *Industrial Crops and Products*, **33**(1), 205-210.
41. Romaní, A., Garrote, G., López, F., Parajó, J.C., 2011. Eucalyptus globulus wood fractionation by autohydrolysis and organosolv delignification. *Bioresource Technology*, **102**(10), 5896-5904.
42. Garrote, G., Domínguez, H., Parajó, J.C., 2004. Production of substituted oligosaccharides by hydrolytic processing of barley husks. *Industrial & Engineering Chemistry Research*, **43**(7), 1608-1614.
43. Ruiz, H.A., Vicente, A.A., Teixeira, J.A., 2012. Kinetic modeling of enzymatic saccharification using wheat straw pretreated under autohydrolysis and organosolv process. *Industrial Crops and Products*, **36**(1), 100-107.
44. Garrote, G., Domínguez, H., Parajó, J.C., 2001. Manufacture of xylose-based fermentation media from corncobs by posthydrolysis of autohydrolysis liquors. *Applied Biochemistry and Biotechnology*, **95**(3), 195-207.
45. Kim, Y., Mosier, N.S., Ladisch, M.R., 2009. Enzymatic digestion of liquid hot water pretreated hybrid poplar. *Biotechnology Progress*, **25**(2), 340-348.
46. Laser, M., Schulman, D., Allen, S.G., Lichwa, J., Antal Jr, M.J., Lynd, L.R., 2002. A comparison of liquid hot water and steam pretreatments of sugar cane bagasse for bioconversion to ethanol. *Bioresource Technology*, **81**(1), 33-44.
47. Yoon, S.H., Van Heiningen, A., 2008. Kraft pulping and papermaking properties of hot-water pre-extracted loblolly pine in an integrated forest products biorefinery. *Tappi Journal*, **7**(7), 22-27.
48. El Hage, R., Chrusciel, L., Desharnais, L., Brosse, N., 2010. Effect of autohydrolysis of *Miscanthus x giganteus* on lignin structure and organosolv delignification. *Bioresource Technology*, **101**(23), 9321-9329.
49. Huijgen, W., Smit, A., De Wild, P., Den Uil, H., 2012. Fractionation of wheat straw by prehydrolysis, organosolv delignification and enzymatic hydrolysis for production of sugars and lignin. *Bioresource Technology*, **114**, 389-398.
50. Esteghlalian, A., Hashimoto, A.G., Fenske, J.J., Penner, M.H., 1997. Modeling and optimization of the dilute-sulfuric-acid pretreatment of corn stover, poplar and switchgrass. *Bioresource Technology*, **59**(2-3), 129-136.
51. Hinman, N.D., Schell, D.J., Riley, C.J., Bergeron, P.W., Walter, P.J., 1992. Preliminary estimate of the cost of ethanol-production for SSF Technology. *Applied Biochemistry and Biotechnology*, **34-5**, 639-649.
52. Nguyen, Q.A., Tucker, M.P., Keller, F.A., Eddy, F.P., 2000. Two-stage dilute-acid pretreatment of softwoods. *Applied Biochemistry and Biotechnology*, **84-6**, 561-576.

53. Kim, J.S., Lee, Y.Y., Park, S.C., 2000. Pretreatment of wastepaper and pulp mill sludge by aqueous ammonia and hydrogen peroxide. *Applied Biochemistry and Biotechnology*, **84-6**, 129-139.
54. Brink, D.L. 1993. Method of treating biomass material, Google Patents.
55. Goldstein, I.S., Easter, J.M., 1992. An improved process for converting cellulose to ethanol. *Tappi Journal*, **75**(8), 135-140.
56. Israilides, C.J., Grant, G.A., Han, Y.W., 1978. Sugar level, fermentability, and acceptability of straw treated with different acids. *Applied and Environmental Microbiology*, **36**(1), 43-46.
57. Mosier, N., Wyman, C., Dale, B., Elander, R., Lee, Y.Y., Holtzapple, M., Ladisch, M., 2005. Features of promising technologies for pretreatment of lignocellulosic biomass. *Bioresource Technology*, **96**(6), 673-686.
58. Alvira, P., Tomás-Pejó, E., Ballesteros, M., Negro, M., 2010. Pretreatment technologies for an efficient bioethanol production process based on enzymatic hydrolysis: a review. *Bioresource Technology*, **101**(13), 4851-4861.
59. Pileidis, F.D., Titirici, M.M., 2016. Levulinic acid biorefineries: new challenges for efficient utilization of biomass. *ChemSusChem*, **9**(6), 562-582.
60. Saha, B., Abu-Omar, M.M., 2014. Advances in 5-hydroxymethylfurfural production from biomass in biphasic solvents. *Green Chemistry*, **16**(1), 24-38.
61. Wang, T.F., Nolte, M.W., Shanks, B.H., 2014. Catalytic dehydration of C-6 carbohydrates for the production of hydroxymethylfurfural (HMF) as a versatile platform chemical. *Green Chemistry*, **16**(2), 548-572.
62. Birgit, K., Patrick R., G., Michael K., 2006. Adding color to green chemistry? An overview of the fundamentals and potential of chlorophylls *Biorefineries-Industrial Processes and Products: Status Quo and Future Directions*. **2**, 325-343.
63. Zeitsch, K.J. 2000. *The chemistry and technology of furfural and its many by-products*. Elsevier Science B.V., Amsterdam, The Netherlands.
64. Jeong, H., Jang, S.K., Hong, C.Y., Kim, S.H., Lee, S.Y., Lee, S.M., Choi, J.W., Choi, I.G., 2017. Levulinic acid production by two-step acid-catalyzed treatment of Quercus mongolica using dilute sulfuric acid. *Bioresource Technology*, **225**, 183-190.
65. vom Stein, T., Grande, P.M., Kayser, H., Sibilla, F., Leitner, W., de Maria, P.D., 2011. From biomass to feedstock: one-step fractionation of lignocellulose components by the selective organic acid-catalyzed depolymerization of hemicellulose in a biphasic system. *Green Chemistry*, **13**(7), 1772-1777.
66. Bian, H.Y., Chen, L.H., Gleisner, R., Dai, H.Q., Zhu, J.Y., 2017. Producing wood-based nanomaterials by rapid fractionation of wood at 80 degrees C using a recyclable acid hydrotrope. *Green Chemistry*, **19**(14), 3370-3379.
67. Guo, F., Fang, Z., Xu, C.C., Smith, R.L., 2012. Solid acid mediated hydrolysis of biomass for producing biofuels. *Progress in Energy and Combustion Science*, **38**(5), 672-690.
68. Shu, Q., Nawaz, Z., Gao, J.X., Liao, Y.H., Zhang, Q., Wang, D.Z., Wang, J.F., 2010. Synthesis of biodiesel from a model waste oil feedstock using a carbon-based solid acid catalyst: Reaction and separation. *Bioresource Technology*, **101**(14), 5374-5384.
69. Lou, W.Y., Zong, M.H., Duan, Z.Q., 2008. Efficient production of biodiesel from high free fatty acid-containing waste oils using various carbohydrate-derived solid acid catalysts. *Bioresource Technology*, **99**(18), 8752-8758.
70. Zong, M.H., Duan, Z.Q., Lou, W.Y., Smith, T.J., Wu, H., 2007. Preparation of a sugar catalyst and its use for highly efficient production of biodiesel. *Green Chemistry*, **9**(5), 434-437.
71. Fukuhara, K., Nakajima, K., Kitano, M., Kato, H., Hayashi, S., Hara, M., 2011. Structure and catalysis of cellulose-derived amorphous carbon bearing HSO_3 groups. *ChemSusChem*, **4**(6), 778-784.

72. Lai, D.M., Deng, L., Guo, Q.X., Fu, Y., 2011. Hydrolysis of biomass by magnetic solid acid. *Energy & Environmental Science*, **4**(9), 3552-3557.
73. Azizi Samir, M.A.S., Alloin, F., Dufresne, A., 2005. Review of recent research into cellulosic whiskers, their properties and their application in nanocomposite field. *Biomacromolecules*, **6**(2), 612-626.
74. O'sullivan, A.C., 1997. Cellulose: the structure slowly unravels. *Cellulose*, **4**(3), 173-207.
75. Rambabu, N., Panthapulakkal, S., Sain, M., Dalai, A.K., 2016. Production of nanocellulose fibers from pinecone biomass: Evaluation and optimization of chemical and mechanical treatment conditions on mechanical properties of nanocellulose films. *Industrial Crops and Products*, **83**, 746-754.
76. Anderson, S.R., Esposito, D., Gillette, W., Zhu, J., Baxa, U., Mcneil, S.E., 2014. Enzymatic preparation of nanocrystalline and microcrystalline cellulose. *TAPPI Journal,* **13**(5), 35-42.
77. Patankar, S.C., Renneckar, S., 2017. Greener synthesis of nanofibrillated cellulose using magnetically separable TEMPO nanocatalyst. *Green Chemistry*, **19**(20), 4792-4797.
78. Yu, H.Y., Qin, Z.Y., Liang, B.L., Liu, N., Zhou, Z., Chen, L., 2013. Facile extraction of thermally stable cellulose nanocrystals with a high yield of 93% through hydrochloric acid hydrolysis under hydrothermal conditions. *Journal of Materials Chemistry A,* **1**(12), 3938-3944.
79. Chen, L.H., Zhu, J.Y., Baez, C., Kitin, P., Elder, T., 2016. Highly thermal-stable and functional cellulose nanocrystals and nanofibrils produced using fully recyclable organic acids. *Green Chemistry*, **18**(13), 3835-3843.
80. Li, B., Xu, W.Y., Kronlund, D., Määttänen, A., Liu, J., Smått, J.H., Peltonen, J., Willför, S., Mu, X.D., Xu, C.L., 2015. Cellulose nanocrystals prepared via formic acid hydrolysis followed by TEMPO-mediated oxidation. *Carbohydrate Polymers*, **133**, 605-612.
81. Xu, W.Y., Grénman, H., Liu, J., Kronlund, D., Li, B., Backman, P., Peltonen, J., Willför, S., Sundberg, A., Xu, C.L., 2017. Mild oxalic-acid-catalyzed hydrolysis as a novel approach to prepare cellulose nanocrystals. *Chemnanomat*, **3**(2), 109-119.
82. Espinosa, S.C., Kuhnt, T., Foster, E.J., Weder, C., 2013. Isolation of Thermally Stable Cellulose Nanocrystals by Phosphoric Acid Hydrolysis. *Biomacromolecules*, **14**(4), 1223-1230.
83. Peyre, J., Pääkkönen, T., Reza, M., Kontturi, E., 2015. Simultaneous preparation of cellulose nanocrystals and micron-sized porous colloidal particles of cellulose by TEMPO-mediated oxidation. *Green Chemistry*, **17**(2), 808-811.
84. Zhou, Y.X., Saito, T., Bergström, L., Isogai, A., 2018. Acid-free preparation of cellulose nanocrystals by TEMPO oxidation and subsequent cavitation. *Biomacromolecules*, **19**(2), 633-639.
85. Eichhorn, S.J., Dufresne, A., Aranguren, M., Marcovich, N.E., Capadona, J.R., Rowan, S.J., Weder, C., Thielemans, W., Roman, M., Renneckar, S., Gindl, W., Veigel, S., Keckes, J., Yano, H., Abe, K., Nogi, M., Nakagaito, A.N., Mangalam, A., Simonsen, J., Benight, A.S., Bismarck, A., Berglund, L.A., Peijs, T., 2010. Review: current international research into cellulose nanofibres and nanocomposites. *Journal of Materials Science*, **45**(1), 1-33.
86. Kim, J.H., Shim, B.S., Kim, H.S., Lee, Y.J., Min, S.K., Jang, D., Abas, Z., Kim, J., 2015. Review of Nanocellulose for Sustainable Future Materials. *International Journal of Precision Engineering and Manufacturing-Green Technology*, **2**(2), 197-213.
87. Hu, S.X., Gu, J., Jiang, F., Hsieh, Y.L., 2016. Holistic Rice Straw Nanocellulose and Hemicelluloses/Lignin Composite Films. *ACS Sustainable Chemistry & Engineering*, **4**(3), 728-737.
88. Fengel, D., Wegener, G. 2011. *Wood: chemistry, ultrastructure, reactions*. Walter de Gruyter.

89. Šušteršic, Ž., Mohareb, A., Chaouch, M., Pétrissans, M., Petrič, M., Gérardin, P., 2010. Prediction of the decay resistance of heat treated wood on the basis of its elemental composition. *Polymer Degradation and Stability*, **95**(1), 94-97.
90. Lundqvist, J., Jacobs, A., Palm, M., Zacchi, G., Dahlman, O., Stalbrand, H., 2003. Characterization of galactoglucomannan extracted from spruce (*Picea abies*) by heat-fractionation at different conditions. *Carbohydrate Polymers*, **51**(2), 203-211.
91. Balakshin, M., Capanema, E., Gracz, H., Chang, H.-m., Jameel, H., 2011. Quantification of lignin-carbohydrate linkages with high-resolution NMR spectroscopy. *Planta*, **233**(6), 1097-1110.
92. Du, X.Y., Gellerstedt, G., Li, J.B., 2013. Universal fractionation of lignin-carbohydrate complexes (LCCs) from lignocellulosic biomass: an example using spruce wood. *Plant Journal*, **74**(2), 328-338.
93. Laurichesse, S., Avérous, L., 2014. Chemical modification of lignins: Towards biobased polymers. *Progress in Polymer Science*, **39**(7), 1266-1290.
94. Zhao, W.W., Simmons, B., Singh, S., Ragauskas, A., Cheng, G., 2016. From lignin association to nano-/micro-particle preparation: extracting higher value of lignin. *Green Chemistry*, **18**(21), 5693-5700.
95. Ralph, J., Lapierre, C., Boerjan, W., 2019. Lignin structure and its engineering. *Current opinion in biotechnology*, **56**, 240-249.
96. Boerjan, W., Ralph, J., Baucher, M., 2003. Lignin biosynthesis. *Annual Review of Plant Biology*, **54**, 519-546.
97. Norgren, M., Edlund, H., 2014. Lignin: Recent advances and emerging applications. *Current Opinion in Colloid & Interface Science*, **19**(5), 409-416.
98. Doherty, W.O.S., Mousavioun, P., Fellows, C.M., 2011. Value-adding to cellulosic ethanol: Lignin polymers. *Industrial Crops and Products*, **33**(2), 259-276.
99. Sarkanen, S., Teller, D.C., Abramowski, E., Mccarthy, J.L., 1982. Lignin .19. Kraft lignin ce-solution. *Macromolecules*, **15**(4), 1098-1104.
100. Glasser, W.G., Barnett, C.A., Muller, P.C., Sarkanen, K.V., 1983. The chemistry of several novel bioconversion lignins. *Journal of Agricultural and Food Chemistry*, **31**(5), 921-930.
101. Glasser, W.G., 2000. Classification of lignin according to chemical and molecular structure. *Lignin : Historical, Biological, and Materials Perspectives*, **742**, 216-238.
102. Chabannes, M., Ruel, K., Yoshinaga, A., Chabbert, B., Jauneau, A., Joseleau, J.P., Boudet, A.M., 2001. In situ analysis of lignins in transgenic tobacco reveals a differential impact of individual transformations on the spatial patterns of lignin deposition at the cellular and subcellular levels. *Plant Journal*, **28**(3), 271-282.
103. Whetten, R., Sederoff, R., 1995. Lignin biosynthesis. *Plant Cell*, **7**(7), 1001-1013.
104. Boudet, A.M., Lapierre, C., Grimapettenati, J., 1995. Tansley review No-80 - biochemistry and molecular-biology of lignification. *New Phytologist*, **129**(2), 203-236.
105. Upton, B.M., Kasko, A.M., 2016. Strategies for the conversion of lignin to high-value polymeric materials: Review and perspective. *Chemical Reviews*, **116**(4), 2275-2306.
106. Zakzeski, J., Bruijnincx, P.C.A., Jongerius, A.L., Weckhuysen, B.M., 2010. The catalytic valorization of lignin for the production of renewable chemicals. *Chemical Reviews*, **110**(6), 3552-3599.
107. Xu, C., Arancon, R.A.D., Labidi, J., Luque, R., 2014. Lignin depolymerisation strategies: towards valuable chemicals and fuels. *Chemical Society Reviews*, **43**(22), 7485-7500.
108. Li, C., Zhao, X., Wang, A., Huber, G.W., Zhang, T., 2015. Catalytic transformation of lignin for the production of chemicals and fuels. *Chemical Reviews*, **115**(21), 11559-11624.
109. Azadi, P., Inderwildi, O.R., Farnood, R., King, D.A., 2013. Liquid fuels, hydrogen and chemicals from lignin: A critical review. *Renewable and Sustainable Energy Reviews*, **21**, 506-523.

110. Lennartsson, P.R., Niklasson, C., Taherzadeh, M.J., 2011. A pilot study on lignocelluloses to ethanol and fish feed using NMMO pretreatment and cultivation with zygomycetes in an air-lift reactor. *Bioresource Technology*, **102**(6), 4425-4432.
111. Constant, S., Wienk, H.L.J., Frissen, A.E., de Peinder, P., Boelens, R., van Es, D.S., Grisel, R.J.H., Weckhuysen, B.M., Huijgen, W.J.J., Gosselink, R.J.A., Bruijnincx, P.C.A., 2016. New insights into the structure and composition of technical lignins: a comparative characterisation study. *Green Chemistry*, **18**(9), 2651-2665.
112. Uraki, Y., Sugiyama, Y., Koda, K., Kubo, S., Kishimoto, T., Kadla, J.F., 2012. Thermal mobility of β-O-4-type artificial lignin. *Biomacromolecules*, **13**(3), 867-872.
113. Pinkert, A., Goeke, D.F., Marsh, K.N., Pang, S.S., 2011. Extracting wood lignin without dissolving or degrading cellulose: investigations on the use of food additive-derived ionic liquids. *Green Chemistry*, **13**(11), 3124-3136.
114. Thakur, V.K., Thakur, M.K., 2015. Recent advances in green hydrogels from lignin: a review. *International Journal of Biological Macromolecules*, **72**, 834-847.
115. Réti, C., Casetta, M., Duquesne, S., Bourbigot, S., Delobel, R., 2008. Flammability properties of intumescent PLA including starch and lignin. *Polymers for Advanced Technologies*, **19**(6), 628-635.
116. Agrawal, A., Kaushik, N., Biswas, S., 2014. Derivatives and applications of lignin-an insight. *The SciTech Journal*, **1**(7), 30-36.
117. Sun, S.N., Li, H.Y., Cao, X.F., Xu, F., Sun, R.C., 2015. Structural variation of eucalyptus lignin in a combination of hydrothermal and alkali treatments. *Bioresource Technology*. **176**, 296–299.
118. Bruijnincx, P.C.A., Weckhuysen, B.M., 2014. Biomass conversion lignin up for break-down. *Nature Chemistry*, **6**(12), 1035-1036.
119. Björkman, A., 1957. Lignin and lignin-carbohydrate complexes-extraction from wood meal with neutral solvents. *Industrial Engineering Chemistry*, **49**, 1395-1398.
120. Jiang, B., Cao, T.Y., Gu, F., Wu, W.J., Jin, Y.C., 2017. Comparison of the structural characteristics of cellulolytic enzyme lignin preparations isolated from wheat straw stem and leaf. *ACS Sustainable Chemistry & Engineering*, **5**(1), 342-349.
121. Tolbert, A., Akinosho, H., Khunsupat, R., Naskar, A.K., Ragauskas, A.J., 2014. Characterization and analysis of the molecular weight of lignin for biorefining studies. *Biofuels Bioproducts & Biorefining*, **8**(6), 836-856.
122. Lin, S.Y., Dence, C.W. 2012. *Methods in lignin chemistry*. Springer Science & Business Media.
123. Baumberger, S., Abaecherli, A., Fasching, M., Gellerstedt, G., Gosselink, R., Hortling, B., Li, J., Saake, B., de Jong, E., 2007. Molar mass determination of lignins by size-exclusion chromatography: towards standardisation of the method. *Holzforschung*, **61**(4), 459-468.
124. Ringena, O., Lebioda, A., Lehnen, R., Saake, B., 2006. Size-exclusion chromatography of technical lignins in dimethyl sulfoxide/water and dimethylacetamide. *Journal of Chromatography A*, **1102**(1-2), 154-163.
125. Braaten, S.M., Christensen, B.E., Fredheim, G.E., 2003. Comparison of molecular weight and molecular weight distributions of softwood and hardwood lignosulfonates. *Journal of Wood Chemistry and Technology*, **23**(2), 197-215.
126. Gidh, A.V., Decker, S.R., Vinzant, T.B., Himmel, M.E., Williford, C., 2006. Determination of lignin by size exclusion chromatography using multi angle laser light scattering. *Journal of Chromatography A*, **1114**(1), 102-110.
127. Jiang, N., Pu, Y.Q., Ragauskas, A.J., 2010. Rapid determination of lignin content via direct dissolution and ^{1}H NMR analysis of plant cell walls. *ChemSusChem*, **3**(11), 1285-1289.

128. Tiainen, E., Drakenberg, T., Tamminen, T., Kataja, K., Hase, A., 1999. Determination of phenolic hydroxyl groups in lignin by combined use of ^{1}H NMR and UV spectroscopy. *Holzforschung*, **53**(5), 529-533.
129. Pu, Y.Q., Chen, F., Ziebell, A., Davison, B.H., Ragauskas, A.J., 2009. NMR characterization of C3H and HCT down-regulated alfalfa lignin. *Bioenergy Research*, **2**(4), 198-208.
130. Pu, Y.Q., Cao, S.L., Ragauskas, A.J., 2011. Application of quantitative ^{31}P NMR in biomass lignin and biofuel precursors characterization. *Energy & Environmental Science*, **4**(9), 3154-3166.
131. Chen, W., McClelland, D.J., Azarpira, A., Ralph, J., Luo, Z.Y., Huber, G.W., 2016. Low temperature hydrogenation of pyrolytic lignin over Ru/TiO2: 2D HSQC and C-13 NMR study of reactants and products. *Green Chemistry*, **18**(1), 271-281.
132. Liu, C.W., Su, M.L., Zhou, X.W., Zhao, R.J., Lu, J.X., Wang, Y.R., 2017. Analysis of content and distribution of lignin in cell wall of transgenic poplar with Fourier Infrared Spectrun (FTIR) and confocal laser scanning microscopy (CLSM). *Spectroscopy and Spectral Analysis*, **37**(11), 3404-3408.
133. Moghaddam, L., Rencoret, J., Maliger, V.R., Rackemann, D.W., Harrison, M.D., Gutierrez, A., del Rio, J.C., Doherty, W.S., 2017. Structural characteristics of bagasse furfural residue and its lignin component. an NMR, Py-GC/MS, and FTIR Study. *ACS Sustainable Chemistry & Engineering*, **5**(6), 4846-4855.
134. Hatakeyama, H., 1972. Thermal analysis of lignin by defferential scanning calorimetry. *Cellulose Chemistry and Technology.*, **6**, 521-529.
135. El Mansouri, N. E., Salvadó, J., 2007. Analytical methods for determining functional groups in various technical lignins. *Industrial Crops and Products*, **26**(2), 116-124.
136. Pouteau, C., Dole, P., Cathala, B., Averous, L., Boquillon, N., 2003. Antioxidant properties of lignin in polypropylene. *Polymer Degradation and Stability*, **81**(1), 9-18.
137. Domenek, S., Louaifi, A., Guinault, A., Baumberger, S., 2013. Potential of lignins as antioxidant additive in active biodegradable packaging materials. *Journal of Polymers and the Environment*, **21**(3), 692-701.
138. Mishra, S.B., Mishra, A.K., Kaushik, N.K., Khan, M.A., 2007. Study of performance properties of lignin-based polyblends with polyvinyl chloride. *Journal of Materials Processing Technology*, **183**(2-3), 273-276.
139. De Chirico, A., Armanini, M., Chini, P., Cioccolo, G., Provasoli, F., Audisio, G., 2003. Flame retardants for polypropylene based on lignin. *Polymer Degradation And Stability*, **79**(1), 139-145.
140. Ragauskas, A.J., Beckham, G.T., Biddy, M.J., Chandra, R., Chen, F., Davis, M.F., Davison, B.H., Dixon, R.A., Gilna, P., Keller, M., Langan, P., Naskar, A.K., Saddler, J.N., Tschaplinski, T.J., Tuskan, G.A., Wyman, C.E., 2014. Lignin valorization: improving lignin processing in the biorefinery. *Science*, **344**(6185), 1246843-1246843.
141. Huber, G.W., Iborra, S., Corma, A., 2006. Synthesis of transportation fuels from biomass: Chemistry, catalysts, and engineering. *Chemical Reviews*, **106**(9), 4044-4098.
142. Wang, H., Tucker, M., Ji, Y., 2013. Recent development in chemical depolymerization of lignin: a review. *Journal of Applied Chemistry*, **2013**.
143. Pandey, M.P., Kim, C.S., 2011. Lignin depolymerization and conversion: A review of thermochemical methods. *Chemical Engineering & Technology*, **34**(1), 29-41.
144. Holladay, J.E., White, J.F., Bozell, J.J., Johnson, D. 2007. Top value-added chemicals from biomass-Volume II-Results of screening for potential candidates from biorefinery lignin. Pacific Northwest National Lab.(PNNL), Richland, WA (United States).
145. Meister, J.J., 2002. Modification of lignin. *Journal of Macromolecular Science-Polymer Reviews*, **C42**(2), 235-289.
146. He, W.M., Fatehi, P., 2015. Preparation of sulfomethylated softwood kraft lignin as a dispersant for cement admixture. *RSC Advances*, **5**(58), 47031-47039.

147. Madzhidova, V., Dalimova, G., Abduazimov, K.A., 1998. Sulfomethylation of lignins. *Chemistry of Natural Compounds*, **34**(2), 179-181.
148. Wu, H.R., Chen, F.G., Feng, Q.G., Yue, X.P., 2012. Oxidation and sulfomethylation of alkali-extracted lignin from corn stalk. *Bioresources*, **7**(3), 2742-2751.
149. Ouyang, X.P., Ke, L.X., Qiu, X.Q., Guo, Y.X., Pang, Y.X., 2009. Sulfonation of alkali lignin and its potential use in dispersant for cement. *Journal of Dispersion Science and Technology*, **30**(1), 1-6.
150. Du, X.Y., Li, J.B., Lindström, M.E., 2014. Modification of industrial softwood Kraft lignin using Mannich reaction with and without phenolation pretreatment. *Industrial Crops and Products*, **52**, 729-735.
151. Gan, L.H., Zhou, M.S., Qiu, X.Q., 2015. Influence of carboxylic group content on the solution behavior of carboxymethylated lignin (CML) in water. *Holzforschung*, **69**(1), 25-32.
152. Matsushita, Y., 2015. Conversion of technical lignins to functional materials with retained polymeric properties. *Journal of Wood Science*, **61**(3), 230-250.
153. Effendi, A., Gerhauser, H., Bridgwater, A.V., 2008. Production of renewable phenolic resins by thermochemical conversion of biomass: A review. *Renewable & Sustainable Energy Reviews*, **12**(8), 2092-2116.
154. Rangan, A., Manjula, M., Satyanarayana, K., Menon, R. 2016. Lignin/nanolignin and their biodegradable composites. in: *Biodegradable Green Composites*, Wiley Online Library, 167-198.
155. Thulluri, C., Pinnamaneni, S.R., Shetty, P.R., Addepally, U., 2016. Synthesis of lignin-based nanomaterials/nanocomposites: Recent trends and future perspectives. *Industrial Biotechnology*, **12**(3), 153-160.
156. Frangville, C., Rutkevičius, M., Richter, A.P., Velev, O.D., Stoyanov, S.D., Paunov, V.N., 2012. Fabrication of environmentally biodegradable lignin nanoparticles. *ChemPhyschem*, **13**(18), 4235-4243.
157. Myint, A.A., Lee, H.W., Seo, B., Son, W.S., Yoon, J., Yoon, T.J., Park, H.J., Yu, J., Yoon, J., Lee, Y.W., 2016. One pot synthesis of environmentally friendly lignin nanoparticles with compressed liquid carbon dioxide as an antisolvent. *Green Chemistry*, **18**(7), 2129-2146.
158. Qian, Y., Deng, Y.H., Qiu, X.Q., Li, H., Yang, D.J., 2014. Formation of uniform colloidal spheres from lignin, a renewable resource recovered from pulping spent liquor. *Green Chemistry*, **16**(4), 2156-2163.
159. Lievonen, M., Valle-Delgado, J.J., Mattinen, M.L., Hult, E.L., Lintinen, K., Kostiainen, M.A., Paananen, A., Szilvay, G.R., Setälä, H., Österberg, M., 2016. A simple process for lignin nanoparticle preparation. *Green Chemistry*, **18**(5), 1416-1422.
160. Gilca, I.A., Pupa, V.I., Crestini, C., 2015. Obtaining lignin nanoparticles by sonication. *Ultrasonics Sonochemistry*, **23**, 369-375.
161. Nypelö, T.E., Carrillo, C.A., Rojas, O.J., 2015. Lignin supracolloids synthesized from (W/O) microemulsions: use in the interfacial stabilization of Pickering systems and organic carriers for silver metal. *Soft Matter*, **11**(10), 2046-2054.
162. Lu, Q., Zhu, M.H., Zu, Y.G., Liu, W.J., Yang, L., Zhang, Y., Zhao, X.H., Zhang, X.N., Zhang, X.N., Li, W.G., 2012. Comparative antioxidant activity of nanoscale lignin prepared by a supercritical antisolvent (SAS) process with non-nanoscale lignin. *Food Chemistry*, **135**(1), 63-67.
163. Yearla, S.R., Padmasree, K., 2016. Preparation and characterisation of lignin nanoparticles: evaluation of their potential as antioxidants and UV protectants. *Journal of Experimental Nanoscience*, **11**(4), 289-302.

164. Nair, S.S., Sharma, S., Pu, Y.Q., Sun, Q.N., Pan, S.B., Zhu, J.Y., Deng, Y.L., Ragauskas, A.J., 2014. High shear homogenization of lignin to nanolignin and thermal stability of nanolignin-polyvinyl alcohol blends. *ChemSusChem*, **7**(12), 3513-3520.
165. Njuguna, J., Pielichowski, K., Desai, S., 2008. Nanofiller-reinforced polymer nanocomposites. *Polymers for Advanced Technologies*, **19**(8), 947-959.
166. Tian, D., Hu, J.G., Bao, J., Chandra, R.P., Saddler, J.N., Lu, C.H., 2017. Lignin valorization: lignin nanoparticles as high-value bio-additive for multifunctional nanocomposites. *Biotechnology for Biofuels*, **10**.
167. Richter, A.P., Brown, J.S., Bharti, B., Wang, A., Gangwal, S., Houck, K., Hubal, E.A.C., Paunov, V.N., Stoyanov, S.D., Velev, O.D., 2015. An environmentally benign antimicrobial nanoparticle based on a silver-infused lignin core. *Nature Nanotechnology*, **10**(9), 817-823.
168. Lintinen, K., Latikka, M., Sipponen, M.H., Ras, R.H.A., Osterberg, M., Kostiainen, M.A., 2016. Structural diversity in metal-organic nanoparticles based on iron isopropoxide treated lignin. *RSC Advances*, **6**(38), 31790-31796.
169. Figueirêdo, P., Lintinen, K., Kiriazis, A., Hynninen, V., Liu, Z.H., Bauleth-Ramos, T., Rahikkala, A., Correia, A., Kohout, T., Sarmento, B., Yli-Kauhaluoma, J., Hirvonen, J., Ikkala, O., Kostiainen, M.A., Santos, H.A., 2017. *In vitro* evaluation of biodegradable lignin-based nanoparticles for drug delivery and enhanced antiproliferation effect in cancer cells. *Biomaterials*, **121**, 97-108.
170. Ge, Y.Y., Li, Z.L., 2018. Application of lignin and its derivatives in adsorption of heavy metal ions in water: A review. *ACS Sustainable Chemistry & Engineering*, **6**(5), 7181-7192.
171. Supanchaiyamat, N., Jetsrisuparb, K., Knijnenburg, J.T.N., Tsang, D.C.W., Hunt, A.J., 2019. Lignin materials for adsorption: Current trend, perspectives and opportunities. *Bioresource Technology*, **272**, 570-581.
172. Li, F.F., Wang, X.L., Yuan, T.Q., Sun, R.C., 2016. A lignosulfonate-modified graphene hydrogel with ultrahigh adsorption capacity for Pb(II) removal. *Journal of Materials Chemistry A*, **4**(30), 11888-11896.
173. Zong, E.M., Huang, G.B., Liu, X.H., Lei, W.W., Jiang, S.T., Ma, Z.Q., Wang, J.F., Song, P.G., 2018. A lignin-based nano-adsorbent for superfast and highly selective removal of phosphate. *Journal of Materials Chemistry A*, **6**(21), 9971-9983.
174. Liang, F.B., Song, Y.L., Huang, C.P., Li, Y.X., Chen, B.H., 2013. Synthesis of novel lignin-based ion-exchange resin and its utilization in heavy metals removal. *Industrial & Engineering Chemistry Research*, **52**(3), 1267-1274.
175. Albadarin, A.B., Collins, M.N., Naushad, M., Shirazian, S., Walker, G., Mangwandi, C., 2017. Activated lignin-chitosan extruded blends for efficient adsorption of methylene blue. *Chemical Engineering Journal*, **307**, 264-272.
176. Bartczak, P., Klapiszewski, Ł., Wysokowski, M., Majchrzak, I., Czernicka, W., Piasecki, A., Ehrlich, H., Jesionowski, T., 2017. Treatment of model solutions and wastewater containing selected hazardous metal ions using a chitin/lignin hybrid material as an effective sorbent. *Journal of Environmental Management*, **204**, 300-310.
177. Mohan, D., Pittman, C.U., Steele, P.H., 2006. Single, binary and multi-component adsorption of copper and cadmium from aqueous solutions on Kraft lignin - a biosorbent. *Journal of Colloid and Interface Science*, **297**(2), 489-504.
178. Guo, X.Y., Zhang, S.Z., Shan, X.Q., 2008. Adsorption of metal ions on lignin. *Journal of Hazardous Materials*, **151**(1), 134-142.
179. Wu, Y., Zhang, S.Z., Guo, X.Y., Huang, H.L., 2008. Adsorption of chromium(III) on lignin. *Bioresource Technology*, **99**(16), 7709-7715.

180. Abdelkafi, F., Ammar, H., Rousseau, B., Tessier, M., El Gharbi, R., Fradet, A., 2011. Structural Analysis of Alfa Grass (*Stipa tenacissima L.*) Lignin Obtained by Acetic Acid/Formic Acid Delignification. *Biomacromolecules*, **12**(11), 3895-3902.
181. Björkman, A., 1954. Isolation of lignin from finely divided wood with neutral solvents. *Nature*, **174**(4440), 1057-1058.
182. Liu, J., Korpinen, R., Mikkonen, K.S., Willför, S., Xu, C.L., 2014. Nanofibrillated cellulose originated from birch sawdust after sequential extractions: a promising polymeric material from waste to films. *Cellulose*, **21**(4), 2587-2598.
183. Zhang, S., Zhou, Y.F., Nie, W.Y., Song, L.Y., 2012. Preparation of Fe_3O_4/chitosan/poly(acrylic acid) composite particles and its application in adsorbing copper ion (II). *Cellulose*, **19**(6), 2081-2091.
184. Li, S., Willoughby, J.A., Rojas, O.J., 2016. Oil-in-water emulsions stabilized by carboxymethylated lignins: Properties and energy prospects. *ChemSusChem*, **9**(17), 2460-2469.
185. Sundberg, A., Sundherg, K., Lillandt, C., Holmhom, B., 1996. Determination of hemicelluloses and pectins in wood and pulp fibres by acid methanolysis and gas chromatography. *Nordic Pulp & Paper Research Journal*, **11**(4), 216-219.
186. Zheng, X., Ma, X., Chen, L., Cao, S., Nasrallah, J., 2016. Lignin extraction and recovery in hydrothermal pretreatment of bamboo. *Journal of Bioresources and Bioproducts*, **1**(3), 145-151.
187. Guo, Y.Z., Zhou, J.H., Wen, J.L., Sun, G.W., Sun, Y.J., 2015. Structural transformations of triploid of Populus tomentosa Carr. lignin during auto-catalyzed ethanol organosolv pretreatment. *Industrial Crops and Products*, **76**, 522-529.
188. Wang, X.Y., Cai, J.H., Zhang, Y.J., Li, L.H., Jiang, L., Wang, C.R., 2015. Heavy metal sorption properties of magnesium titanate mesoporous nanorods. *Journal of Materials Chemistry A*, **3**(22), 11796-11800.
189. Ge, X., Song, X.Y., Ma, Y., Zhou, H.J., Wang, G.Z., Zhang, H.M., Zhang, Y.X., Zhao, H.J., Wong, P.K., 2016. Fabrication of hierarchical iron-containing MnO_2 hollow microspheres assembled by thickness-tunable nanosheets for efficient phosphate removal. *Journal of Materials Chemistry A*, **4**(38), 14814-14826.
190. Xu, Q.H., Wang, Y.L., Jin, L.Q., Wang, Y., Qin, M.H., 2017. Adsorption of Cu (II), Pb (II) and Cr (VI) from aqueous solutions using black wattle tannin-immobilized nanocellulose. *Journal of Hazardous Materials*, **339**, 91-99.
191. Vázquez, G., Antorrena, G., González, J., 1995. Kinetics of acid-catalyzed delignification of eucalyptus-globulus wood by acetic-acid. *Wood Science and Technology*, **29**(4), 267-275.
192. Pan, X.J., Sano, Y., 2005. Fractionation of wheat straw by atmospheric acetic acid process. *Bioresource Technology*, **96**(11), 1256-1263.
193. Huijgen, W.J.J., Reith, J.H., den Uil, H., 2010. Pretreatment and fractionation of wheat sraw by an acetone-based organosolv process. *Industrial & Engineering Chemistry Research*, **49**(20), 10132-10140.
194. Wildschut, J., Smit, A.T., Reith, J.H., Huijgen, W.J.J., 2013. Ethanol-based organosolv fractionation of wheat straw for the production of lignin and enzymatically digestible cellulose. *Bioresource Technology*, **135**, 58-66.
195. El Hage, R., Brosse, N., Chrusciel, L., Sanchez, C., Sannigrahi, P., Ragauskas, A., 2009. Characterization of milled wood lignin and ethanol organosolv lignin from miscanthus. *Polymer Degradation and Stability*, **94**(10), 1632-1638.
196. Jahan, M.S., Chowdhury, D.A.N., Islam, M.K., Moeiz, S.M.I., 2007. Characterization of lignin isolated from some nonwood available in Bangladesh. *Bioresource Technology*, **98**(2), 465-469.

197. Li, Q., He, Y.C., Xian, M., Jun, G., Xu, X., Yang, J.M., Li, L.Z., 2009. Improving enzymatic hydrolysis of wheat straw using ionic liquid 1-ethyl-3-methyl imidazolium diethyl phosphate pretreatment. *Bioresource Technology*, **100**(14), 3570-3575.
198. Wen, J.L., Sun, S.N., Yuan, T.Q., Xu, F., Sun, R.C., 2013. Fractionation of bamboo culms by autohydrolysis, organosolv delignification and extended delignification: Understanding the fundamental chemistry of the lignin during the integrated process. *Bioresource Technology*, **150**, 278-286.
199. Li, J.B., Henriksson, G., Gellerstedt, G., 2007. Lignin depolymerization/repolymerization and its critical role for delignification of aspen wood by steam explosion. *Bioresource Technology*, **98**(16), 3061-3068.
200. Sannigrahi, P., Ragauskas, A.J., Miller, S.J., 2010. Lignin structural modifications resulting from ethanol organosolv treatment of Loblolly Pine. *Energy & Fuels*, **24**(1), 683-689.
201. Hallac, B.B., Ray, M., Murphy, R.J., Ragauskas, A.J., 2010. Correlation between anatomical characteristics of ethanol organosolv pretreated buddleja davidii and its enzymatic conversion to glucose. *Biotechnology and Bioengineering*, **107**(5), 795-801.
202. Lagerwall, J.P.F., Schütz, C., Salajkova, M., Noh, J., Park, J.H., Scalia, G., Bergström, L., 2014. Cellulose nanocrystal-based materials: from liquid crystal self-assembly and glass formation to multifunctional thin films. *Npg Asia Materials*, **6**.
203. Li, Z.L., Ge, Y.Y., Wan, L., 2015. Fabrication of a green porous lignin-based sphere for the removal of lead ions from aqueous media. *Journal of Hazardous Materials*, **285**, 77-83.
204. Hambardzumyan, A., Foulon, L., Bercu, N.B., Pernes, M., Maigret, J.E., Molinari, M., Chabbert, B., Aguié-Beghin, V., 2015. Organosolv lignin as natural grafting additive to improve the water resistance of films using cellulose nanocrystals. *Chemical Engineering Journal*, **264**, 780-788.
205. Ma, Y.B., Asaadi, S., Johansson, L.S., Ahvenainen, P., Reza, M., Alekhina, M., Rautkari, L., Michud, A., Hauru, L., Hummel, M., Sixta, H., 2015. High-strength composite fibers from cellulose-lignin blends regenerated from ionic liquid solution. *ChemSusChem*, **8**(23), 4030-4039.
206. Yang, W.J., Fortunati, E., Gao, D.Q., Balestra, G.M., Giovanale, G., He, X.Y., Torre, L., Kenny, J.M., Puglia, D., 2018. Valorization of acid isolated high yield lignin nanoparticles as innovative antioxidant/antimicrobial organic materials. *ACS Sustainable Chemistry & Engineering*, **6**(3), 3502-3514.
207. Yen, C.H., Lien, H.L., Chung, J.S., Yeh, H.D., 2017. Adsorption of precious metals in water by dendrimer modified magnetic nanoparticles. *Journal of Hazardous Materials*, **322**, 215-222.
208. Uddin, M.K., 2017. A review on the adsorption of heavy metals by clay minerals, with special focus on the past decade. *Chemical Engineering Journal*, **308**, 438-462.
209. Charpentier, T.V.J., Neville, A., Lanigan, J.L., Barker, R., Smith, M.J., Richardson, T., 2016. Preparation of magnetic carboxymethylchitosan nanoparticles for adsorption of heavy metal Ions. *ACS Omega*, **1**(1), 77-83.
210. Liu, Q., Li, F., Lu, H., Li, M., Liu, J., Zhang, S.L., Sun, Q.J., Xiong, L., 2018. Enhanced dispersion stability and heavy metal ion adsorption capability of oxidized starch nanoparticles. *Food Chemistry*, **242**, 256-263.
211. Cai, Y.C., Li, C.L., Wu, D., Wang, W., Tan, F.T., Wang, X.Y., Wong, P.K., Qiao, X.L., 2017. Highly active MgO nanoparticles for simultaneous bacterial inactivation and heavy metal removal from aqueous solution. *Chemical Engineering Journal*, **312**, 158-166.
212. Zhu, H.S., Tan, X.L., Tan, L.Q., Zhang, H.F., Liu, H.N., Fang, M., Hayat, T., Wang, X.K., 2018. Magnetic porous polymers prepared via high internal phase emulsions for efficient removal of Pb^{2+} and Cd^{2+}. *ACS Sustainable Chemistry & Engineering*, **6**(4), 5206-5213.

213. Wu, J., Zhu, H.S., Liu, G., Tan, L.Q., Hu, X.Y., Chen, C.L., Alharbi, N.S., Hayat, T., Tan, X.L., 2017. Fabrication of core-Shell CMNP@PmPD nanocomposite for efficient As(V) adsorption and reduction. *ACS Sustainable Chemistry & Engineering*, **5**(5), 4399-4407.
214. Mu, B., Wang, A.Q., 2015. One-pot fabrication of multifunctional superparamagnetic attapulgite/Fe_3O_4/polyaniline nanocomposites served as an adsorbent and catalyst support. *Journal of Materials Chemistry A*, **3**(1), 281-289.
215. Roto, R., Yusran, Y., Kuncaka, A., 2016. Magnetic adsorbent of Fe_3O_4@SiO_2 core-shell nanoparticles modified with thiol group for chloroauric ion adsorption. *Applied Surface Science*, **377**, 30-36.
216. Cheng, F.Y., Su, C.H., Yang, Y.S., Yeh, C.S., Tsai, C.Y., Wu, C.L., Wu, M.T., Shieh, D.B., 2005. Characterization of aqueous dispersions of Fe_3O_4 nanoparticles and their biomedical applications. *Biomaterials*, **26**(7), 729-738.
217. Moorthy, M.S., Seo, D.J., Song, H.J., Park, S.S., Ha, C.S., 2013. Magnetic mesoporous silica hybrid nanoparticles for highly selective boron adsorption. *Journal of Materials Chemistry A*, **1**(48), 15556-15556.
218. Ren, Y., Abbood, H.A., He, F.B., Peng, H., Huang, K.X., 2013. Magnetic EDTA-modified chitosan/SiO_2/Fe_3O_4 adsorbent: Preparation, characterization, and application in heavy metal adsorption. *Chemical Engineering Journal*, **226**, 300-311.
219. Zhang, M.Y., Song, L.H., Jiang, H.F., Li, S., Shao, Y.F., Yang, J.Q., Li, J.F., 2017. Biomass based hydrogel as an adsorbent for the fast removal of heavy metal ions from aqueous solutions. *Journal of Materials Chemistry A*, **5**(7), 3434-3446.

ISBN 978-952-12-3920-5